$$Q_I = \frac{2\pi p}{(r_i - r_j)(r_i - r_k)} \left[\frac{(r_k^4 - r_i^4)}{4} - \frac{(r_j + r_k)(r_k^3 - r_i^3)}{3} + \frac{r_j r_k}{2} (r_k^2 - r_i^2) \right] \quad (3B.17)$$

$$Q_J = \frac{2\pi p}{(r_j - r_k)(r_j - r_i)} \left[\frac{(r_k^4 - r_i^4)}{4} - \frac{(r_i + r_k)(r_k^3 - r_i^3)}{3} + \frac{r_k r_i}{2} (r_k^2 - r_i^2) \right] \quad (3B.18)$$

$$Q_K = \frac{2\pi p}{(r_k - r_i)(r_k - r_j)} \left[\frac{(r_k^4 - r_i^4)}{4} - \frac{(r_i + r_j)(r_k^3 - r_i^3)}{3} + \frac{r_i r_j}{2} (r_k^2 - r_i^2) \right] \quad (3B.19)$$

CHAPTER FOUR

ANALYSIS OF SINGLE GRANULAR PILES AND SMALL GROUPS

4.1 INTRODUCTION

Stone columns are frequently used either singly or in small groups to support isolated strip or pad footings. In this chapter the finite element analysis described in the previous chapter is used to determine the important parameters affecting the load-settlement behaviour of a single stone column. This method of analysis is then used to reproduce the load-settlement response of a full-scale load test. When slip at the granular pile-soft clay interface is allowed, the agreement between observed and predicted behaviour is very good.

The results of a parametric study of the settlement of two piles at varying spacing are presented. These results were obtained using the elastic method described by Poulos (1968a) and are used in conjunction with a finite element analysis of a single stone column to predict the load-settlement response of small groups of stone columns.

The strength and deformation properties of the pile and soil along with the initial stress conditions are required for a finite element analysis of the load-settlement behaviour of a stone column. Field and laboratory methods for estimating this dat. are discussed and some recommendations made.

4.2 SINGLE PILES

In this section the finite element analysis described in the previous chapter is used to obtain theoretical results which indicate that the use of granular piles as a method of soil stabili-

sation results in significant improvement in the load-settlement behaviour of a foundation.

The prediction of the load-settlement response of a full scale load test on a single stone column (Hughes et al., 1975) using this method of analysis is presented. A comparison between the finite element solutions and the results using the method of Mattes and Poulos (1969) for the analysis of conventional piles is made. The finite element solutions show that considerable yield of both the granular material and the clay would take place unless conservative working loads are adopted in comparison to the ultimate bearing capacity. Thus the method described by Mattes and Poulos for the load-settlement analysis of conventional piles underestimates the settlements except at low working loads.

4.2.1 Typical Results From Finite Element Analysis

To illustrate the application of the preceding analysis and examine some of the general trends in the behaviour of granular piles, a number of solutions were obtained for an idealised case (Fig. 4.1). The solutions presented in this section fall into two categories; those in which all three modes of failure in the pile-soil system are considered (Fig. 4.3) and those in which slip at the pile soil interface is not included in the analysis (Figs. 4.2, 4.4, 4.5).

The axisymmetric finite element mesh consisted of 224 triangular elements. The outer boundary was located at 10.8 pile radii from the pile axis and was assumed to be stress free. The elastic deflection given by the mesh for a uniform pressure applied to a homo-

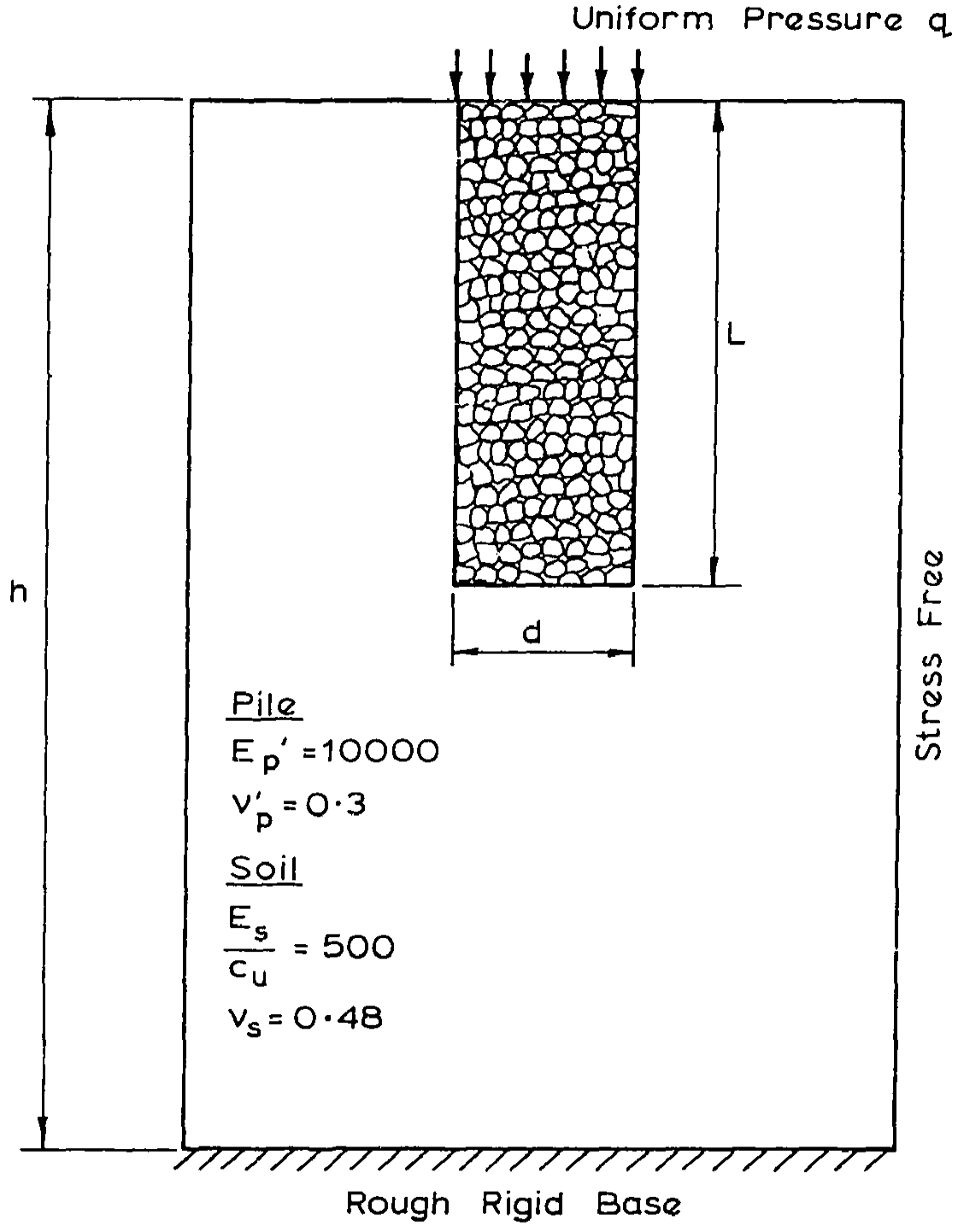

FIG.4·1 IDEALISED CASE FOR THEORETICAL SOLUTIONS

geneous soil layer was compared with that given by Poulos and Davis (1974) and found to differ by 4.2%. Since only relative behaviour and general trends were being sought the mesh was considered to be adequate.

A granular pile of dimensionless length L/d = 4, Poisson's ratio ν_p' = 0.3 and Young's Modulus E_p' = 10,000 situated in a homogeneous soil layer of depth h = 2L was initially considered. The Poisson's ratio of the soil layer ν_s was taken to be 0.48 to represent undrained loading of the pile and the ratio of soil modulus E_s to cohesion c_u was constant and equal to 500. The coefficient of earth pressure at rest K_o' was taken to be 1.0 in both the pile and soil. The unit weight of both the pile and soil was assumed to be 1.92 times that of water. The pile was taken to have zero cohesion, an angle of friction ϕ and an angle of dilatancy ψ, while the soil was assumed to be purely cohesive. The soil layer was underlain by a rough rigid base and a uniform pressure q applied across the top of the pile.

For a given ϕ, L and modular ratio E_p'/E_s, the ultimate load of a single pile is proportional to the undrained cohesion of the soil c_u. By plotting deflections in the non-dimensional form $\delta E_s/d c_u$ the load-deflection curves for a particular value of ϕ and of E_p'/E_s is unique, i.e. independent of the ratio E_s/c_u.

Fig. 4.3 illustrates the difference in predicted load settlement behaviour when slip at the pile-soil interface is included in the analysis. The pile has $\phi = 40°$ and $\psi = 20°$. Solutions have been computed for the cases when the pile-soil adhesion c_a is taken equal to the cohesion and half the cohesion of the soil respectively. These are

In Fig. 4.2, load-deflection curves for the pile with various angles of friction ϕ are shown. The angle of dilatancy is taken to be equal to $\phi/2$. The increased load capacity with increasing ϕ of the pile is evident.

Fig. 4.3 illustrates the difference in predicted load settlement behaviour when slip at the pile-soil interface is included in the analysis. The pile has $\phi = 40°$ and $\psi = 20°$. Solutions have been computed for the cases when the pile-soil adhesion c_a is taken equal to the cohesion and half the cohesion of the soil respectively. These are

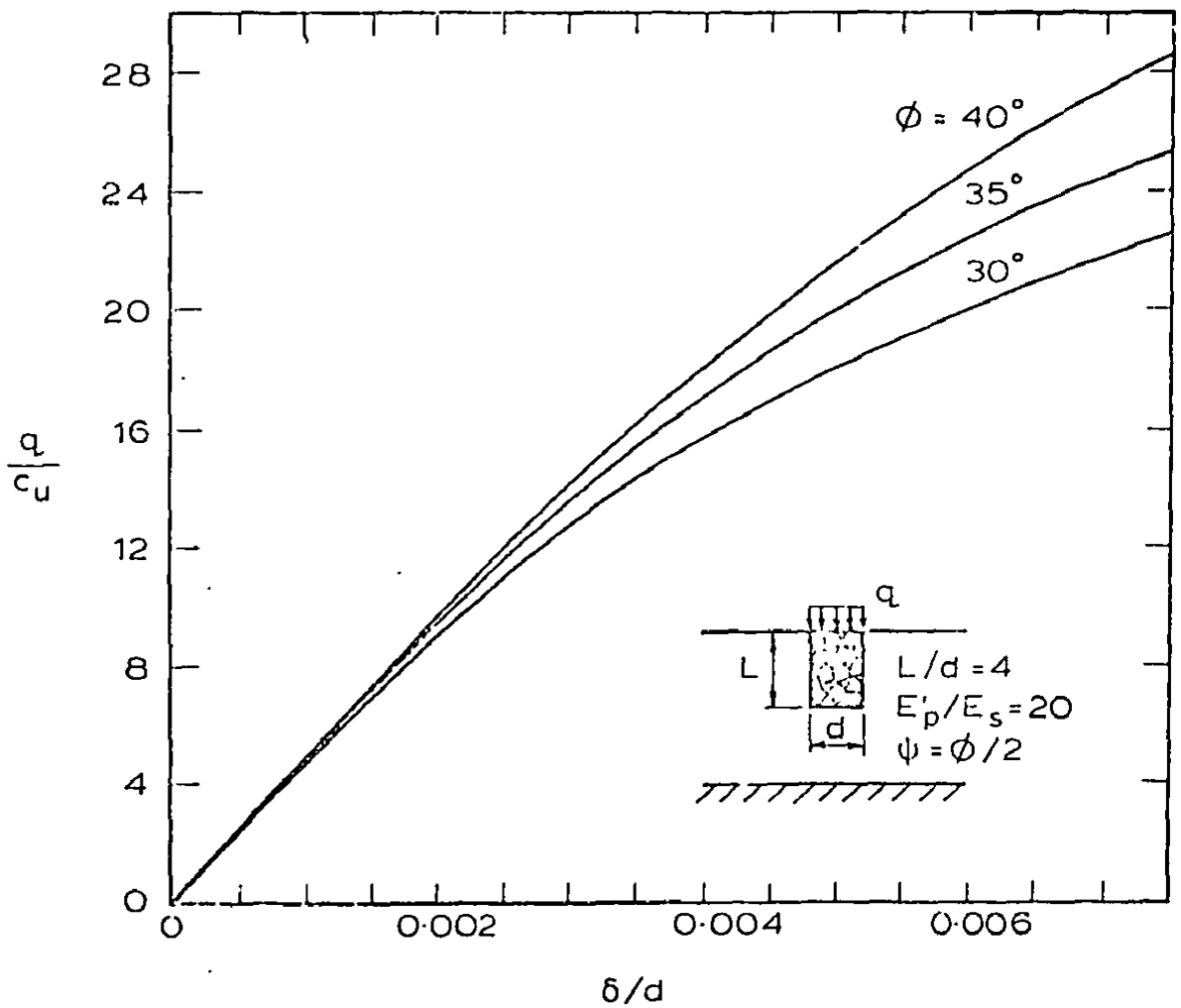

FIG.4·2 EFFECT OF INTERNAL FRICTION Ø ON THE LOAD DEFLECTION BEHAVIOUR

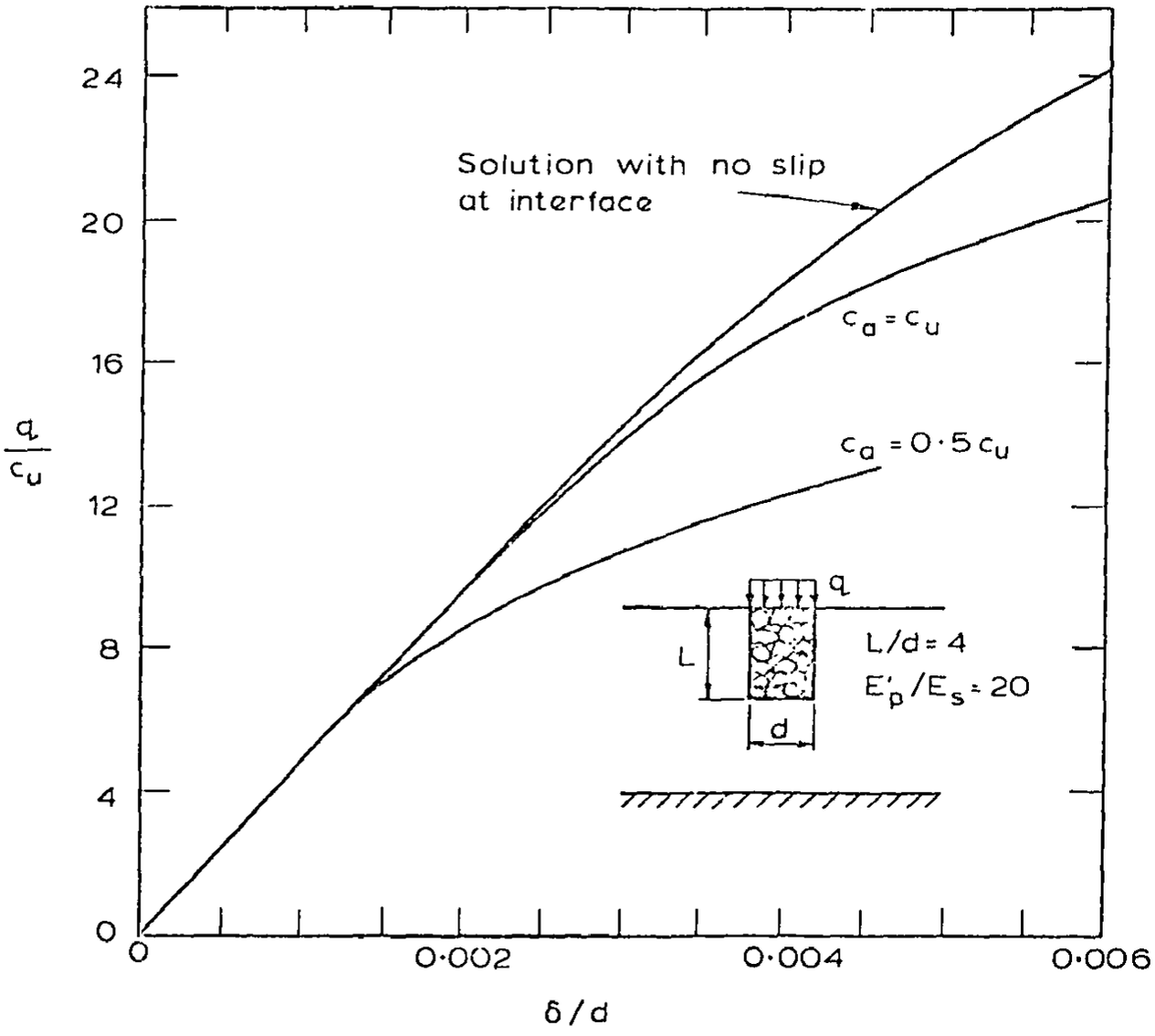

FIG. 4.3 SOLUTIONS WITH ADHESIVE SLIP AT INTERFACE

plotted together with the solution for no slip at the interface. As might be expected, the advent of slip decreases the load capacity.

The value of E_s/c_u = 500 was assumed for the theoretical analyses as this value appears to be representative for many clays, although the kaolin used in the laboratory tests was found to have a value of E_s/c_u of about 250.

ment and load carrying capacity. However, even a short pile leads to a great improvement in the load-settlement performance, thus confirming the value of granular piles for soil stabilisation. In Fig. 4.5, the results of analysing the pile with L/d = 4 and $\phi = 40°$, $\psi = 20°$, for varying ratios of E_p'/E_s are shown. Both settlement and load capacity are very significantly affected by the value of E_p'/E_s.

In Fig. 4.6 the zones of yielding within the pile and soil are shown for the case illustrated in Fig. 4.3 (with $c_a = 0.5c_u$) for q/c_u = 12.0 and 13.6, the latter being the estimated ultimate bearing capacity. In both cases slip has occurred over the full length of the shaft.

The growth of the plastic zones obtained from the finite element analyses shows that the mechanism of failure by bulging of the stone columns, causing passive failure of the soil, is similar to that assumed by Hughes and Withers.

(ii) The depth to which the pile is installed, L

(iii) The cohesion of the insitu soil, c_u

The angle of dilatancy of the pile material is of little importance. If allowance for slip at the pile-soil interface is included in the

The result of varying the dimensionless length L/d of the pile when $\phi = 40°$, $\psi = 20°$ is shown in Fig. 4.4. The limiting cases of no pile and the fully penetrating pile are shown. For this case, the pile length has a very significant influence on both the settlement and load carrying capacity. However, even a short pile leads to a great improvement in the load-settlement performance, thus confirming the value of granular piles for soil stabilisation. In Fig. 4.5, the results of analysing the pile with L/d = 4 and $\phi = 40°$, $\psi = 20°$, for varying ratios of E_p'/E_s are shown. Both settlement and load capacity are very significantly affected by the value of E_p'/E_s.

The theoretical results presented in this section indicate that the three most important factors affecting the ultimate bearing capacity of a stone column are;

(i) The friction angle of the pile material, ϕ

(ii) The depth to which the pile is installed, L

(iii) The cohesion of the insitu soil,

The angle of dilatancy of the pile material is of little importance. If allowance for slip at the pile-soil interface is included in the

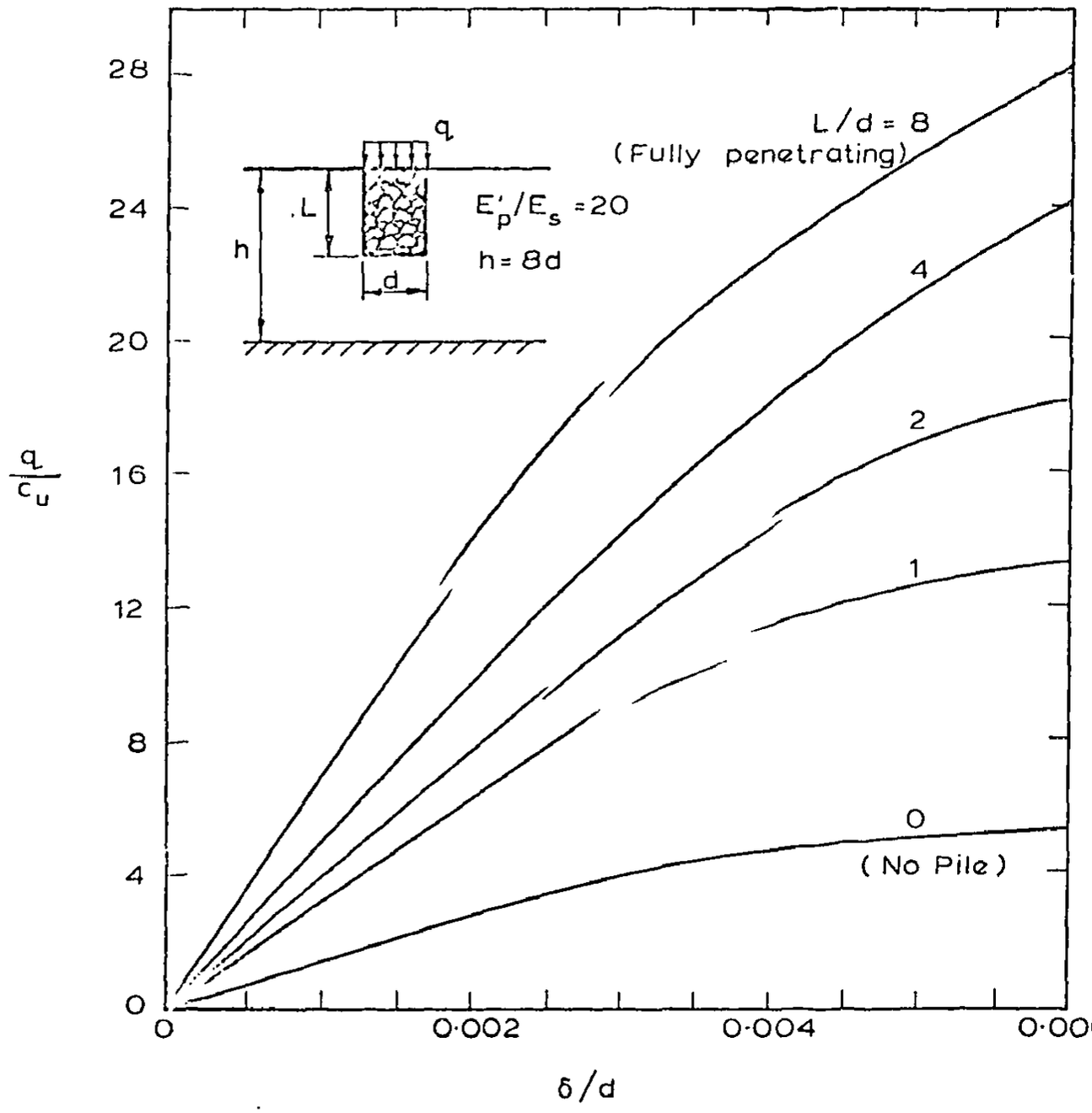

FIG. 4.4 LOAD-SETTLEMENT CURVES FOR PILES OF VARYING LENGTH

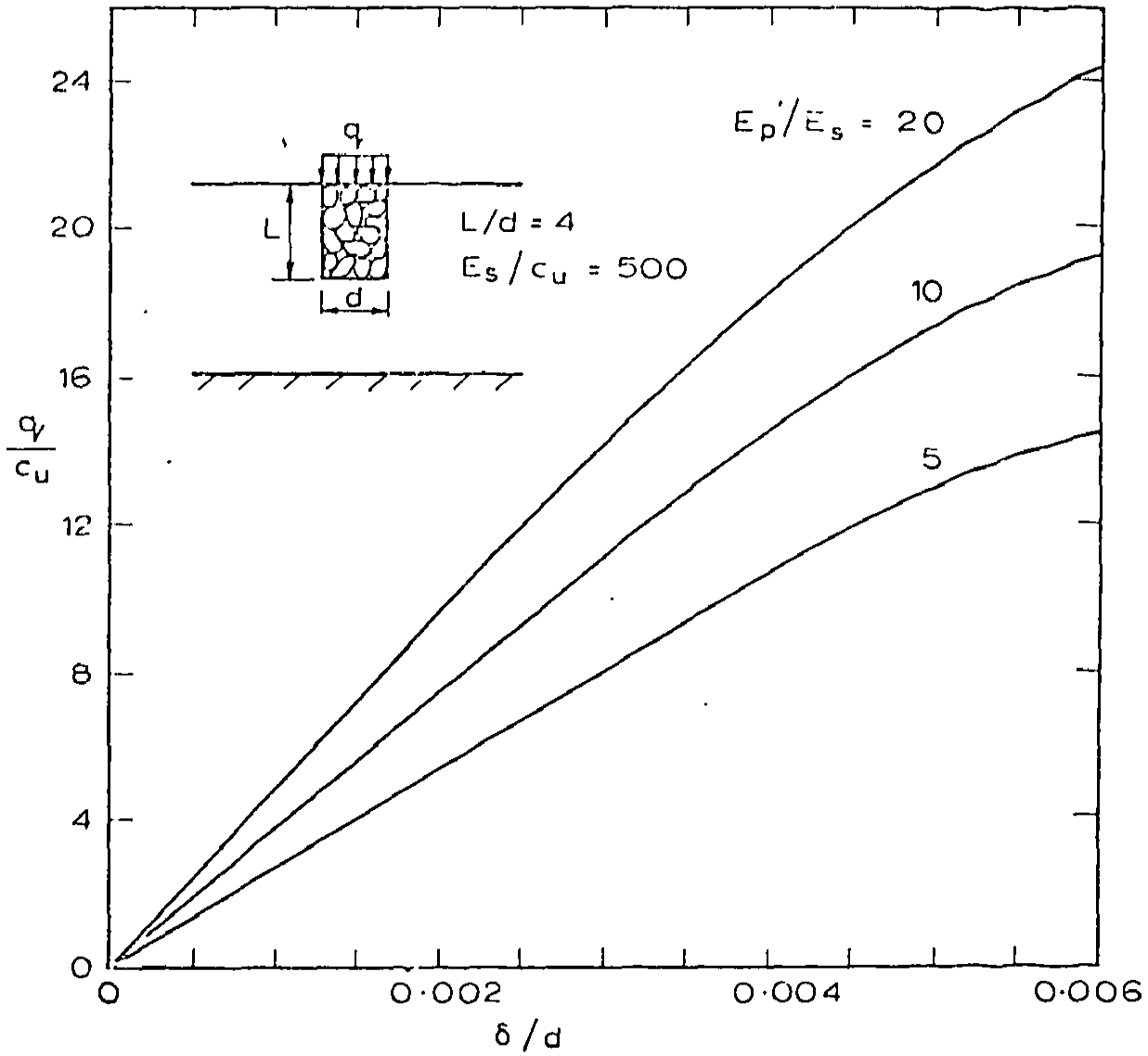

FIG. 4·5 THE EFFECT OF RELATIVE STIFFNESS E_p'/E_s ON THE LOAD – DISPLACEMENT BEHAVIOUR

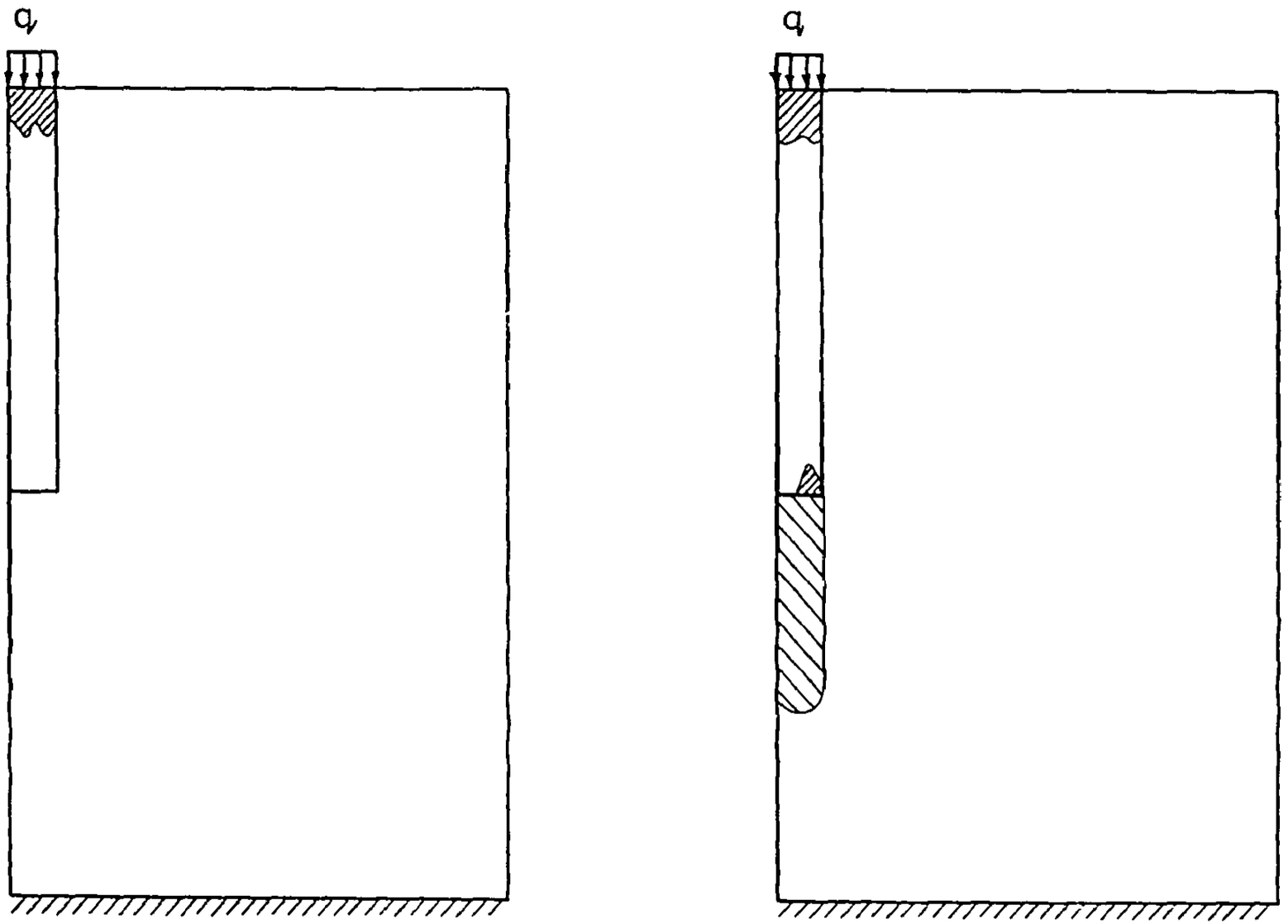

$q = 12 \cdot 0 c_u$ $q = 13 \cdot 6 c_u$

FIG. 4·6 ZONES OF YIELDING AFTER WHOLE OF SHAFT HAS SLIPPED

analysis, the value for the adhesive strength c_a needs to be chosen carefully as it affects the load-settlement response significantly. As expected, the settlement behaviour of the stone column is affected by the E_s/c_u ratio and the ratio of pile to soil moduli, E_p'/E_s.

The results confirm the findings in practice that the use of granular piles leads to significant improvements in the load-settlement behaviour of the soil.

4.2.2 Comparison Between Theoretical Results and a Full Scale Load Test

Hughes et al., (1975) have presented in detail the results of a plate loading test on an isolated stone column installed in soft clay at Canvey Island (Britain). The results of a site investigation, supplemented by Cambridge and Ménard pressuremeter tests, are also presented.

The authors predicted the result of the test prior to the field testing using the theory outlined by Hughes and Withers (1974) which was discussed in Chapter 2. When an accurate assessment of the column diameter was obtained the prediction of the load carrying capacity was excellent. However, the settlements were underestimated at low load levels. The column strength calculated by the authors was based on the lowest value of measured passive restraint over the critical length of the column where the critical length was defined as the minimum length at which both bulging and bearing failure occurred simultaneously.

In this section the finite element analysis presented in Chapter 3 is used to reproduce the load-settlement response of the stone column. The test took half an hour to complete and therefore it is assumed that the soil deformed under undrained conditions. The pile is treated as a purely frictional dilatant material whereas the soil is taken to be purely cohesive.

On a macro scale the site is uniform with a top crust of 1-2m thick and then soft clay to a depth of about 9m where the stiffer stratum is found. The water table is 2m below the surface. On excavating the column after testing, the initial column diameter was estimated at 730mm. The load was applied to the top of the column by a circular plate. The isoparametric finite element mesh used for the analyses is shown in Fig. 4.7.

The data given enables an intuitive assessment of the basic soil parameters required for a finite element analysis. The profile of insitu lateral stresses measured by the Cambridge pressuremeter along with that used for the finite element analyses is reproduced in Fig. 4.8. The soil shear strength profile was measured using the Ménard and Cambridge pressuremeters, Dutch Cone and conventional undrained triaxial tests supplemented by vane tests. The Cambridge pressuremeter results indicate a relatively homogeneous soil with an average cohesion of approximately 22 kN/m^2. The profile obtained from the conventional undrained triaxial tests and vane tests along with that used in the finite element analyses is reproduced in Fig. 4.9. This profile was used because normally the availability of the results from the pressuremeters would be rare. To determine the Young's modulus of the clay, the radial stress-strain curves from the Cambridge

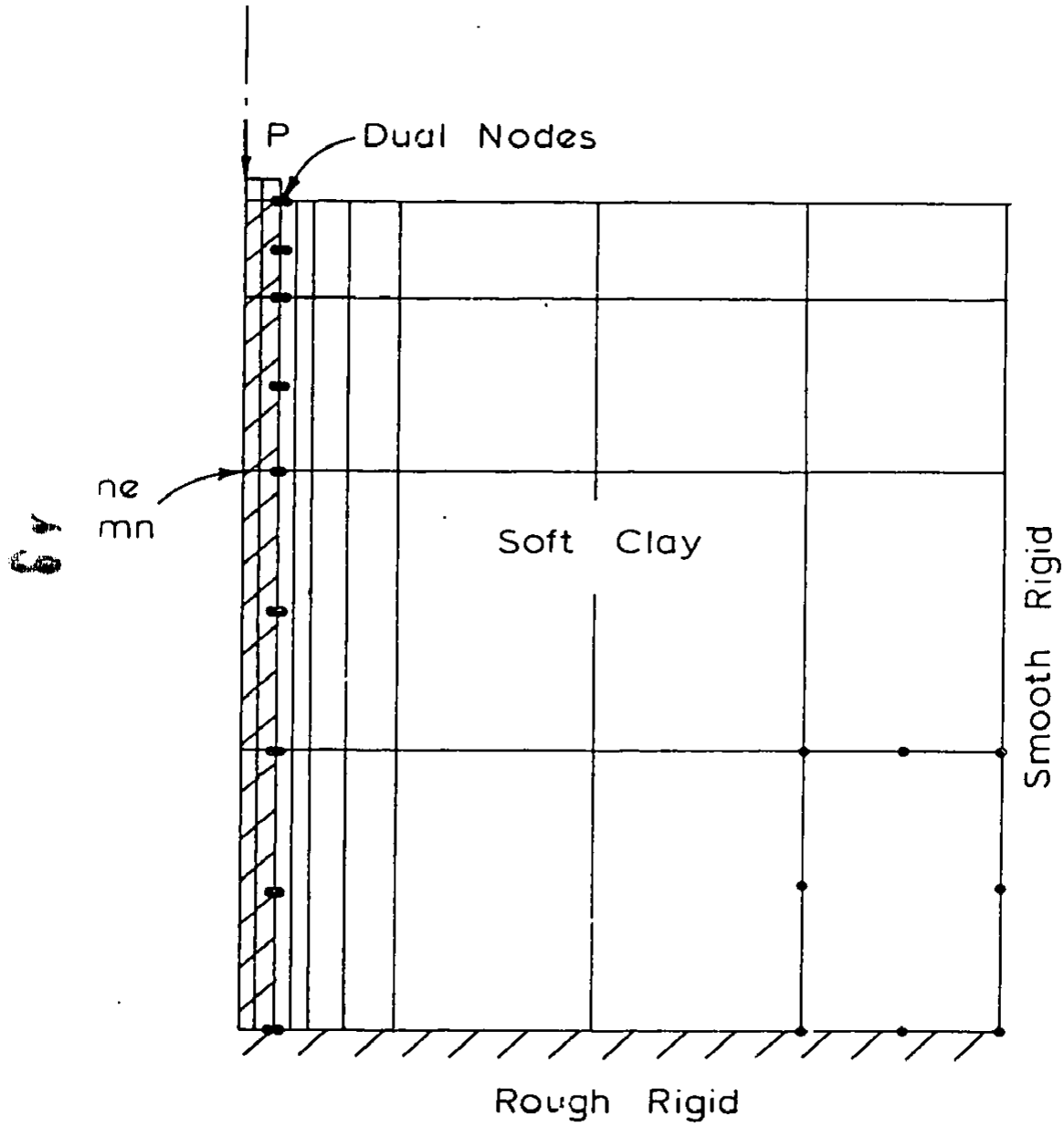

IG. 4·7 ISOPARAMETRIC FINITE ELEMENT MESH USED FOR ANA YSES OF HUGHES et al LOAD TEST

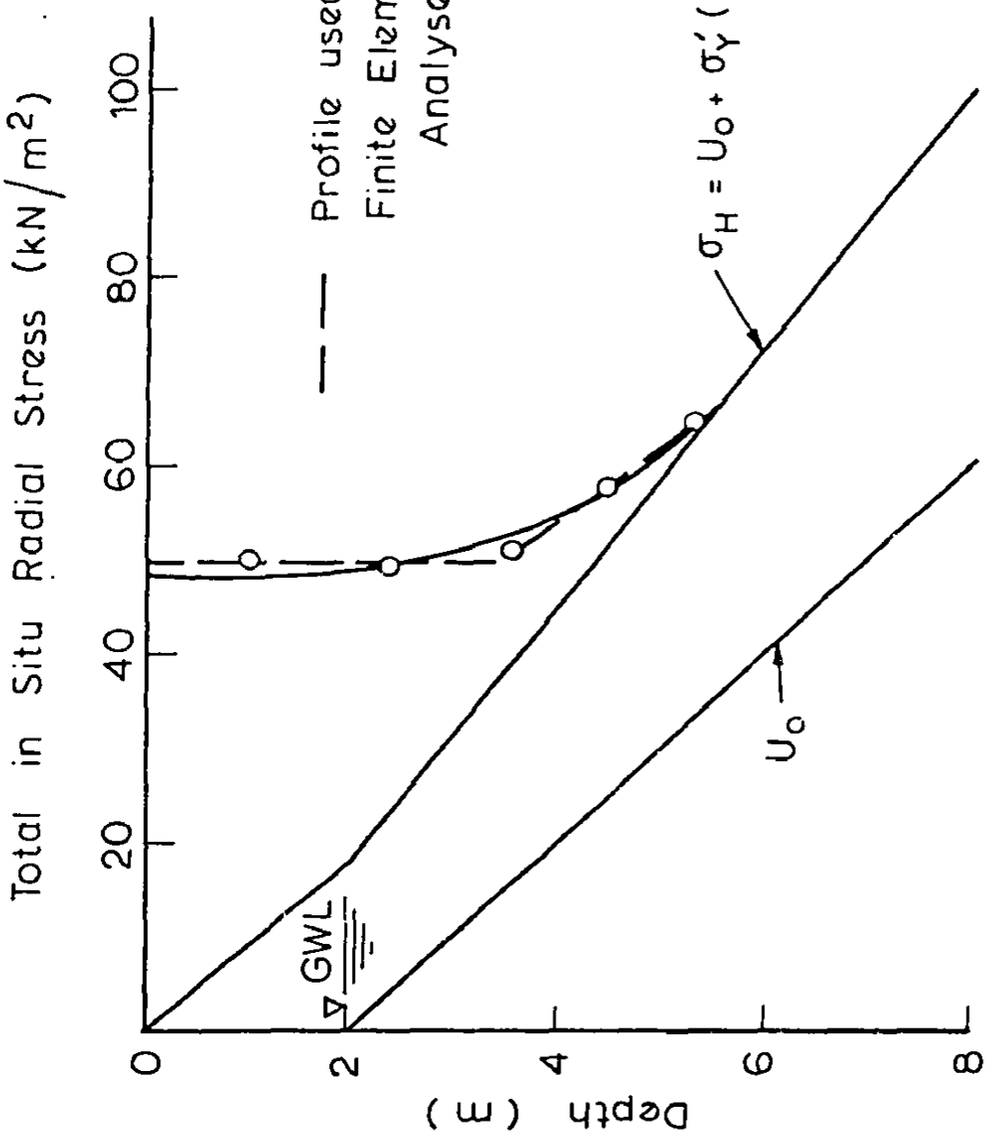

FIG. 4·8 PROFILE OF IN SITU LATERAL STRESS FROM CAMBRIDGE PRESSUREMETER (AFTER ; HUGHES et al 1975)

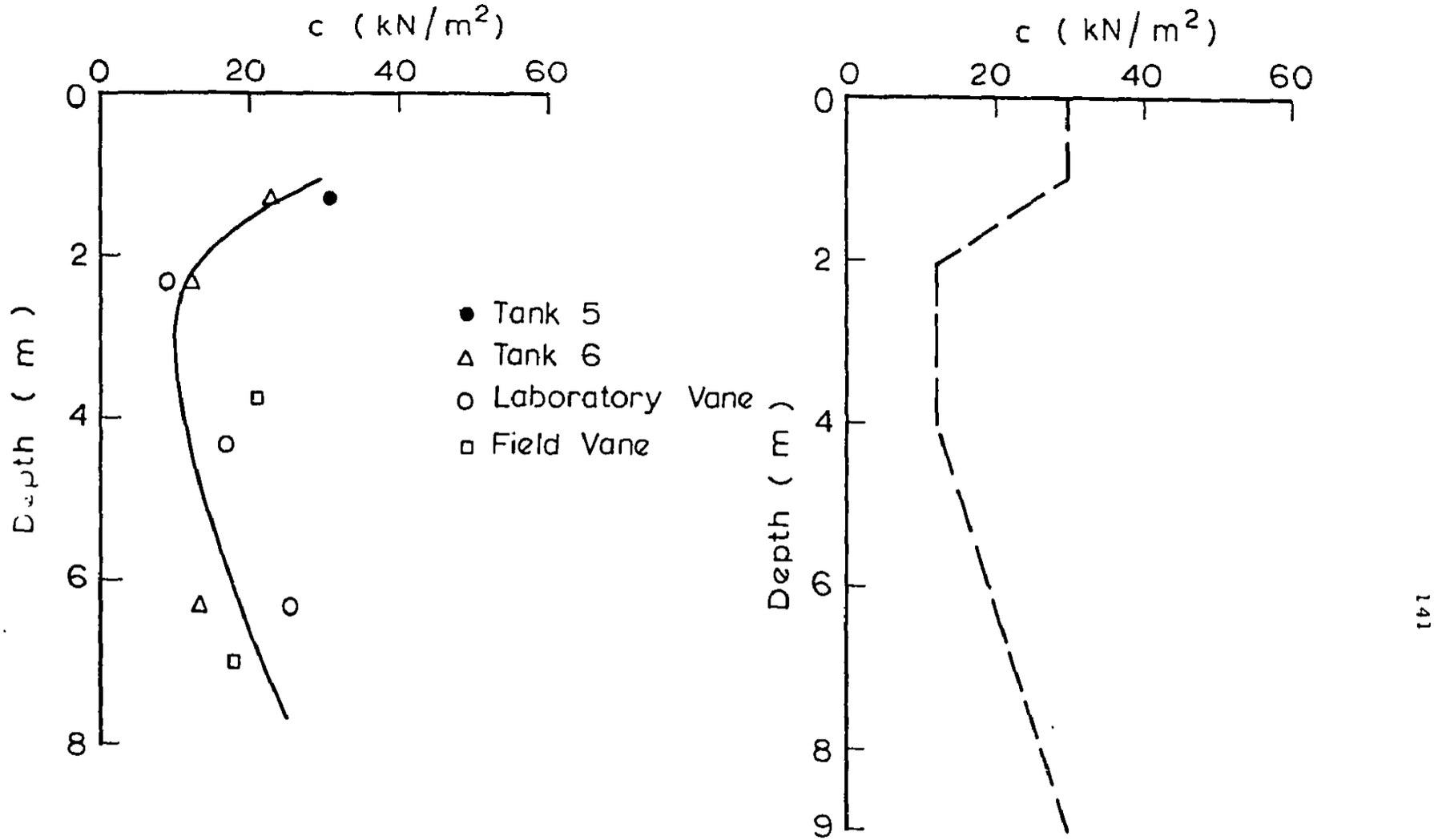

(a) Conventional Undrained Triaxial And Vane Tests (After Hughes et al 1975)

(b) Cohesion Profile Used In Finite Element Analyses

FIG. 4·9 SOIL SHEAR STRENGTH PROFILE

pressuremeter were used to construct shear stress versus strain curves (Ladd et al., 1977). From these an average value of 8000 kN/m^2 was adopted. A unit weight of 18 kN/m^3 was assumed for both the column and soil. The angle of internal friction of the pile assumed by the authors to be 38° was used and an angle of dilatancy ψ = 12° assumed. Because the pile is rammed into the soft clay, the coefficient of earth pressure at rest, K_o', is taken to be 1.0 in the pile. Finally, the modulus for the pile of 50,000 kN/m^2 was backfigured from the elastic portion of the load-settlement curve. This value compares favourably with 58,000 kN/m^2 suggested by Engelhardt and Kirsch (1977) for the modulus of a single stone column.

The results of five analyses along with the measured load-settlement curve are shown in Fig. 4.10. The first analysis was performed to estimate the increased bearing capacity of the circular plate due to the installation of the column. As reported by Hughes et al., the stone column causes a significant increase in bearing capacity.

The second analysis, which closely reproduces the measured load deflection curve, is obtained when the interface strength is purely adhesive. The adhesion is taken to be the full cohesion of the soil as shown in Fig. 4.9(b). The third analysis is for an interface strength which is purely frictional and dilatant. In this analysis the friction angle governing slip at the interface ϕ_a is 38° and the dilatancy angle of the interface ψ_a is 12°, these being identical to the friction and dilatancy angles of the pile material. The curve is not continued past the point plotted because of the advent of negative plastic work in elements at the column-clay inter-

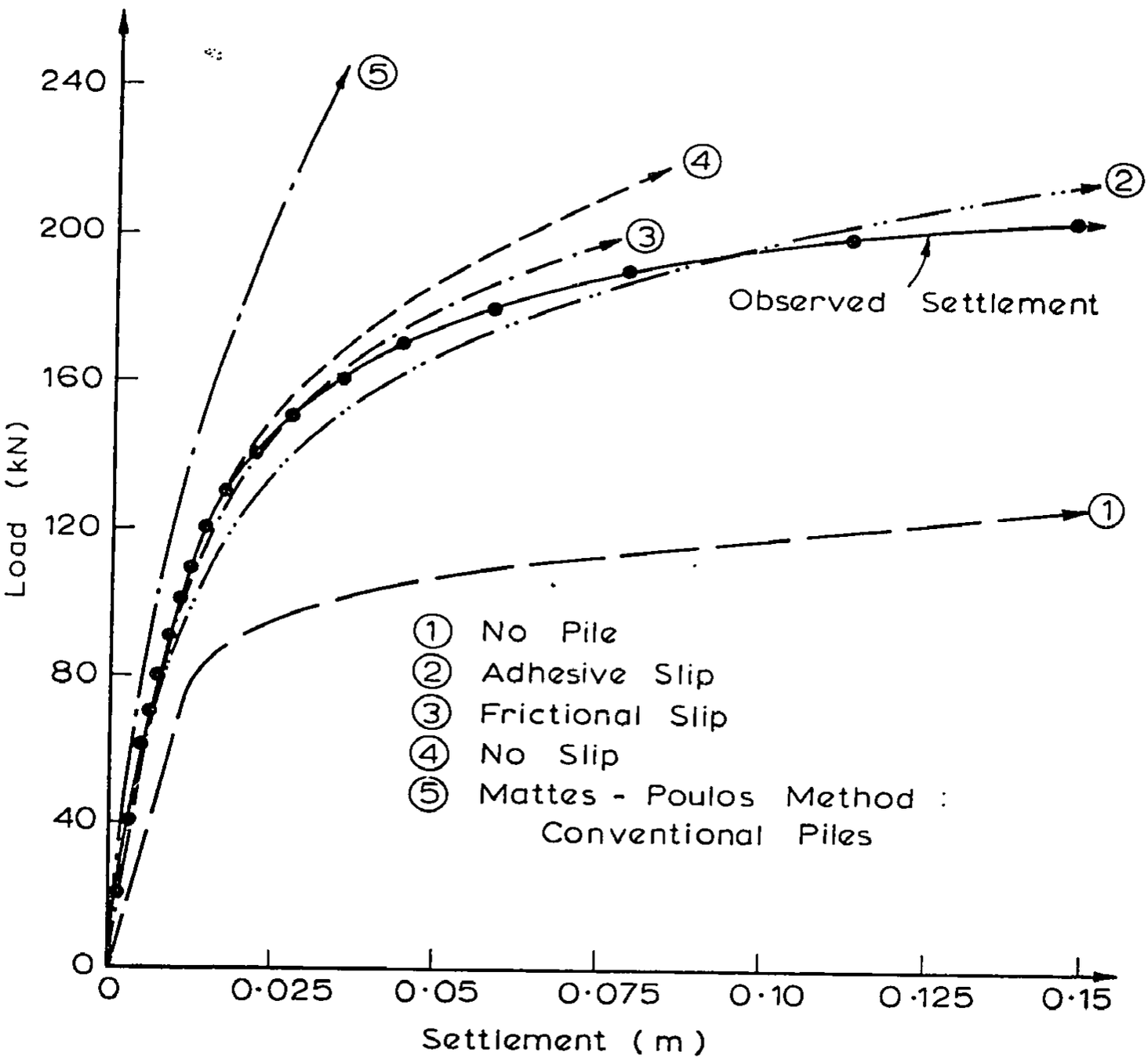

FIG. 4·10 HUGHES AND WITHERS LOAD TEST – FINITE ELEMENT RESULTS

face. This may occur because the interface dilatancy being imposed is not compatible with the plastic deformation in the pile and soil materials. However, it may be a numerical problem eliminated by reducing the size of the load steps. Nevertheless, the frictional slip will clearly not model the measured behaviour as closely as the adhesive slip.

In the fourth analysis the stone column-clay interface strength is made sufficiently large so that no slip occurs. This results in an overestimate of the load carrying capacity of the column. Finally, the results from an analysis using the method described by Mattes and Poulos (1969) for conventional piles is presented. In this analysis a limiting interface strength and base resistance is specified. The adhesive slip criterion adopted in the second analysis was employed along with a base resistance calculated from the standard penetration numbers of the underlying grey silty sand. Yield within the pile and soil are not taken into account in this analysis, and consequently the predicted settlements are too small except at low working loads.

In Fig. 4.11 the results of the second analysis are replotted along with the two predictions of Hughes, Withers and Greenwood. The authors' predictions are in close agreement with the observed results when the shearing resistance at the interface is taken into account. If the interface is assumed to have no shear resistance the ultimate load is underestimated and poor agreement results.

The growth of the yielded zones within the pile and soil, obtained from the second finite element analysis in which an adhesive

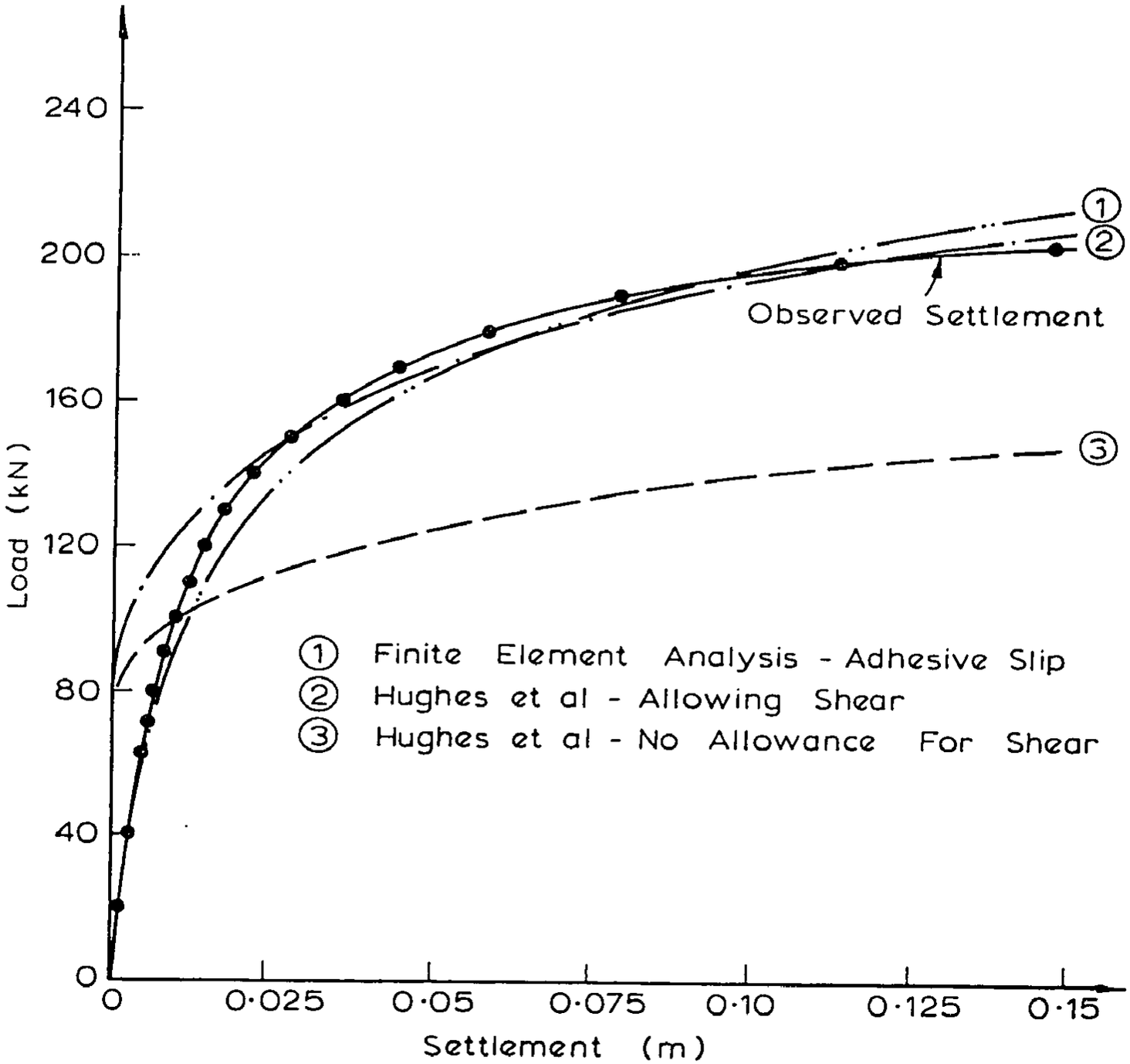

FIG. 4·11 FINITE ELEMENT RESULTS COMPARED TO HUGHES et al (1975) PREDICTIONS

interface strength is specified, is shown in Fig. 4.12. These results verify the mechanism of passive failure of the soil by bulging of the pile which was adopted by Hughes and Withers (1974) for their theory of the ultimate load of a single column.

The results from this load test illustrate that close agreement between observed and predicted behaviour can be achieved from the finite element analysis when an adhesive interface strength is specified. Although the method of Hughes and Withers (1974) predicts the ultimate load closely it underestimates the settlements for small load levels.

4.3 SMALL GROUPS

In this section the elastic method described by Poulos (1968a) is used to obtain theoretical solutions which, when used in conjunction with the results of a finite element analysis of a single stone column, enable an estimate of the load-settlement response of small groups of granular piles installed to support isolated footings.

In an attempt to verify the applicability of the elastic solutions, the results are used to predict the settlements from a load test on a group of seven columns performed by Datye and Nagaraju (1975). The predicted settlements are too small, but the soil data is incomplete and the test arrangement is such that several assumptions are necessary for an analysis. Better agreement could possibly be obtained if the soil properties were more clearly defined.

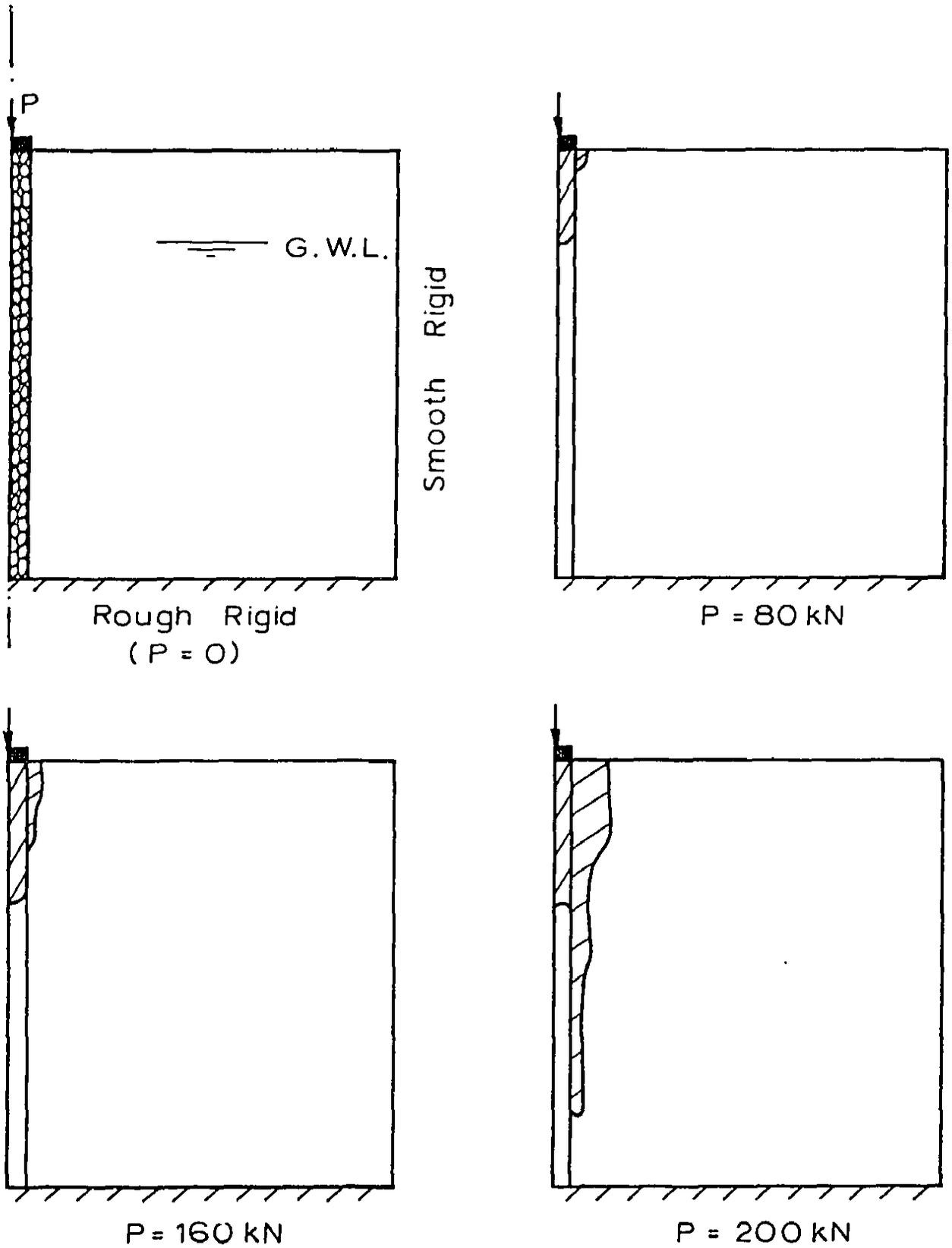

FIG. 4·12 GROWTH OF YIELDED ZONES IN SOIL AND PILE

4.3.1 Load-Settlement Analysis of Small Groups

The load-settlement behaviour of a small group of stone columns can be estimated from the results of a finite element analysis of a single stone column using the procedure outlined below:

(i) The load-settlement response of a single stone column, installed at the site being considered, is predicted by the finite element analysis described in Chapter 3.

(ii) The relationship between the average load on a column in the group and settlement is then constructed using the following relationship [Fig. 4.13(a)]

$$S_G = R_s S_1 \qquad (4.1)$$

where S_G = Settlement of the group

S_1 = Settlement of the single pile from the finite element analysis

$R_s = \sum_{i=1}^{n} \alpha_f$

and n = number of piles

α_f = interaction factors computed from an elastic analysis of two identical piles (Poulos, 1968a).

(iii) The total load versus settlement relationship for the group is computed by multiplying the average load on each pile by the number of piles in the group [Fig. 4.13(b)].

An important assumption in the above approach is that the elastic inter-

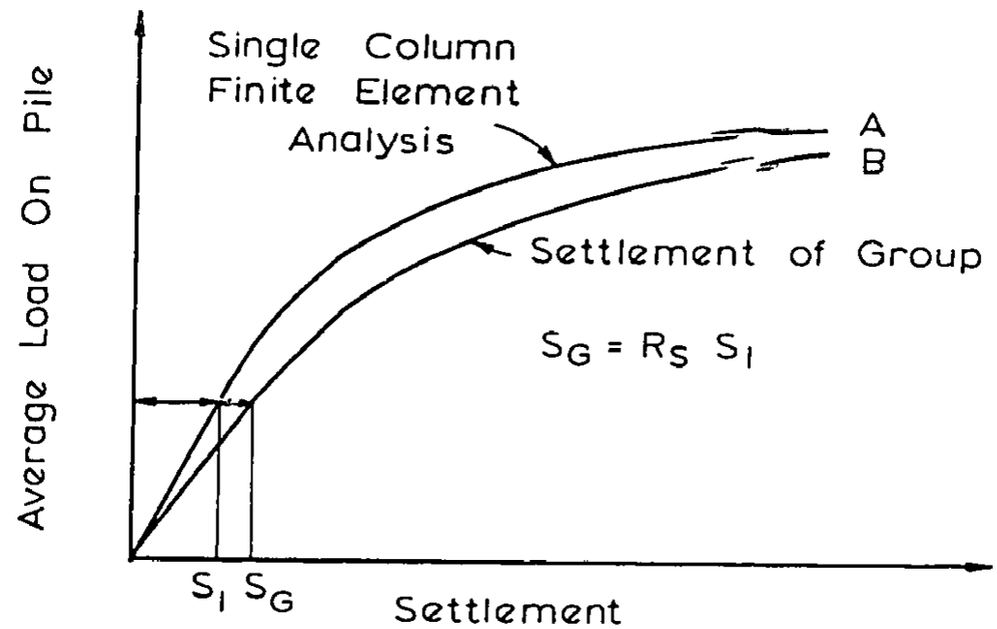

(a) Average Load on Pile in Group VS Settlement

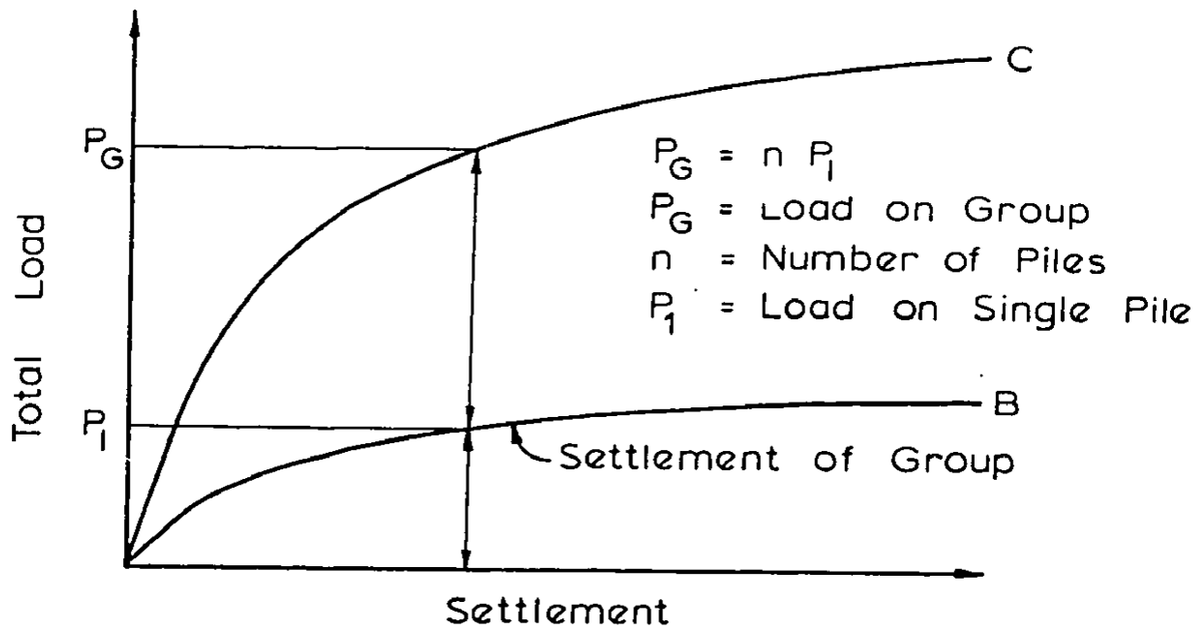

(b) Load - Settlement Curve For Pile Group

FIG. 4·13

action factors can be used to construct the entire load settlement curve, even though yielding in both the piles and soil will result in a non-linear response of the mass. In addition, it is assumed that the ultimate load of the group is not affected by interactions between the piles.

4.3.1 (i) Theoretical Solutions for Interaction Factors

The method of analysis used in this section has been described in detail by Poulos (1968a) and thus only the relevant equations are reproduced here for completeness. The results presented in this section were obtained using a computer program for pile analysis (AXPL4) which was developed at Sydney University.

From an elastic analysis of two identical piles of length L, diameter d and at a spacing s (Fig. 4.14), an interaction factor α_f is computed where

$$\alpha_f = \frac{\text{increase in settlement of pile 1 due to pile 2}}{\text{settlement of pile 1 due to own lo}} \qquad (4.2)$$

In Figs. 4.15, 4.16 and 4.17 interaction factors α_f are presented for L/d = 5, 10, 20 and h/L = 1 and 2 for the complete range of spacings s/d. Three values of relative stiffness K (5, 10 and 20) are considered where

$$K = \frac{E_p'}{E} \qquad (4.3)$$

where E_p' = drained pile modulus

E = soil modulus (drained or undrained as appropriate)

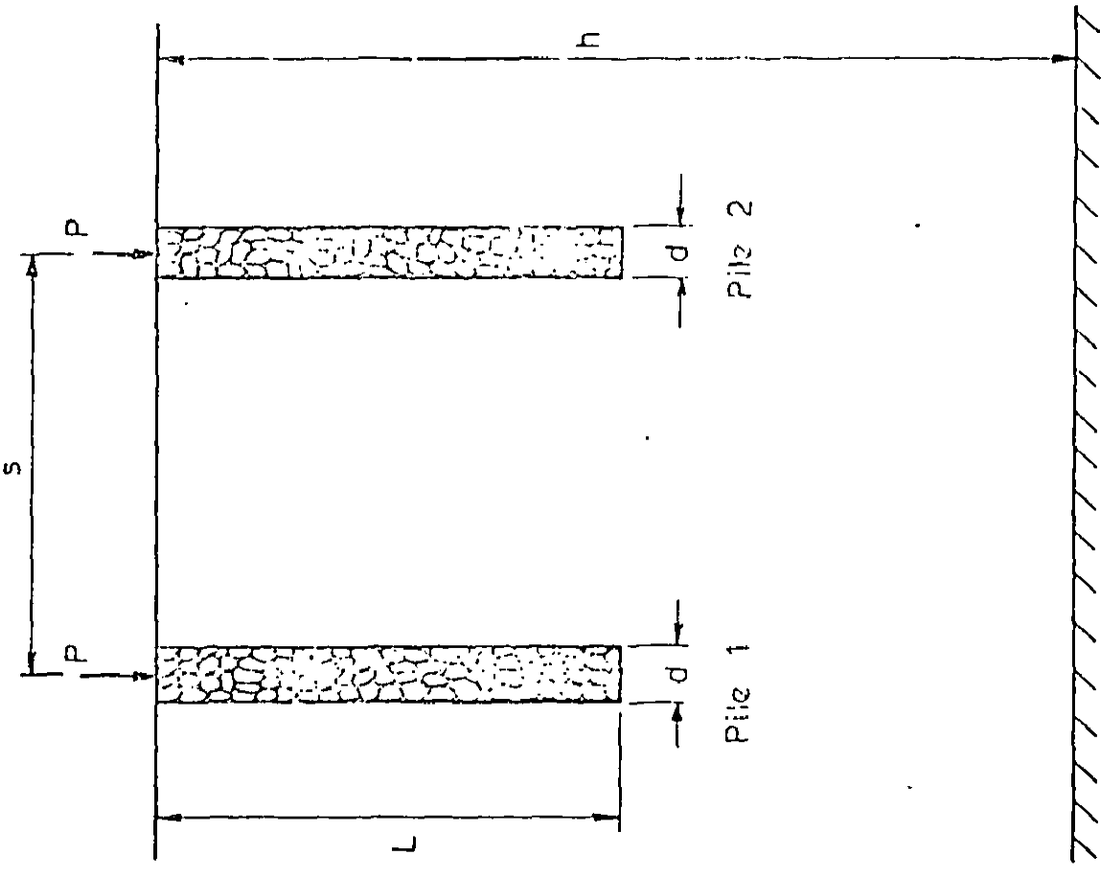

FIG. 4.14 GROUP OF TWO PILES USED TO COMPUTE INTERACTION FACTORS

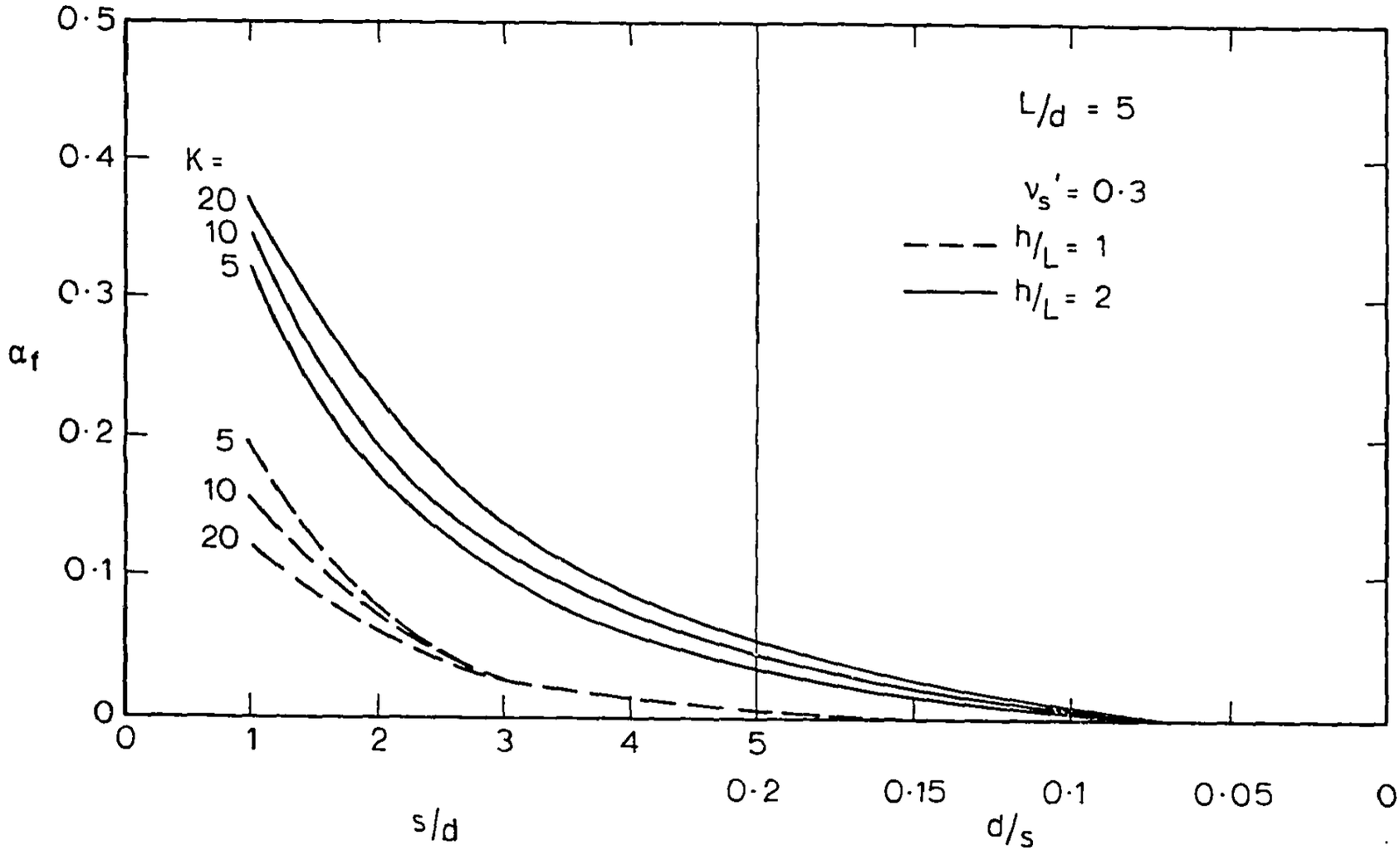

FIG. 4·15 INTERACTION FACTORS FOR SETTLEMENT ANALYSIS OF SMALL GROUPS

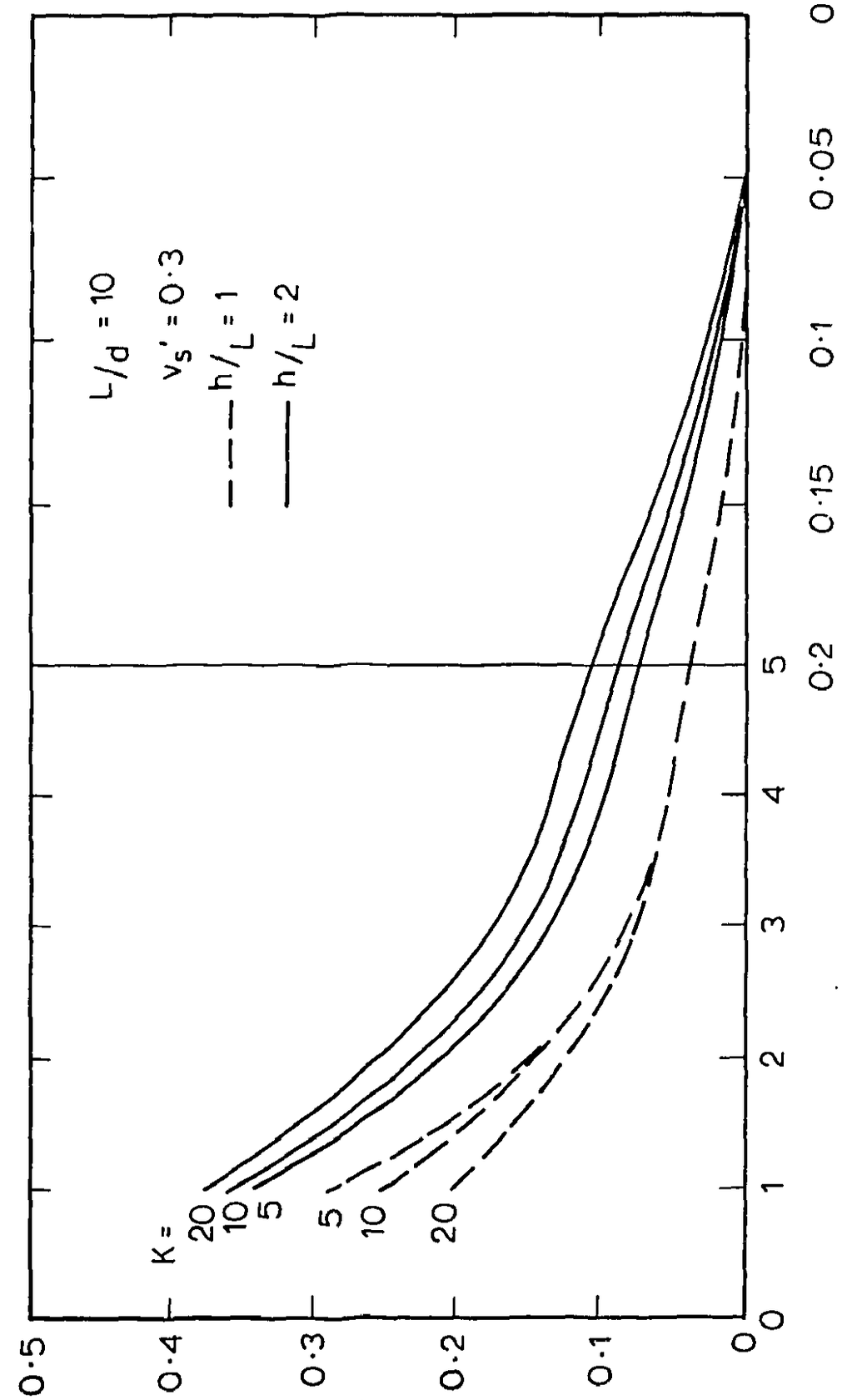

FIG. 4·16 INTERACTION FACTORS FOR SETTLEMENT ANALYSIS OF SMALL GROUPS

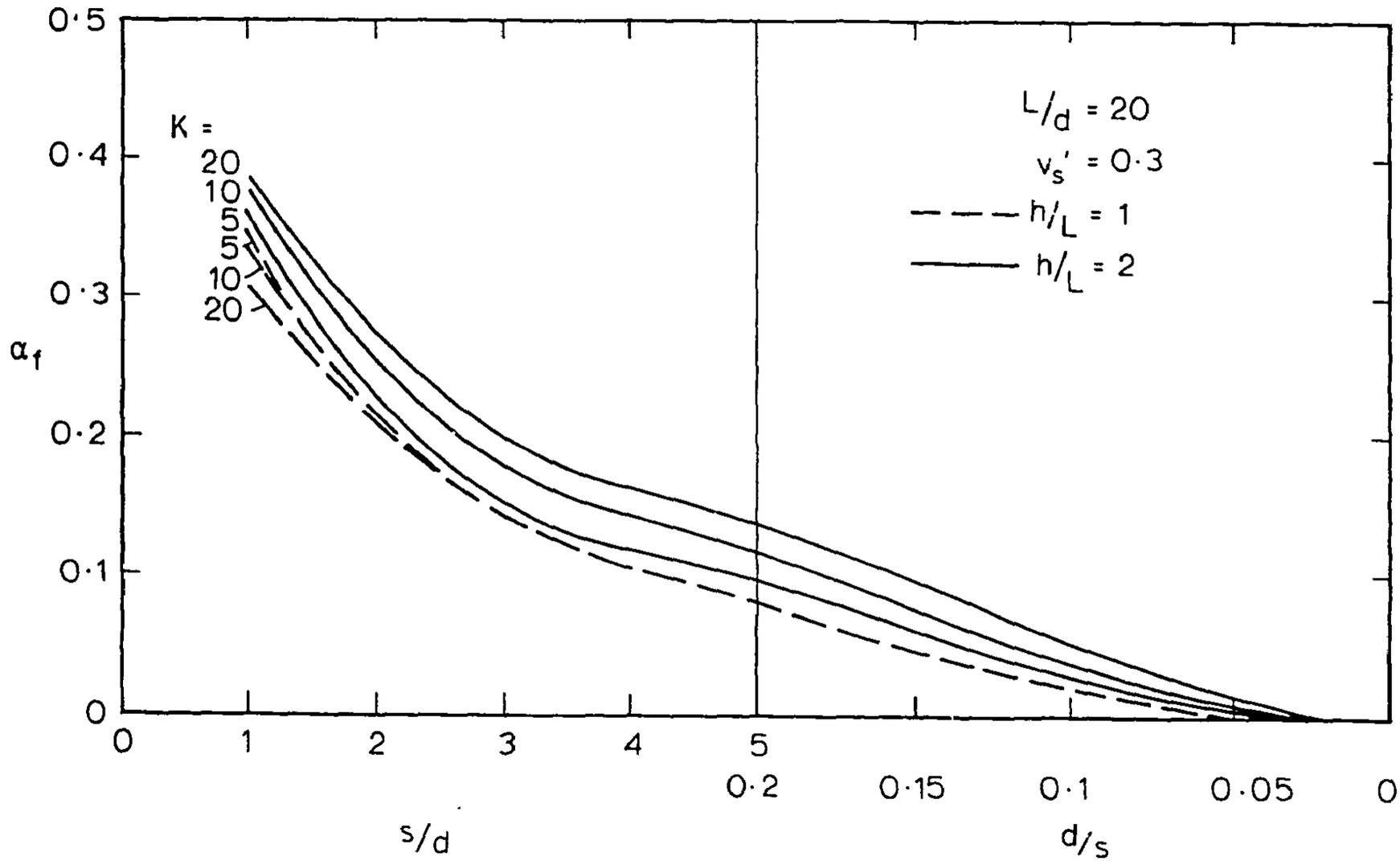

FIG. 4·17 INTERACTION FACTORS FOR SETTLEMENT ANALYSIS OF SMALL GROUPS

To analyse the elastic settlement behaviour of a pile group the principle of superposition is used. Therefore, the settlement of the ith pile S_i in a group of n identical piles is given by

$$S_i = S_I \sum_{j=1}^{n} (P_j \alpha_{ij}) \qquad (4.4)$$

where S_I = settlement of a single pile under a unit load

P_j = applied load on pile j

α_{ij} = is the interaction factor computed for a spacing (s/d) where s is the spacing between piles i and j.

In the process of computing the interaction factors shown in Figs. 4.15, 4.16 and 4.17, the settlement of a single pile is calculated. In Fig. 4.18 the influence factors I_ρ for the settlement of a single pile are plotted against the dimensionless length L/d for K = 5, 10 and 20 where the settlement of a single pile is given by

$$S = \frac{P}{E'_s d} \cdot I_\rho \qquad (4.5)$$

where P = applied load

With these results an elastic settlement of two types of groups can be calculated:

(i) a group with a rigid cap - all piles in the group have equal settlement,

(ii) a group with a flexible cap - the load on each pile is known.

For the rigid cap case, the settlements of each pile are equated giving n simultaneous equations which together with equilibrium can be solved to give n unknown loads and the settlement of the cap. If a flexible cap is being analysed the loads on each of the piles is known and thus

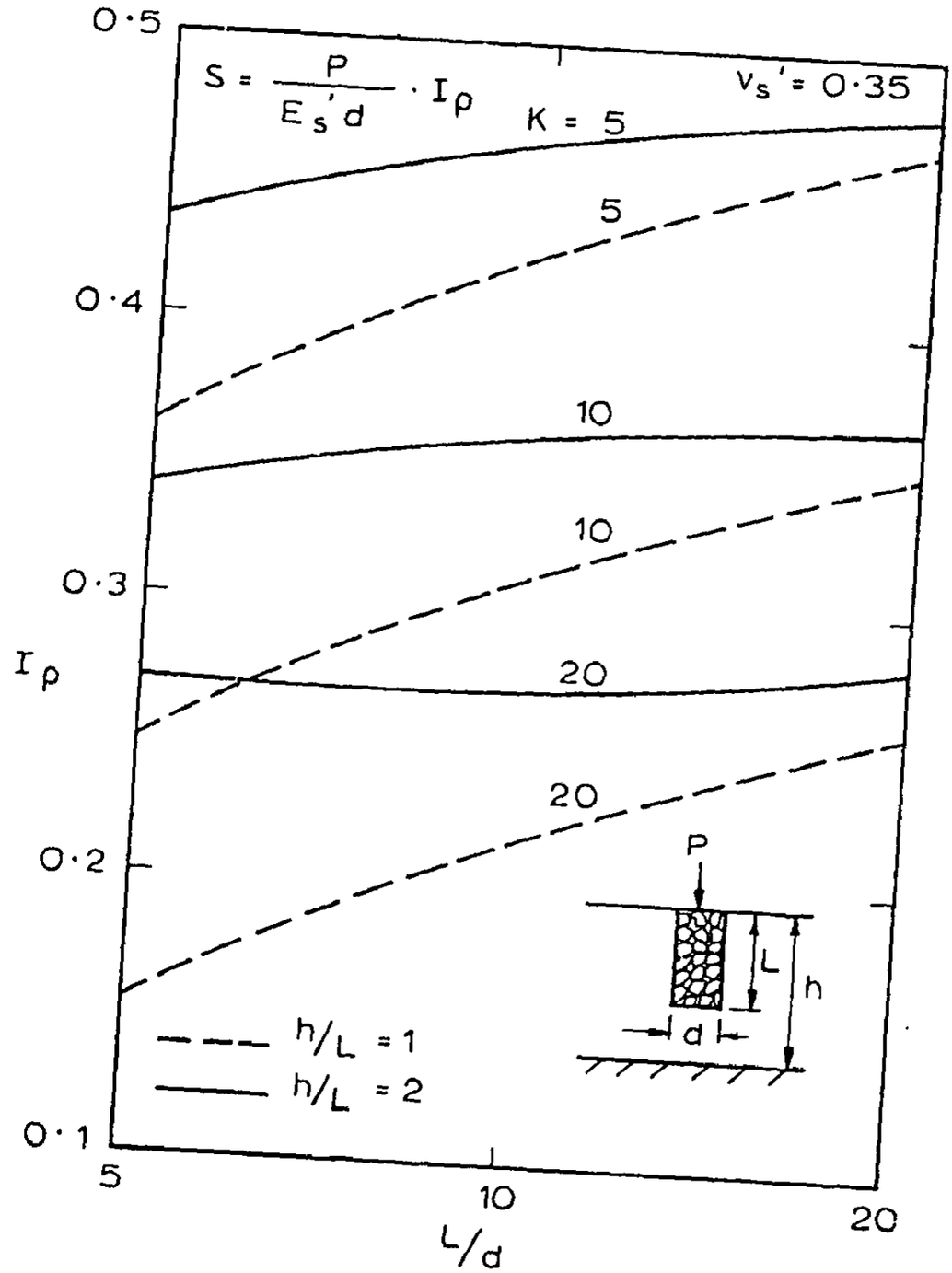

FIG. 4·18 SETTLEMENT OF SINGLE GRANULAR PILE

settlements of each pile in the group can be obtained directly n equation 4.4.

The results presented in this section enable an assessment the elastic settlement characteristics of small groups of granular s for use in preliminary design work. However, if used in con- tion with the results of a finite element analysis of a single column, the entire load-settlement response of a small group be predicted.

Finally, it is worth noting that the theoretical solutions me that the load from a group is only carried by the piles. In ctice this would generally not be the case as the soil between the s would carry a proportion of the load. A typical pile group was lysed for two cases; (i) the load being carried entirely by the les and (ii) the load being applied over the soil surface and there- ore being shared by the piles and soil in the ratio of their areas. he program AXPL4 was used for both analyses.

The computed settlement from the analysis assuming the load is taken entirely by the piles is 13% greater than for the case where the load is shared by the soil and piles. However, except for perfectly flexible footings, the load shared by the piles and soil is a function of the geometry of the pile layout and the modular and area ratios of the pile and soil materials. In many instances, the analyses assuming the piles carry all the load adequately represents the practical situation.

4.3.1 (ii) Datye and Nagaraju Load Test

Datye and Nagaraju (1975) have presented the results of load tests on four single stone columns and a group of seven columns. The elastic analysis described in the previous section was employed to backfigure the soil modulus from the single column tests and then predict the elastic settlement of the group of seven columns. Only limited data on the soil properties are given and thus it was not possible to construct the theoretical load-settlement relationship for the small group using the method described previously. Therefore, it is assumed that the reported settlement is within the elastic range for the small group.

The test arrangement is shown in Fig. 4.19. Several assumptions were necessary in order to backfigure the soil modulus. One of the single column tests was not considered because the load was applied onto a fill placed over the column making analysis difficult. The load in the other three tests was applied to a casing installed through the fill and seated onto the top of the column. Only two of these tests are considered as the load-settlement response from the remaining test was not consistent with the other results. The load carried through to the column was estimated assuming full shear was developed along the casing. On the basis of the vane tests a stiff stratum was placed at 9.5m and a modulus of 4000t/m^2 was assumed, which is approximately 500 times the cohesion. A pile modulus of 6000t/m^2 was adopted and the soil modulus was then backfigured. The theoretical curve for settlement versus E_s' is shown in Fig. 4.20 along with the backfigured moduli for the two piles considered, referred to by the authors as C9 and C13 respectively. The moduli suggest that

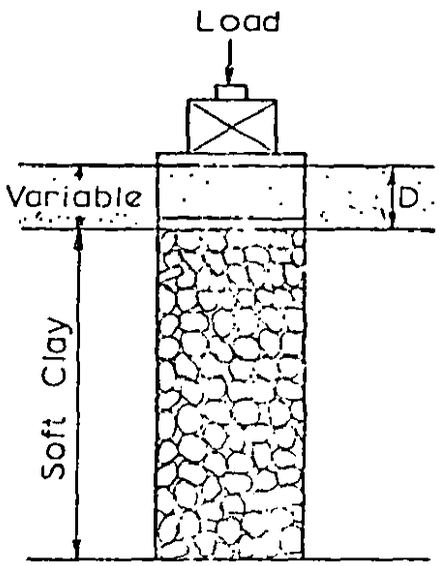

(a) Load Arrangement For Piles C9 & C13 (D = 2·1 m)

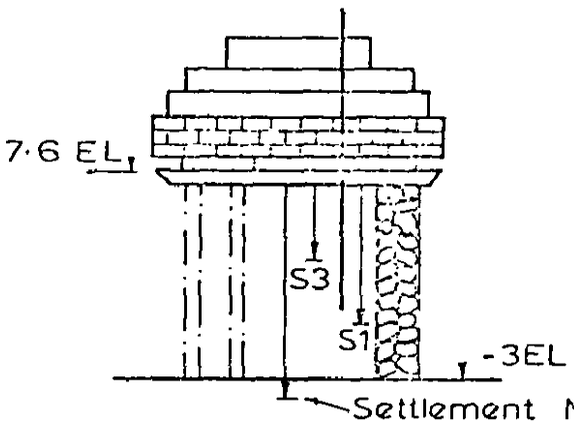

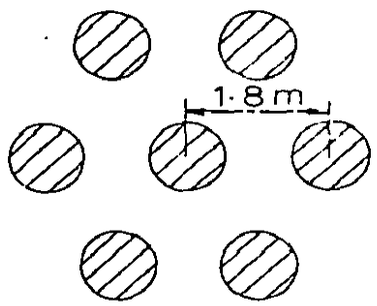

(b) Schematic Diagram of Load Arrangement (c) Plan of Column Layout

FIG. 4·19 LOADING ARRANGEMENT FOR SINGLE AND GROUP PILE TESTS (After Datye and Nagaraju, 1975)

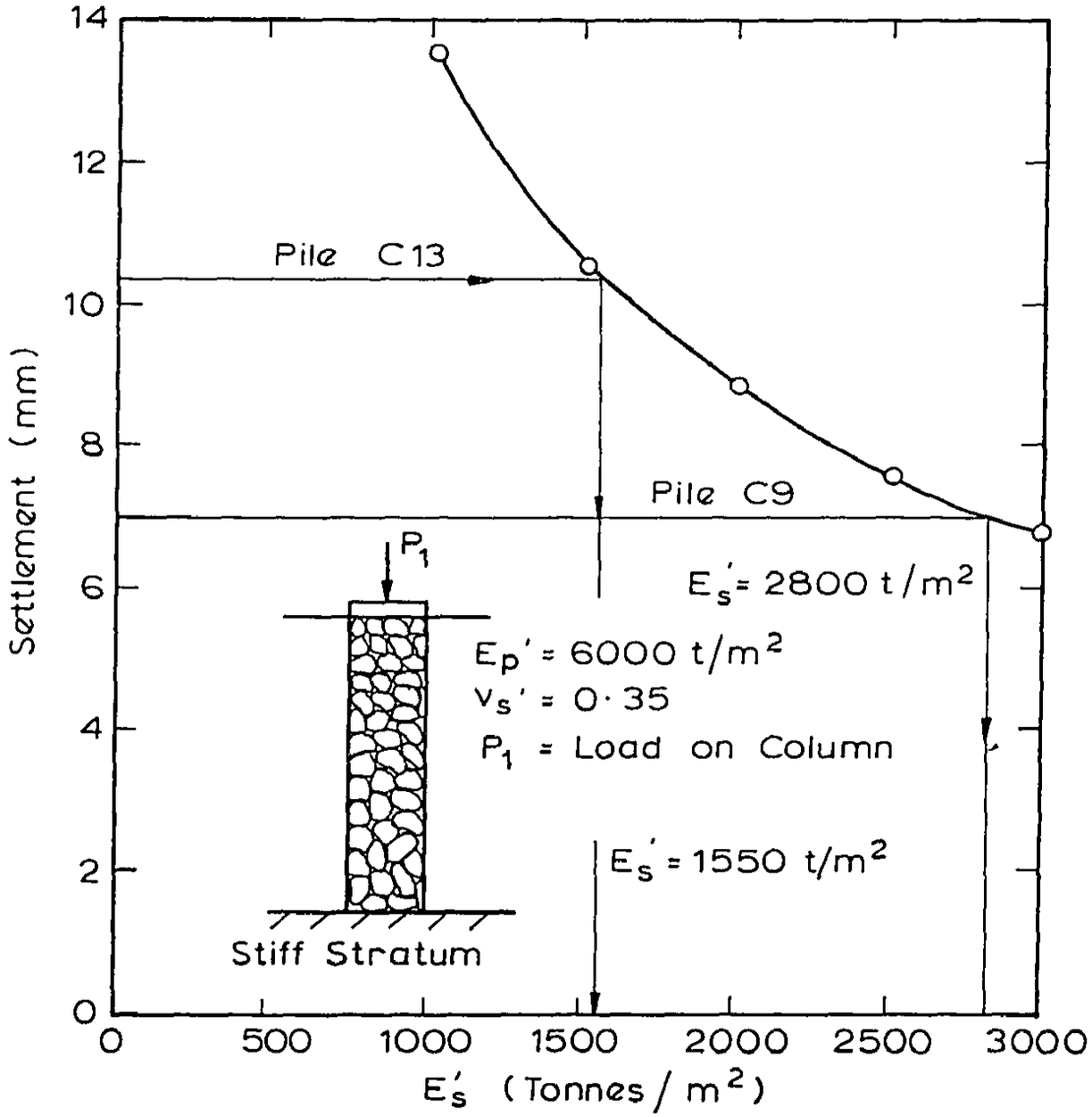

FIG. 4·20 BACKFIGURING SOIL MODULUS FOR PILES C9 AND C13 - PILE MODULUS CONSTANT

the site is non-uniform, with the modulus backfigured from pile C9 being consistent with a very stiff clay.

These two moduli were used to predict the settlement of the group of seven columns. The authors report a measured settlement of 86mm at 350 tonnes. A layer of fill material was placed over the group prior to loading and thus a flexible cap analysis is considered relevant. The results of the predictions are tabulated below:

TABLE 4.1

Backfigured Value of E_s'	Computed Group Settlements	
	Centre	Edge
1550 t/m^2 (From Pile C13)	55mm	61mm
2800 t/m^2 (From Pile C9)	37mm	41mm
Measured Settlement = 86mm		

The predicted settlements are too small, although the modulus backfigured from pile C13 gives reasonable agreement with the measured settlement. Close agreement is obtained when a value of $E_s' = 900\ t/m^2$ is adopted which corresponds to a E_s'/c_u ratio of approximately 450. However, more reported load tests are required before a reliable assessment can be made of the applicability of the analysis.

4.4 ESTIMATION OF THE MATERIAL PROPERTIES FOR USE IN THE ANALYSES

The finite element analyses of stone column behaviour require the following strength and deformation parameters of the pile and soil:

(i) E_u, undrained Young's modulus of the soil

(ii) c_u, undrained cohesion of the soil

(iii) E_s', Young's modulus of the soil skeleton

(iv) c', ϕ', drained cohesion and friction angle of the pile and soil materials

(v) K_o coefficient of lateral earth pressure at rest in both the pile and soil

(vi) ν_s', Poisson's ratio of soil skeleton

(vii) E_p', Young's modulus of pile material

(viii) ν_p', Poisson's ratio of the pile material.

In this section methods for estimating these properties are discussed.

The undrained Young's modulus E_u of the soil may be determined by the following procedures:

(a) plate loading tests- E_u backfigured from the immediate settlement of the plate, using elastic theory

(b) triaxial testing using the stress path method (Davis and Poulos, 1963; Lambe, 1964)
correlations with c_u (Ladd et al., 1977); these indicate a range in the ratio E_u/c_u of approximately 100-800 when the clay is normally consolidated. This ratio reduces with increasing stress level and OCR (overconsolidation ratio).

It should be noted that E_u is very sensitive to stress level and the initial stress state (Poulos and Ahlston, 1974) and thus an accurate assessment of this property is very difficult.

The undrained cohesion of the soil c_u can be readily determined by the conventional laboratory methods, preferably from consolidated undrained triaxial or simple shear tests. The undrained cohesion can also be determined by field testing methods, ie. plate loading tests, vane shear tests and Ménard or self-boring pressuremeter testing.

The Young's modulus of the soil skeleton E_s' can also be determined by the methods (a) and (b) above. In addition, if a Poisson's ratio ν_s' is assumed, the following relationship for an ideal elastic soil can often be used with fair accuracy:

$$E_s' = \frac{(1+\nu_s')(1-2\nu_s')}{m_v(1-\nu_s')} \qquad (4.6)$$

where m_v = coefficient of volume decrease (measured in an oedometer test).

In the absence of any data, the following typical values (Poulos, 1975) are suggested:

Soft clays	1.4	-	4.2	MN/m^2
Medium clays	4.2	-	8.4	MN/m^2
Stiff clays	8.4	-	20 +	MN/m^2

The drained cohesion and friction angle of the soil skeleton can be determined from triaxial tests.

The coefficient of lateral earth pressure at rest K_o for normally consolidated soils can be estimated from correlations with the plasticity index or friction angle (Ladd et al., 1977). These correlations are reproduced in Fig. 4.21. For overconsolidated soils the following relationship can be used

$$K_o(OC)/K_o(NC) = OCR^m \qquad (4.7)$$

where $K_o(OC)$ = K_o if the soil is overconsolidated

$K_o(NC)$ = K_o if the soil is normally consolidated

m = index.

A plot of the index m as a function of the plasticity index is reproduced from Ladd et al., (1977) in Figure 4.22. The above values of K_o apply to the soil. For the pile, which is rammed into place by the vibroflot, a value of K_o equal to one may give an adequate representation of the complex stress state in the pile.

The Poisson's ratios ν_s' and ν_p' can be determined from triaxial testing using the stress path method. However, in the absence of data an adopted value for the pile of 0.3 can be used. Typical values for the soil (Poulos, 1975) are:

Soft N/C clays	0.35 - 0.45
Medium clays	0.30 - 0.35
Stiff O/C clays	0.10 - 0.30

For undrained analyses the Poisson's ratio of the soil, ν_u, is 0.5.

Finally, the Young's modulus E_p' and strength parameters c'

Remoulded	Undisturbed	Referance
○		Brooker & Ireland (1965)
□	■	R Ladd (1965)
△	●	Bishop (1958)
	◆	Simons (1958)
	▲	Campanella & Vaid (1972)
▽		Compiled by Wroth (1972)
	▼	Geot. Eng. Inc. (1976)
◇		Abdelhamid & Krizek (1976)

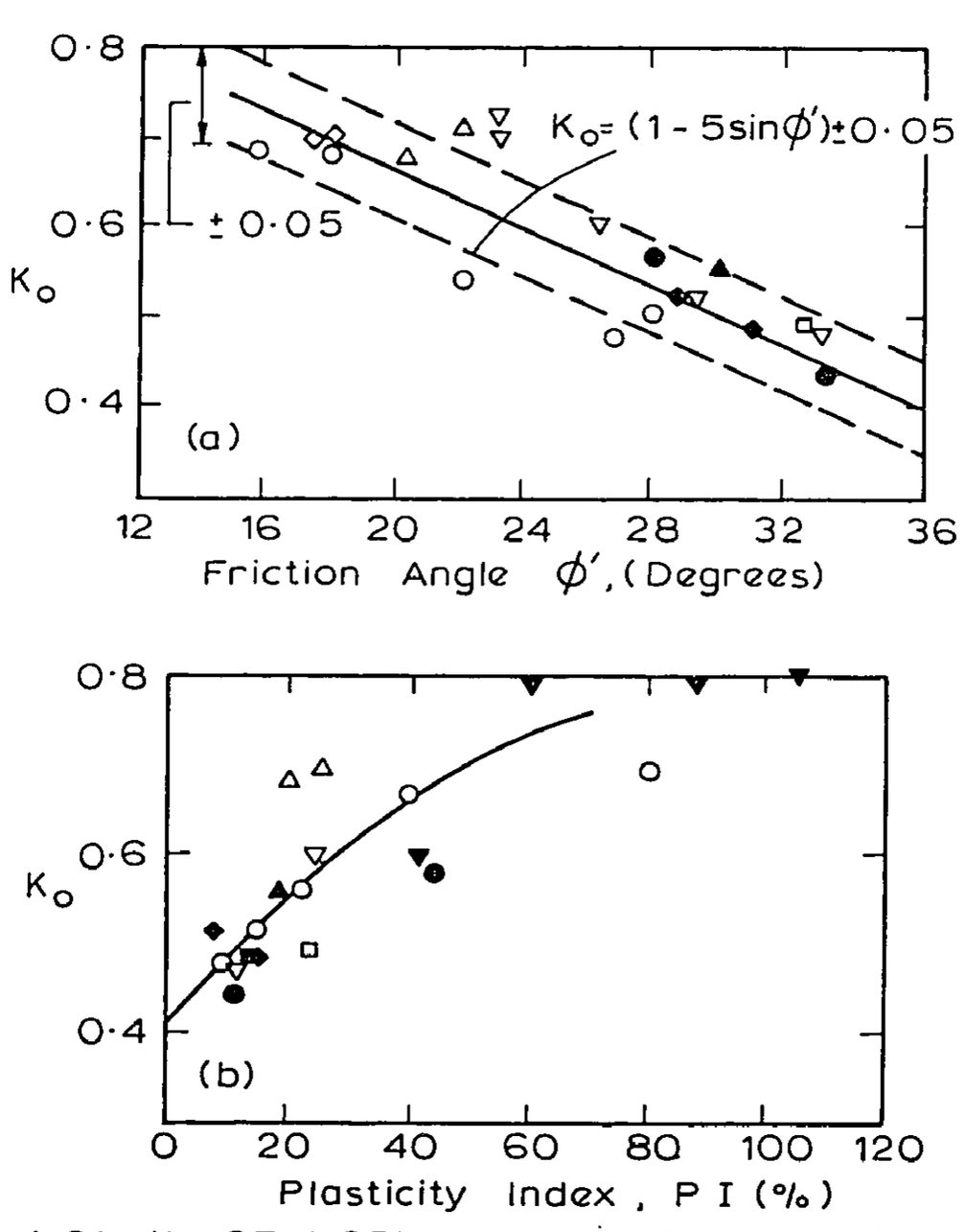

FIG. 4·21 K_o OF NORMALLY CONSOLIDATED CLAYS VS FRICTION ANGLE (a) AND PLASTICITY INDEX (b)(AFTER; LADD ET AL, 1977)

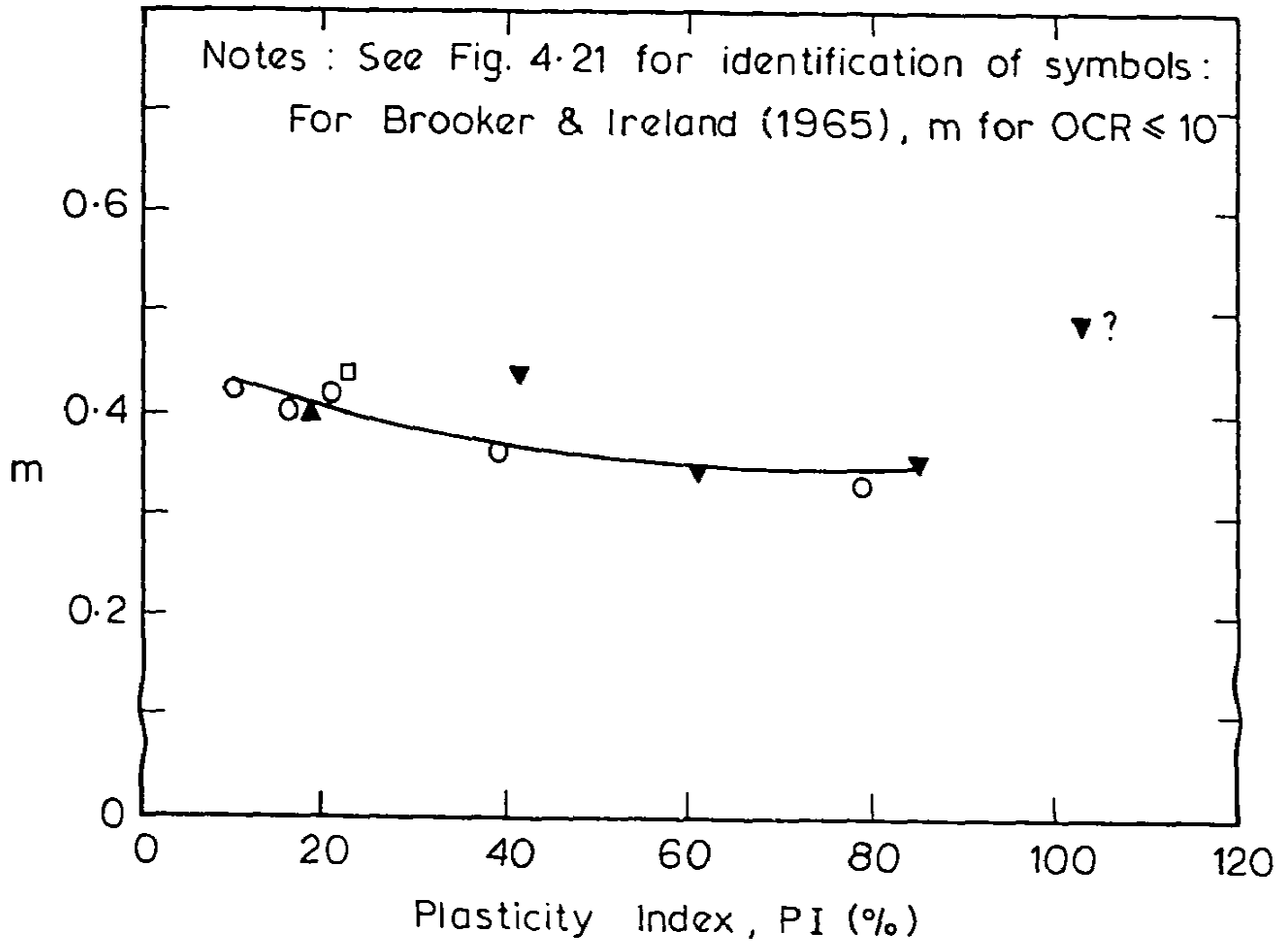

FIG. 4·22 COEFFICIENT m RELATING Ko AND OCR VS PLASTICITY INDEX (After Ladd et al, 1977)

and ϕ' for the pile could be determined from large diameter triaxial tests but this would normally not be feasible. Published data on the deformation properties of the stone comprising the columns is scant. However, the available published data suggests that in the absence of any test results, the drained cohesion can be assumed to be zero and the angle of friction ϕ' taken to be 35-40°. Engelhardt and Kirsch (1977) suggest a modulus of 600 kp/cm^2 (58000 kN/m^2) as being a representative value. If it were considered necessary, the modulus could be backfigured from a plate loading test. The limited data available suggests that an appropriate value lies between 40000 - 70000 kN/m^2.

4.5 SUMMARY AND CONCLUSIONS

In this chapter the finite element analysis described in Chapter 3 has been used to obtain theoretical solutions for idealised cases. These solutions illustrate the improved load carrying capacity of a circular footing due to the installation of a single stone column.

The theoretical results indicate that the three most important factors affecting the ultimate bearing capacity of a stone column are;

(i) The friction angle of the pile material

(ii) The depth to which the pile is installed

(iii) The cohesion of the insitu soil.

The finite element analysis has then been used to reproduce the load-settlement response of a single stone column reported in a pre-

viously published full scale load test. The agreement between the measured response and the finite element solution is very good when an adhesive strength is specified for the stone column-clay interface. The adhesion is taken equal to the cohesion of the insitu clay. The growth of the plastic zones within the pile and soil verify the mechanism of failure adopted by Hughes and Withers (1974) ie. bulging of the pile which results in a passive failure of the soil.

Elastic solutions are presented which enable the load-settlement response of small groups of stone columns to be estimated when used in conjunction with a finite element analysis of a single stone column. The elastic solutions are compared with the settlements measured in a full scale load test on a group of seven columns. The predicted settlements are too small, which may be due to the extent of local yield within the pile and soil at the test load. However, many assumptions were necessary due to the lack of reported data and thus more comparisons of this type are required before reliable conclusions can be drawn.

CHAPTER FIVE

STABILISATION OF EXTENSIVE AREAS

5.1 INTRODUCTION

In Chapters 5, 6 and 7 attention is focussed on the use of large numbers of granular piles installed in a regular array to stabilise soft clays over an extensive area. In this case the behaviour of the stabilised soil may be analysed by considering a typical pile-soil 'unit'. The presence of the stiffer pile results in a reduction in settlement of the clay. In this chapter the effects of geometric factors such as pile length, diameter, spacing and soil layer depth on the settlement characteristics of the reinforced soil are examined using an elastic finite element analysis. The solutions presented are applicable to a uniform vertical pressure such as might be imposed by a flexible raft foundation, an oil or water storage tank or an embankment. In Chapter 6 solutions to diffusion theory are presented for the rate of settlement of a flexible foundation. Attention is then focussed in Chapter 7 on the magnitude and rate of settlement of rigid foundations supported by the stabilised clay.

The finite element analysis used in this Chapter is capable of taking account of elasto-plastic behaviour of the soil and of elasto-plastic and dilatant behaviour of the pile material. This is utilised to illustrate the comparatively small effect of local yield within the pile and soil materials on the settlement behaviour for what is considered a representative range of working pressures.

Under widespread loads the limiting factor in design will be the settlement of the reinforced ground, as a mechanism for a general shear failure is only possible near the edges of the loaded area. The

results of conventional slip circle analyses of an embankment supported by reinforced soil are presented in the final portion of this chapter. This method of analysis has been used successfully by Rathgeb and Kutzner (1975) to find the most economical number and arrangement of stone columns beneath an embankment for a motorway according to a given factor of safety in the stability analysis. The results suggest that near the edges of the load precautionary measures such as reducing the spacing of the piles and extending them to full depth of the soft layer is desirable.

5.2 SETTLEMENT ANALYSIS OF REINFORCED CLAY

A regular pattern of vertical granular piles may be analysed by considering a typical pile-soil 'unit'. For a triangular arrangement each pile has a hexagonal domain of influence [Fig. 5.1(a)] whereas for a square arrangement each pile has a square domain of influence. These domains are replaced by a cylindrical unit of diameter d_e for ease of analysis. For a triangular spacing an equal area of influence is given by a circular domain of diameter $d_e = 1.05s$ where s is the pile spacing. For a square arrangement of piles, $d_e = 1.13s$. A finite element model such as that shown in Fig. 5.1(b) is used for the analysis of settlement magnitude.

5.2.1 Finite Element Analysis

The elastic finite element solutions presented illustrating the reduction in settlement, under drained conditions, of soft clays reinforced with granular piles are applicable to a uniform vertical pressure applied over a large area such as might be imposed by a flexible

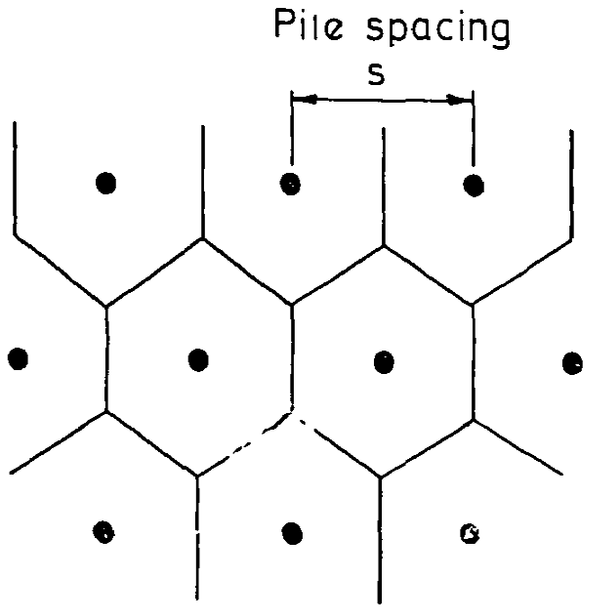

(a) Plan of regular triangular pattern of granular piles

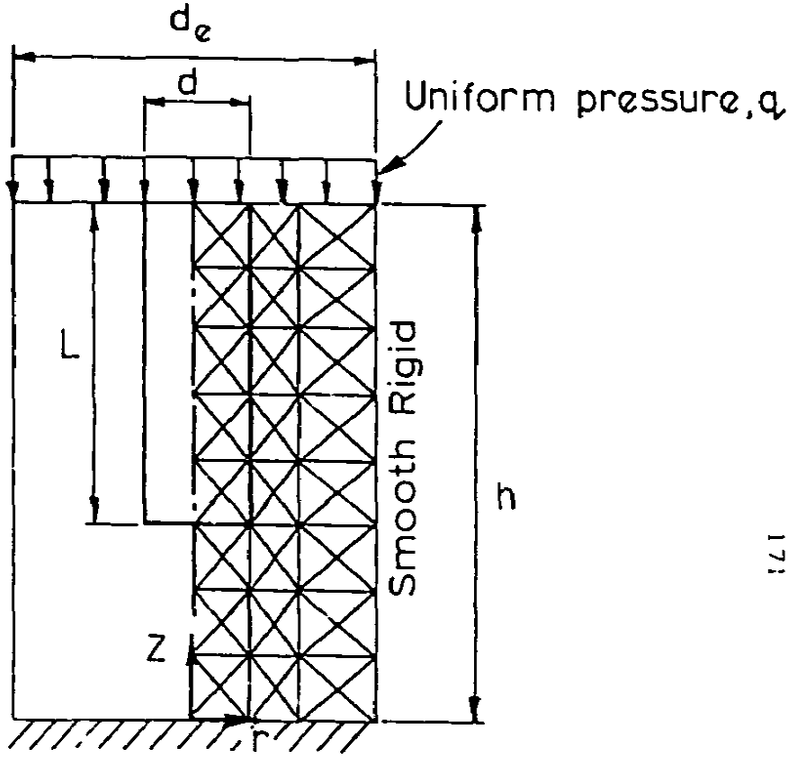

(b) Finite element model of a pile-soil unit

FIG.5·1 FINITE ELEMENT MODEL USED FOR SETTLEMENT ANALYSIS OF LARGE GROUPS OF GRANULAR PILES

raft foundation, an oil or water storage tank or an embankment. Since strains are primarily vertical, undrained settlements are likely to be small and are therefore not considered.

The elastic finite element calculations were based on the following assumptions:

(i) the drained Poisson's ratios of the pile material and soil (ν_p', ν_s') are 0.3

(ii) at any point the undrained and drained Young's moduli of the soil (E_s, E_s') are related by the equation

$$\frac{E_s}{1.5} = \frac{E_s'}{(1+\nu_s')} \qquad (5.1)$$

(iii) at any depth the ratio of the drained Young's modulus of the pile material to E_s is constant and equal to 20 unless otherwise specified

(iv) any variation of modulus with depth is linear.

As the loading pressure q is increased, local yield in the form of contained plastic flow will develop within the pile and/or soil. The extent to which this causes an increase in settlement compared with settlement from an elastic analysis under drained conditions is shown in Fig. 5.2 for h/d = 5, d_e/d = 2, L/h = 0.5, and the material properties shown in Table 5. The settlements δ are presented in the dimensionless form $\delta G_o/hq$ (where G_o is the shear modulus of the soil at the surface) and the elasto-plastic profile is for $q = 0.5\gamma h$ (γ = unit weight of soil) which is considered representative of the upper limit of working load. The inset to Fig. 5.2 shows the

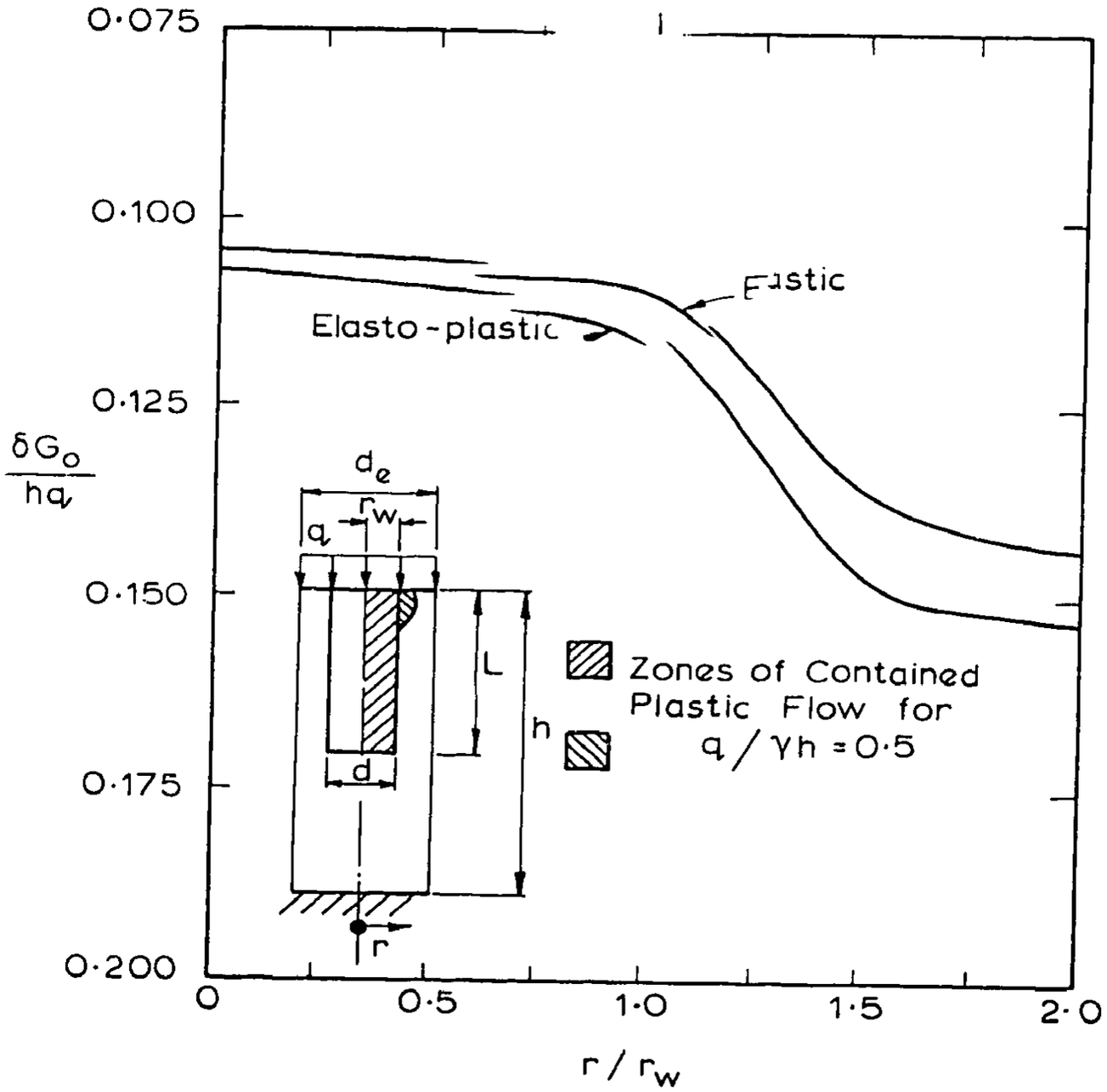

FIG. 5.2 EFFECT OF LOCAL YIELD ON DRAINED SURFACE PROFILE

corresponding areas of yield in the pile and soil.

TABLE 5.1

MATERIAL PROPERTIES USED FOR FIGURE 5.2

Property	Pile Material	Soil
Coefficient of horizontal effective stress at rest, K'_o	1.0	1.0
Drained cohesion c'	0	0
Drained angle of internal friction, ϕ'	40°	30°
Angle of dilatancy, ψ	20°	15°
Ratio of surface Young's modulus $E_s(0)$ to modulus at depth h, $E_s(h)$	0.5	0.5

The maximum settlement and the maximum discrepancy between the elastic and the elasto-plastic settlements occurs at the boundary of the pile-soil unit. The increased settlement due to local yield is shown in Fig. 5.3. The ratio of the elastic settlement to the settlement with local yield taken into account is plotted against $q/\gamma h$ for the centre and edge of the pile-soil unit. As the pressure increases the discrepancy also increases with a maximum of some 5% at the edge of the pile-soil unit for $q/\gamma h = .5$. The growth of the plastic zones within the pile and soil as the pressure is increased is shown diagrammatically in Fig. 5.4.

These results suggested that the relative effects of various changes in a pile-soil unit could be determined to satisfactory accuracy by means of a parametric study of elastic settlements. A para-

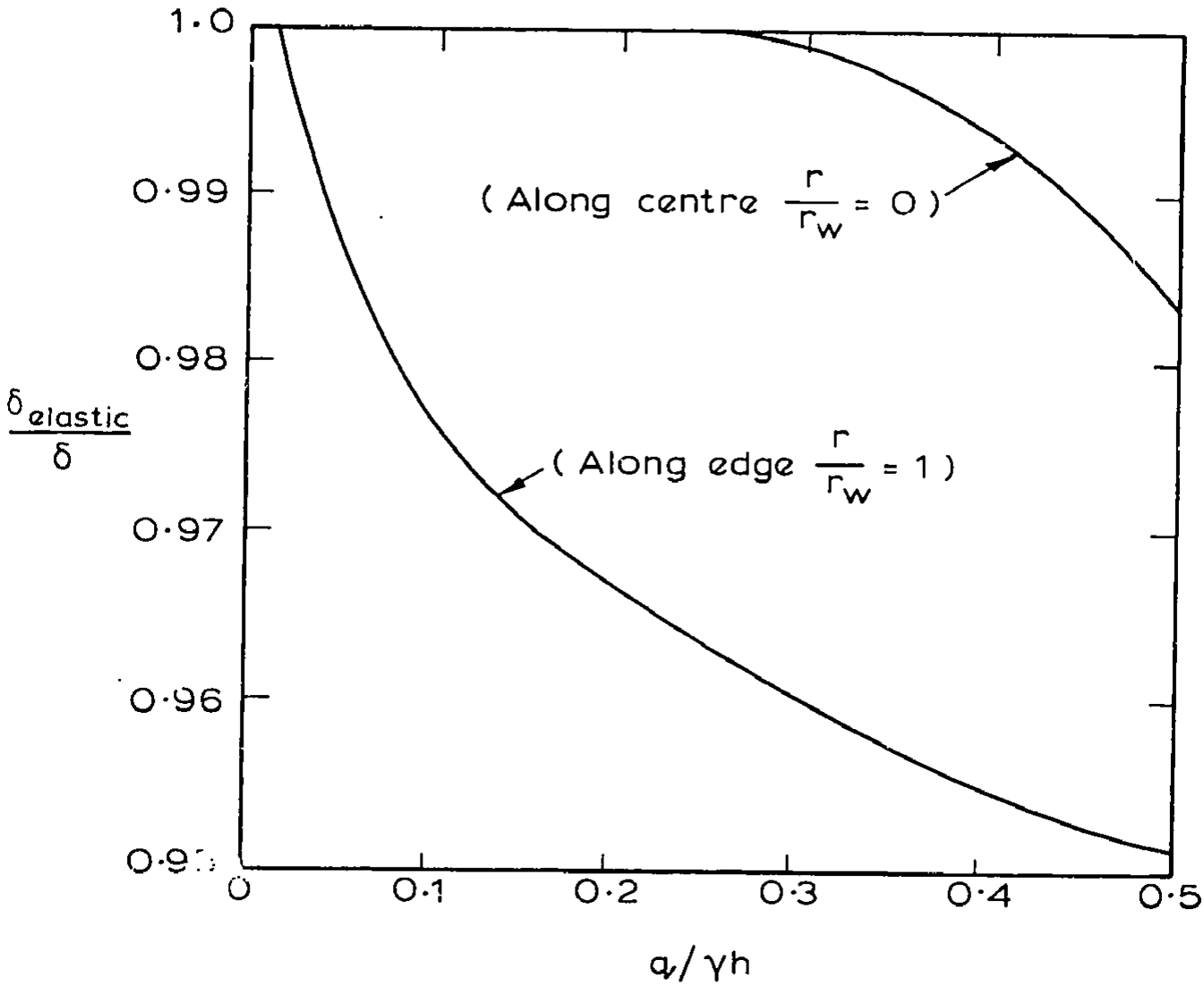

FIG. 5.3 EFFECT OF LOCAL YIELD ON SETTLEMENT AT EDGE AND CENTRE OF PILE-SOIL UNIT

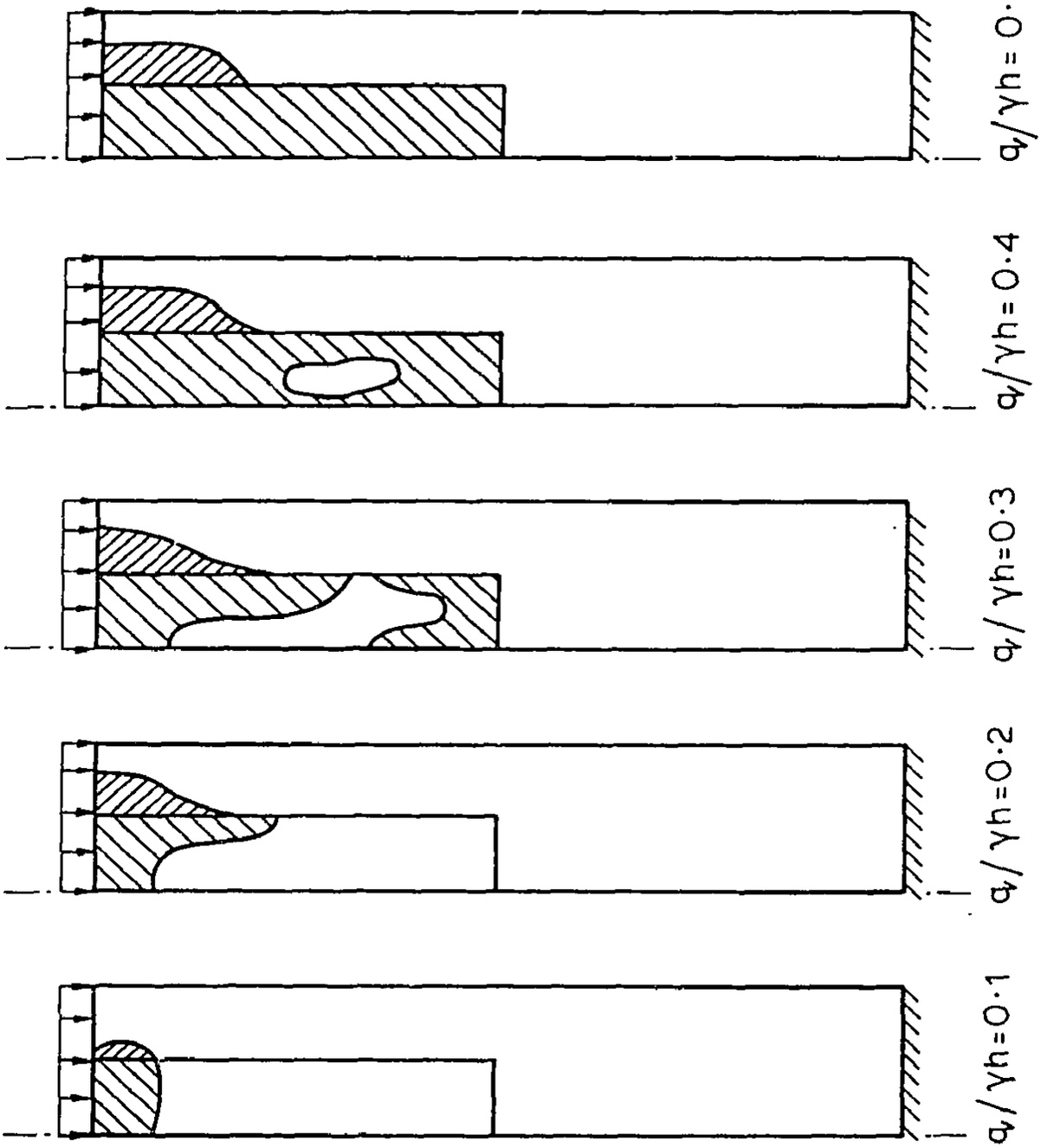

FIG. 5.4 GROWTH OF PLASTIC ZONES IN GRANULAR PILE AND SOIL

metric study investigating the effects of strength and deformation characteristics of both the pile and soil would be very incomplete or extremely cumbersome. However, where insitu stress conditions or the magnitude of the applied pressure suggests that local yield will be widespread, a full elasto-plastic analysis should be performed for predicting the settlement.

Figs. 5.5 to 5.11 summarise the results of a parametric study of elastic drained settlements at the boundary of a pile-soil unit, in which the settlement is presented in dimensionless form as the ratio of settlement of the pile-soil unit, to the settlement which would occur if there were no pile.

The ratio of pile volume to the volume of a pile-soil unit, ie. the fraction of the original soil volume occupied by granular pile material, is given by

$$\frac{\text{Pile Volume}}{\text{Original Soil Volume}} = \left(\frac{d}{d_e}\right)^2 \cdot \left(\frac{L}{h}\right) \qquad (5.2)$$

Consequently for a given degree of pile penetration (L/h), the curves for constant d_e/d which have been plotted in Figs. 5.5, 5.6 and 5.7 represent curves for constant pile/soil volume ratio. Because the value of this ratio is the major factor in determining the relative costs of various pile arrangements, for purposes of preliminary design, these curves may be regarded as constant cost curves in determining the optimum proportions of the pile system.

Fig. 5.5 shows the effect on soil settlement of variation of the ratio of pile and soil moduli (E_p'/E_s), when both moduli are

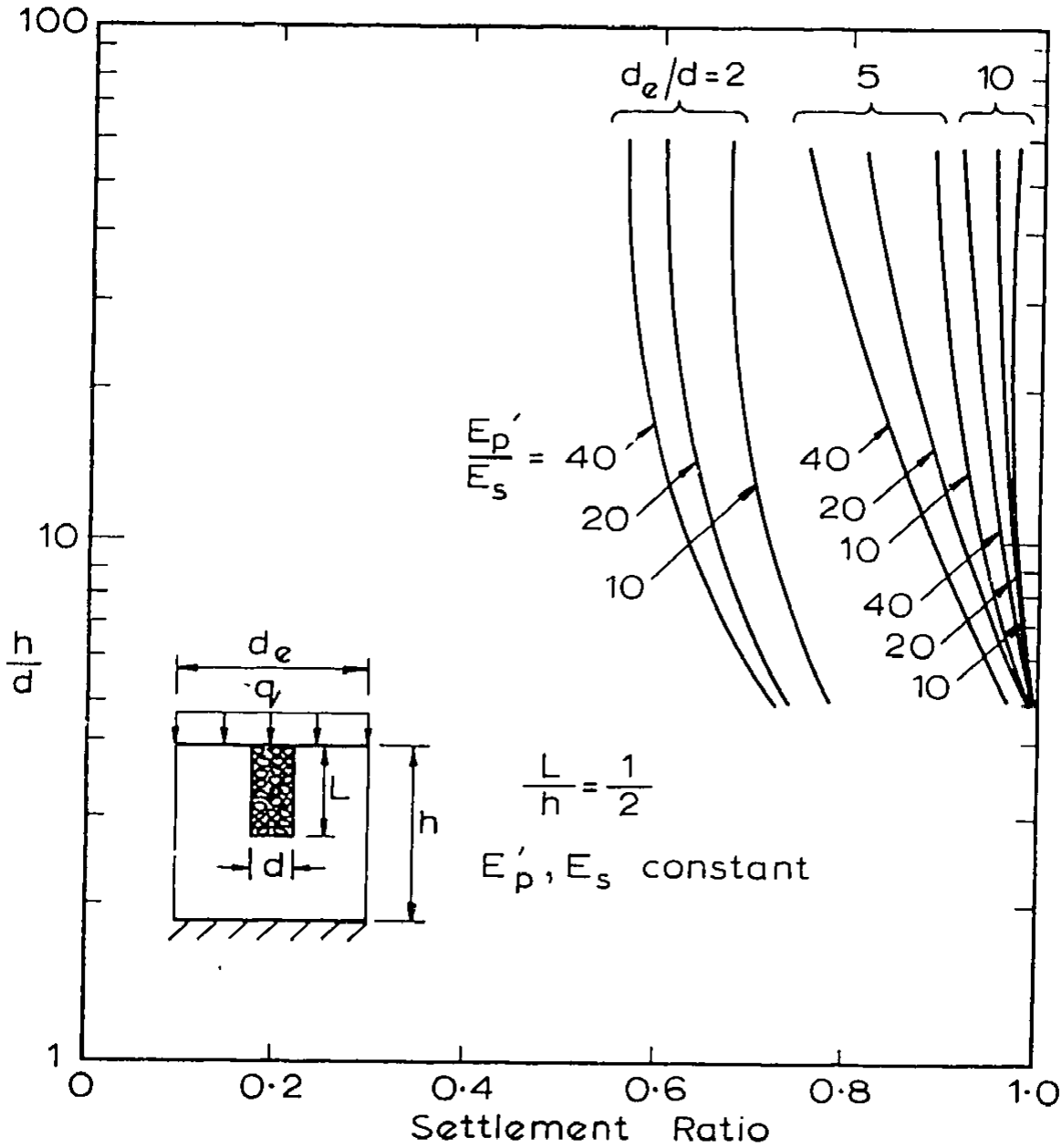

FIG. 5·5 SETTLEMENT VARIATION WITH CHANGES IN E_p'/E_s RATIO

constant with depth and L/h = 0.5. While the value of the ratio of moduli has some effect on the results, it can be seen that it is not of major significance. The subsequent results presented in Figs. 5.6 and 5.7 are for $E_p'/E_s = 20$, which is considered to be representative of the ratios likely to be encountered in practice (Baumann and Bauer, 1974).

Fig. 5.6 shows the effect on soil settlement of increasing the degree of pile penetration (L/h) from 0.5 to 1.0, when both the pile and soil moduli are constant with depth. It is of interest to note that Settlement Ratios are approximately equal for $d_e/d = 2$, $L/h = 0.5$ and $d_e/d = 5$, $L/h = 1.0$, although the fully penetrating piles occupy 4 percent of the total volume compared with 12.5 percent of the total volume when the piles are only installed to half the layer depth.

Fig. 5.7 shows the effect on soil settlement of increasing the degree of pile penetration from 0.5 to 1.0 when both pile and soil moduli increase linearly with depth. This increase in modulus over the value at the surface is 50% at half the layer depth and 100% at the layer base.

A more complete set of Settlement Ratios for fully penetrating piles are presented in Figs. 5.8 to 5.11 for h/d = 5, 10, 15 and 20 for a range of d_e/d between 1.0 and 3.0 which is considered representative of the values found in practice. The pile and soil moduli are assumed constant.

Analyses of cases where the pile penetration is a quarter

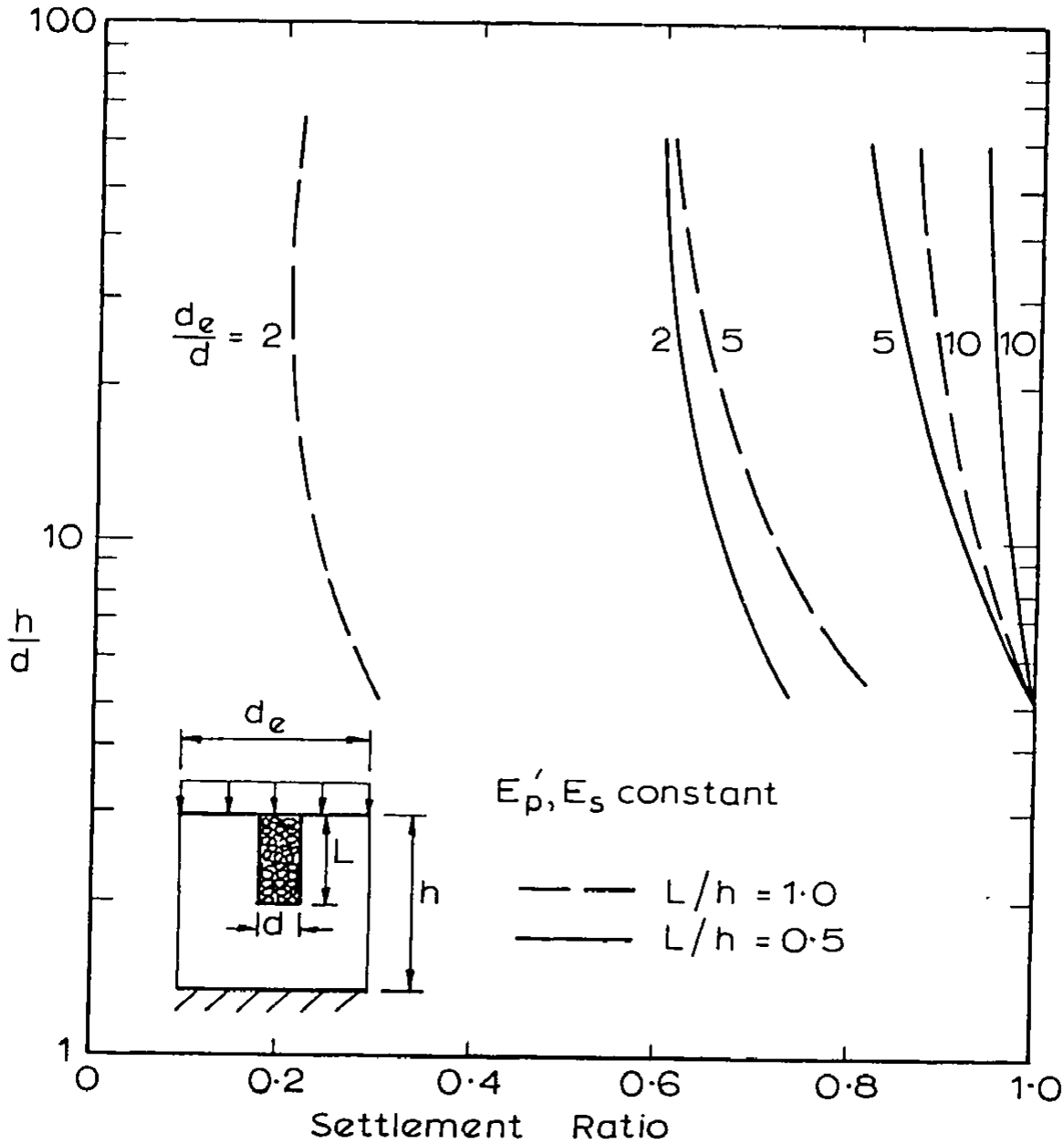

FIG. 5·6 SETTLEMENT VARIATION WITH CHANGES IN DEGREE OF PENETRATION OF PILES

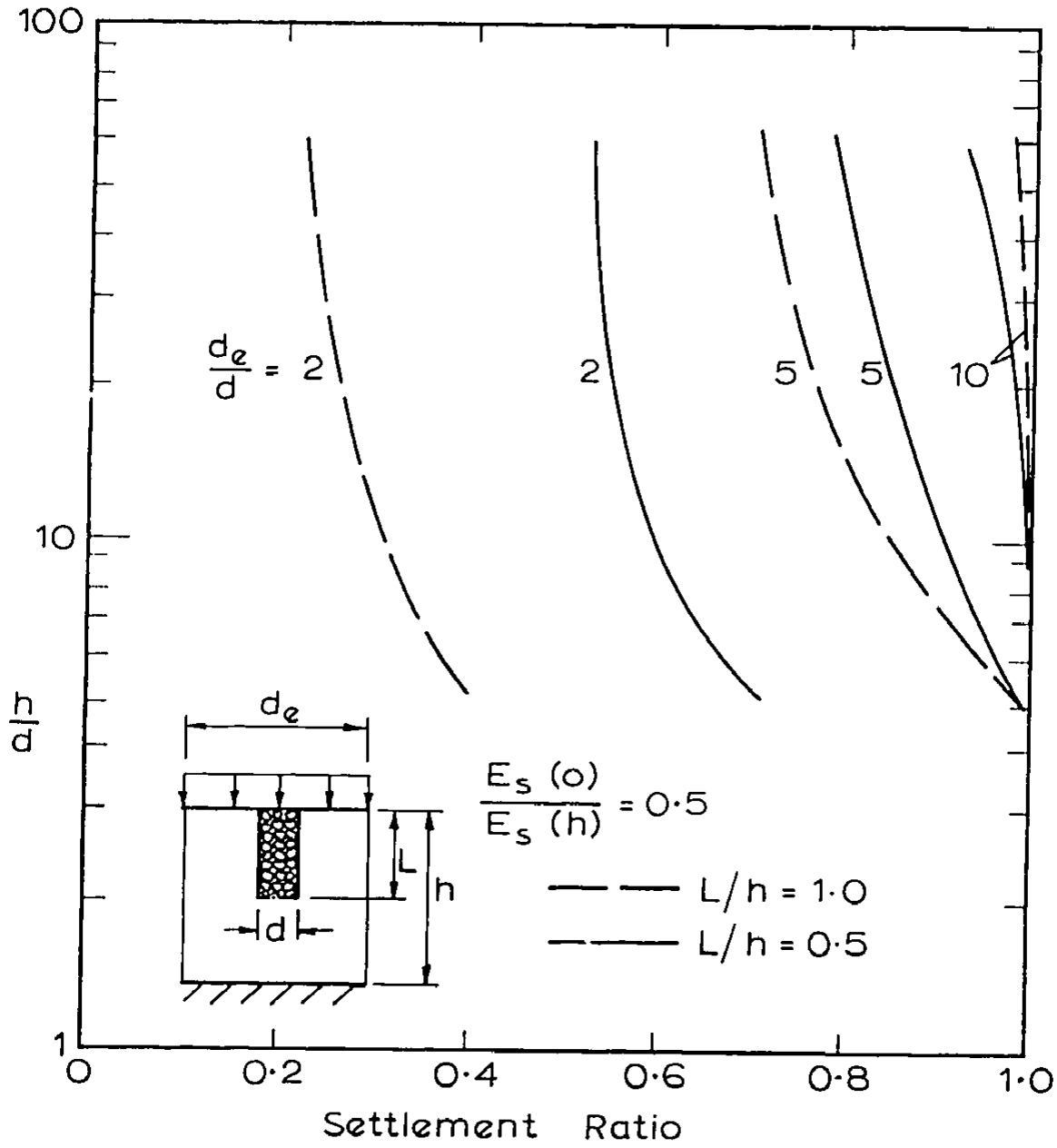

FIG. 5·7 SETTLEMENT VARIATION FOR LINEARLY VARYING MODULUS IN PILE AND SOIL

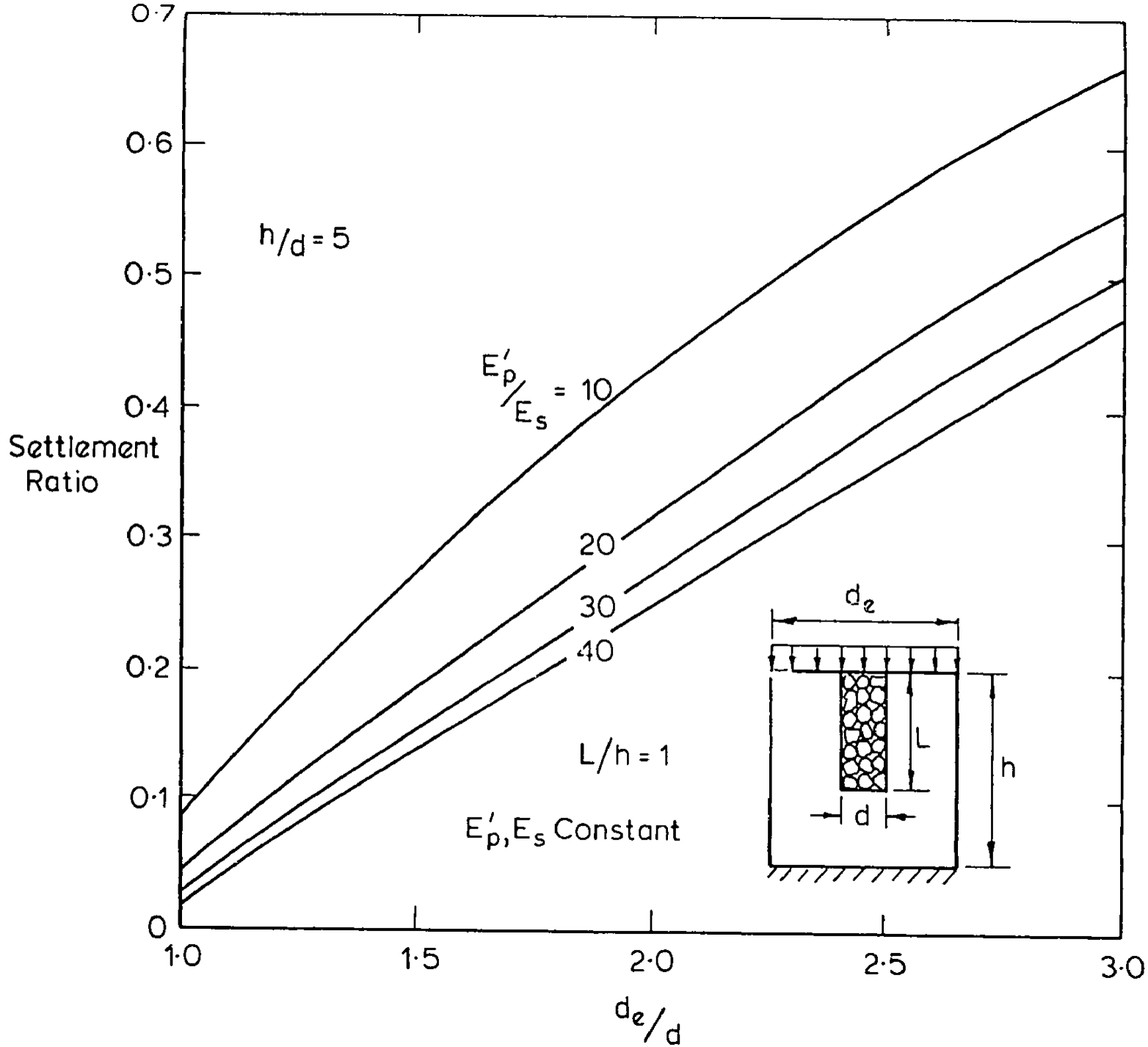

FIG. 5·8 SETTLEMENT REDUCTION FACTORS FOR FULLY PENETRATING PILES

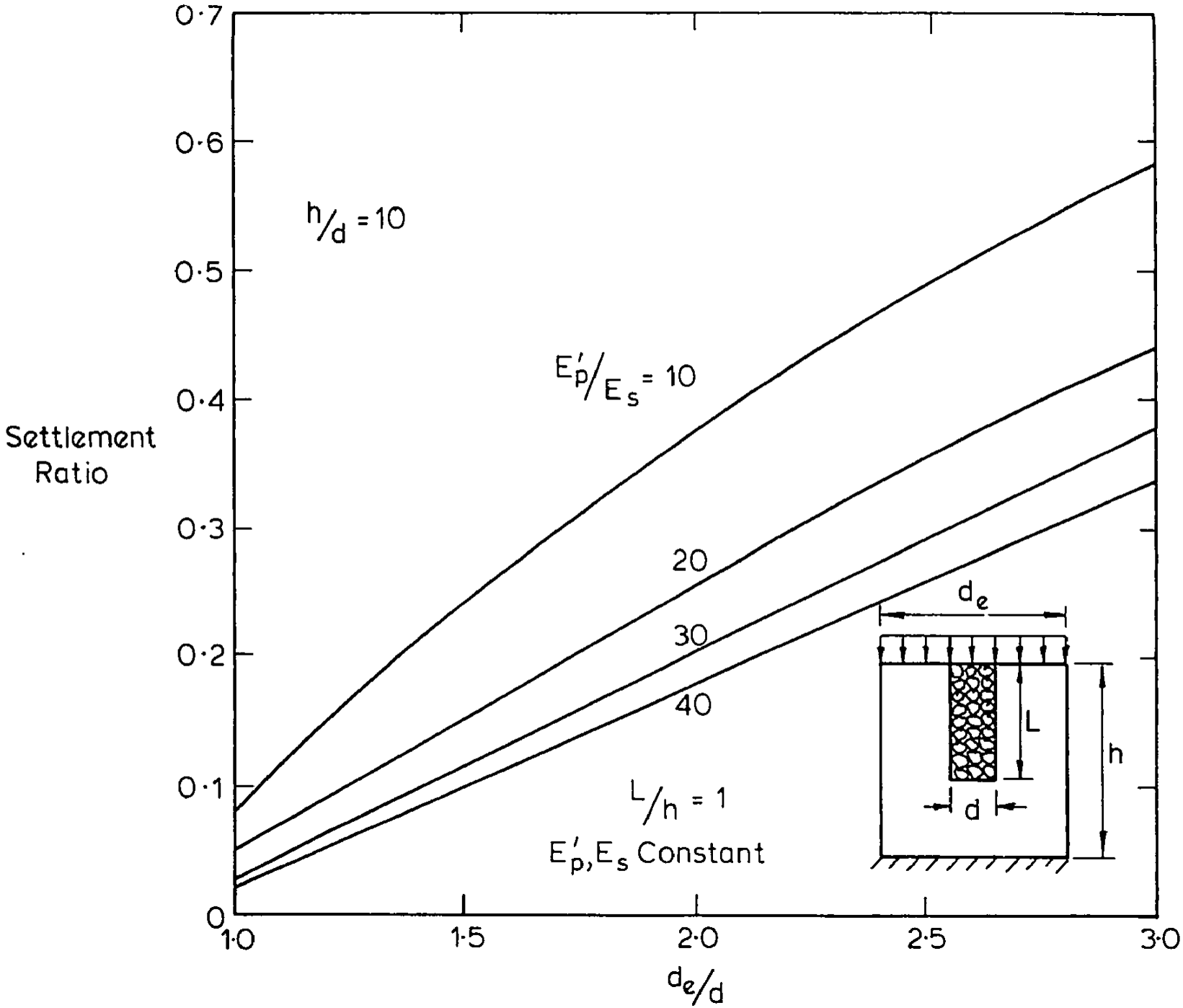

FIG. 5·9 SETTLEMENT REDUCTION FACTORS FOR FULLY PENETRATING PILES

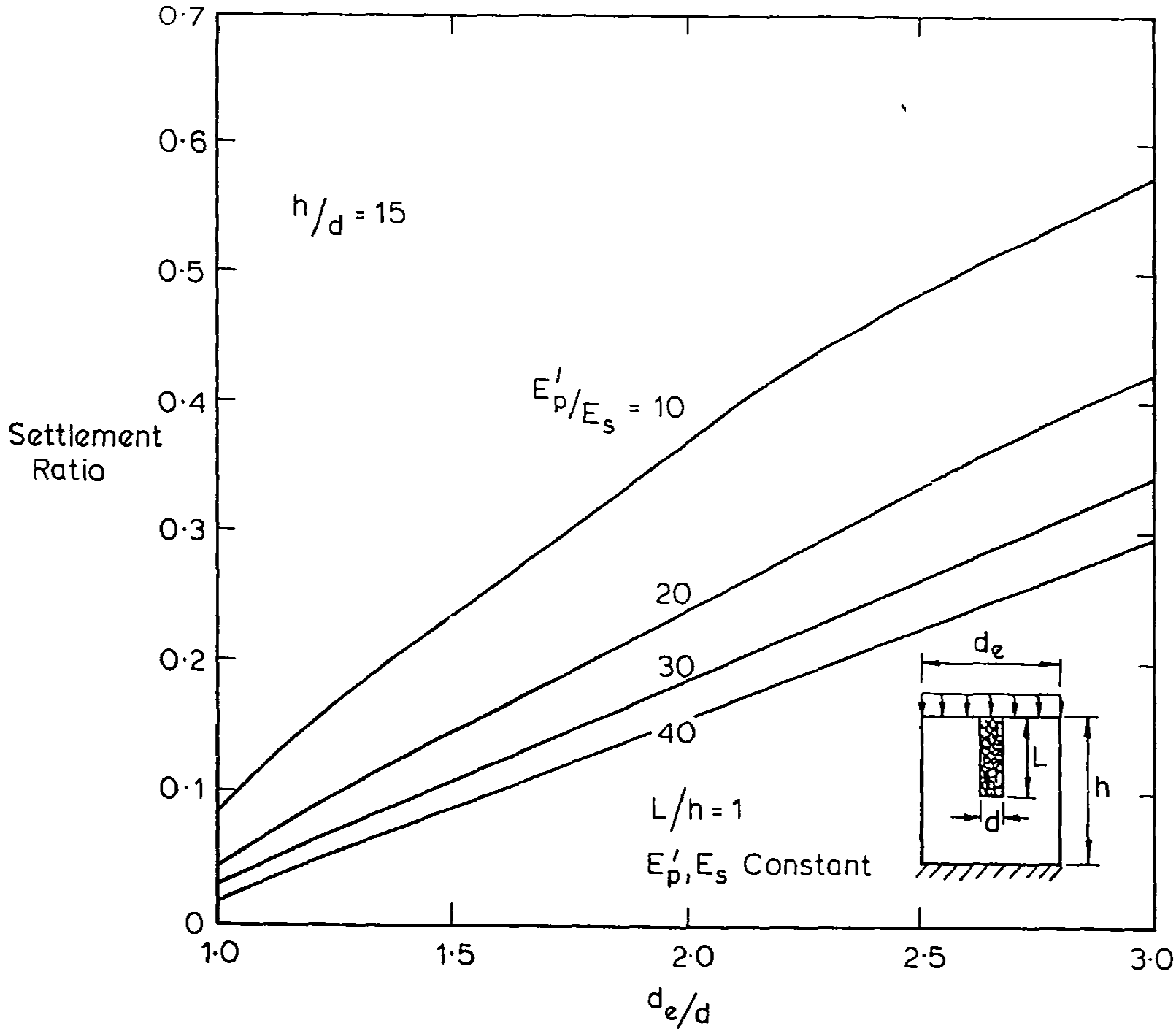

FIG. 5·10 SETTLEMENT REDUCTION FACTORS FOR FULLY PENETRATING PILES

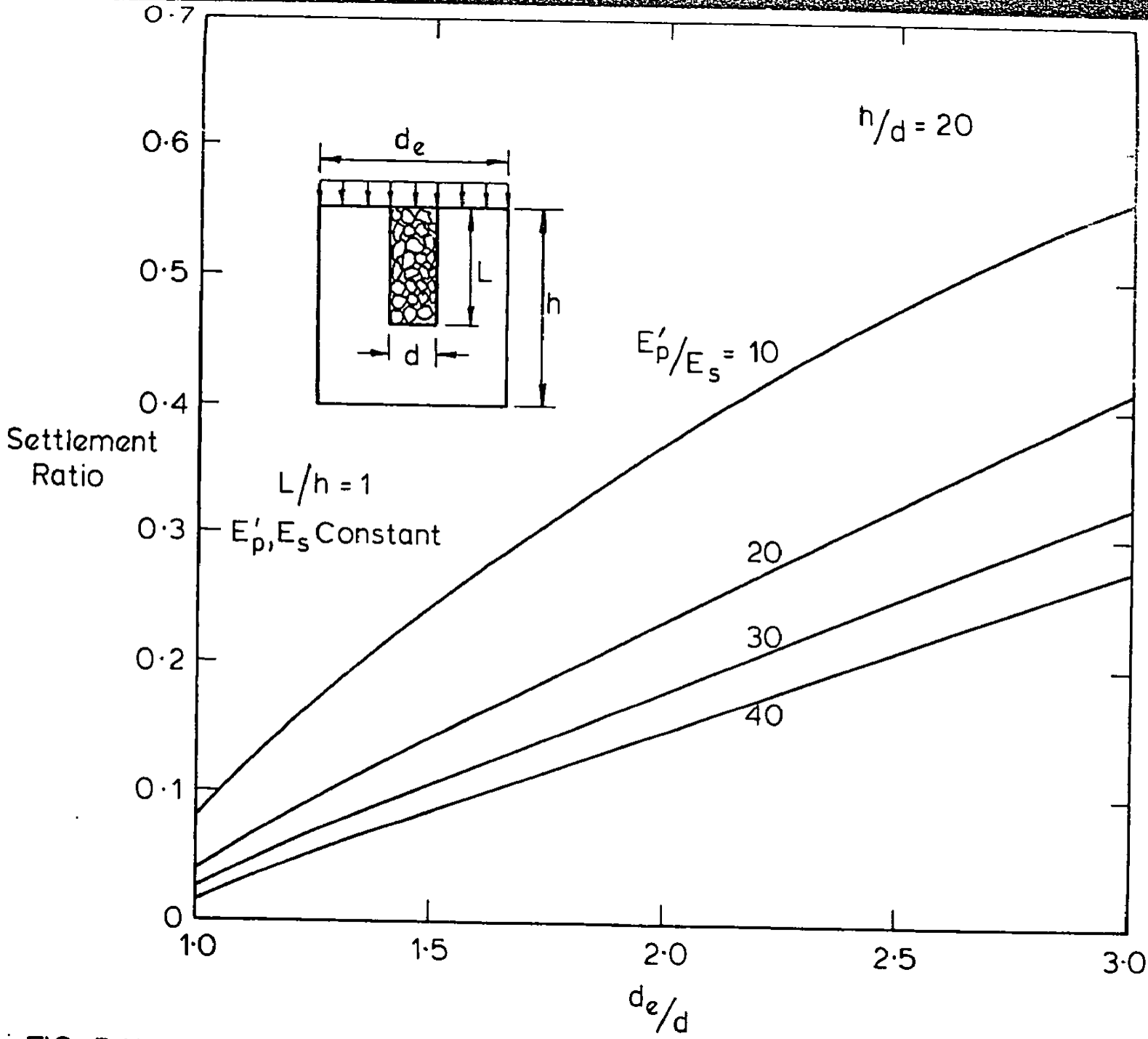

FIG. 5·11 SETTLEMENT REDUCTION FACTORS FOR FULLY PENETRATING PILES

of the layer depth indicate that even if the piles are closely spaced, the settlement reduction is not significant. Fig. 5.12 shows the effect of the degree of penetration of the piles on the Settlement Ratio when $h/d = 60$ for $d_e/d = 2$ and 5. For closely spaced piles ($d_e/d = 2$) the reduction in settlement diminishes rapidly when $L/h < 0.5$ whereas for larger spacings ($d_e/d = 5$), the reduction in settlement is not significant if $L/h < 0.5$. The rate of increase of pile and soil moduli with depth and the value of Poisson's ratio of the pile and soil materials had a negligible effect on the Settlement Ratios.

Although the results presented are limited in terms of the number of parameters, they should provide a sound basis for estimating the reduction in settlement due to pile installation. The results presented in Figs. 5.5 to 5.11 indicate that when granular piles are installed in a regular pattern over a large area, significant reductions in settlement occur only if the piles are closely spaced ($s/d \leq 5$) and usually only if the piles are installed to the full depth of the consolidating layer.

5.2.2 Comparisons Between Observed Settlements, Existing Methods for Predicting Settlements and Elastic Analyses

A demonstration of the applicability of the elastic solutions is difficult because of the lack of published data. In an attempt to illustrate their usefulness comparisons between field data and the elastic solutions are made.

Greenwood's (1970) curves for estimating consolidation settlements under widespread loads for uniform soft clays strengthened by

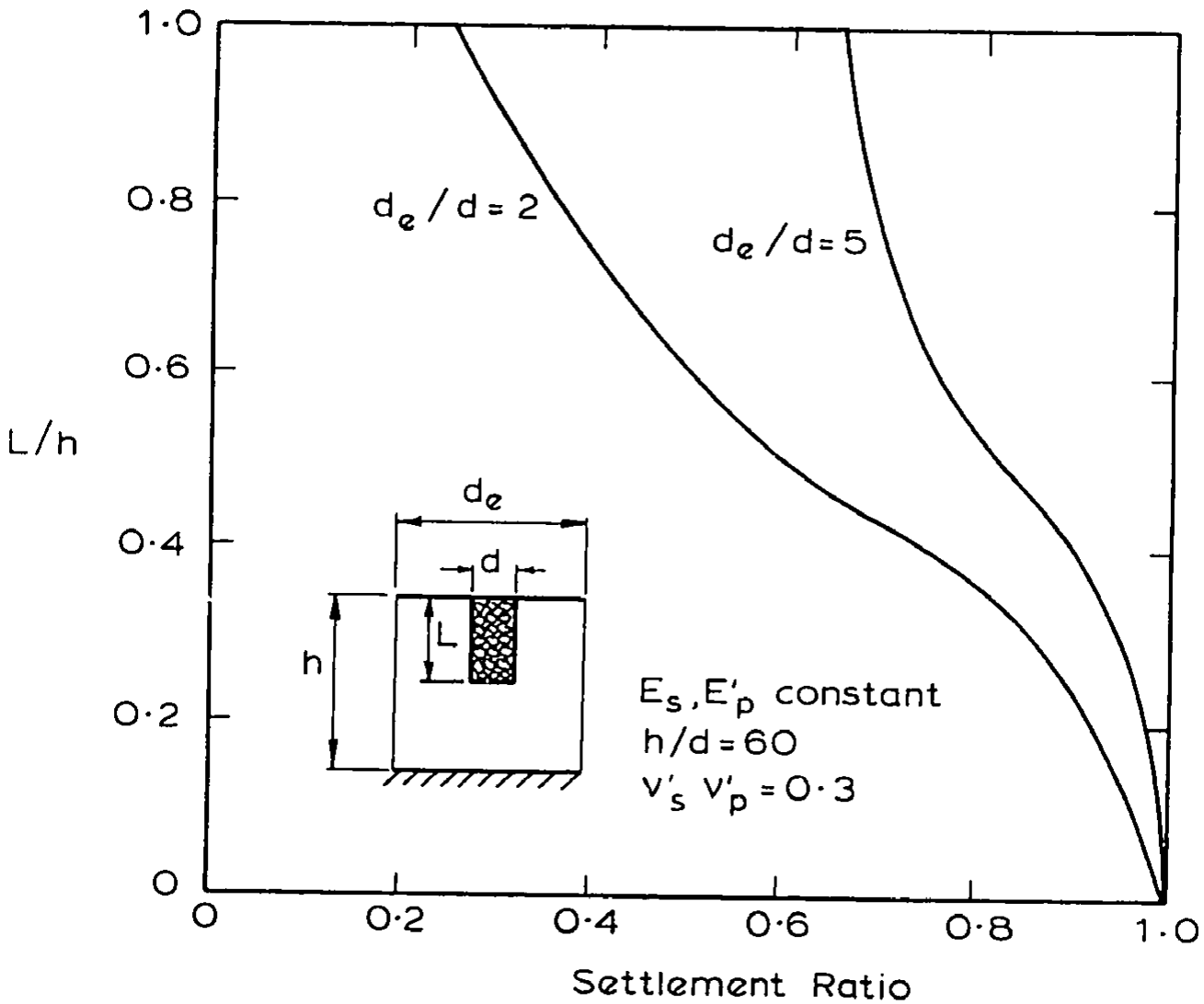

FIG. 5.12 EFFECT OF DEGREE OF PENETRATION ON SETTLEMENT RATIO

granular piles, which were discussed in Chapter 2, are reproduced in Fig. 5.13. The shaded region represents the expected ratio of settlement of the stabilised clay to the settlement if there were no piles, when the wet process of construction is employed. These reductions (or ratios) in settlement could be expected when the columns rested on firm clay, sand or harder ground and thus correspond to the fully penetrating pile solutions from the previous section. Watt, de Boer and Greenwood (1967) suggested that the use of the wet process of construction is preferable and is usually employed because without a jetting fluid the soil immediately surrounding the vibrator is remoulded and disturbed to some extent. The elastic solutions cannot therefore be directly applied when the dry process of construction is adopted and for this reason comparisons between the elastic results and Greenwood's predicted reductions in settlement are restricted to those referring to the wet process of construction. It is worth noting however, that Thorburn and MacVicar (1968) suggest that the use of jetting water should be limited and generally restricted to virgin sites with good natural drainage facilities. According to Greenwood the wet technique results in piles whose diameters are normally 0.9m to 1.04m and thus a representative value of 1.0m is used throughout for purposes of the comparisons.

On Fig. 5.13 the range in Settlement Ratios from the elastic analyses is superimposed on Greenwood's plot. This spread has been determined in the following way. For a given spacing of piles the equivalent diameters d_e are calculated for both a square and triangular pattern of piles. A range of d_e/d values is then obtained using the representative value for the diameter of 1.0m. With this range in d_e/d values a spread of predicted ratios is found by interpolation of

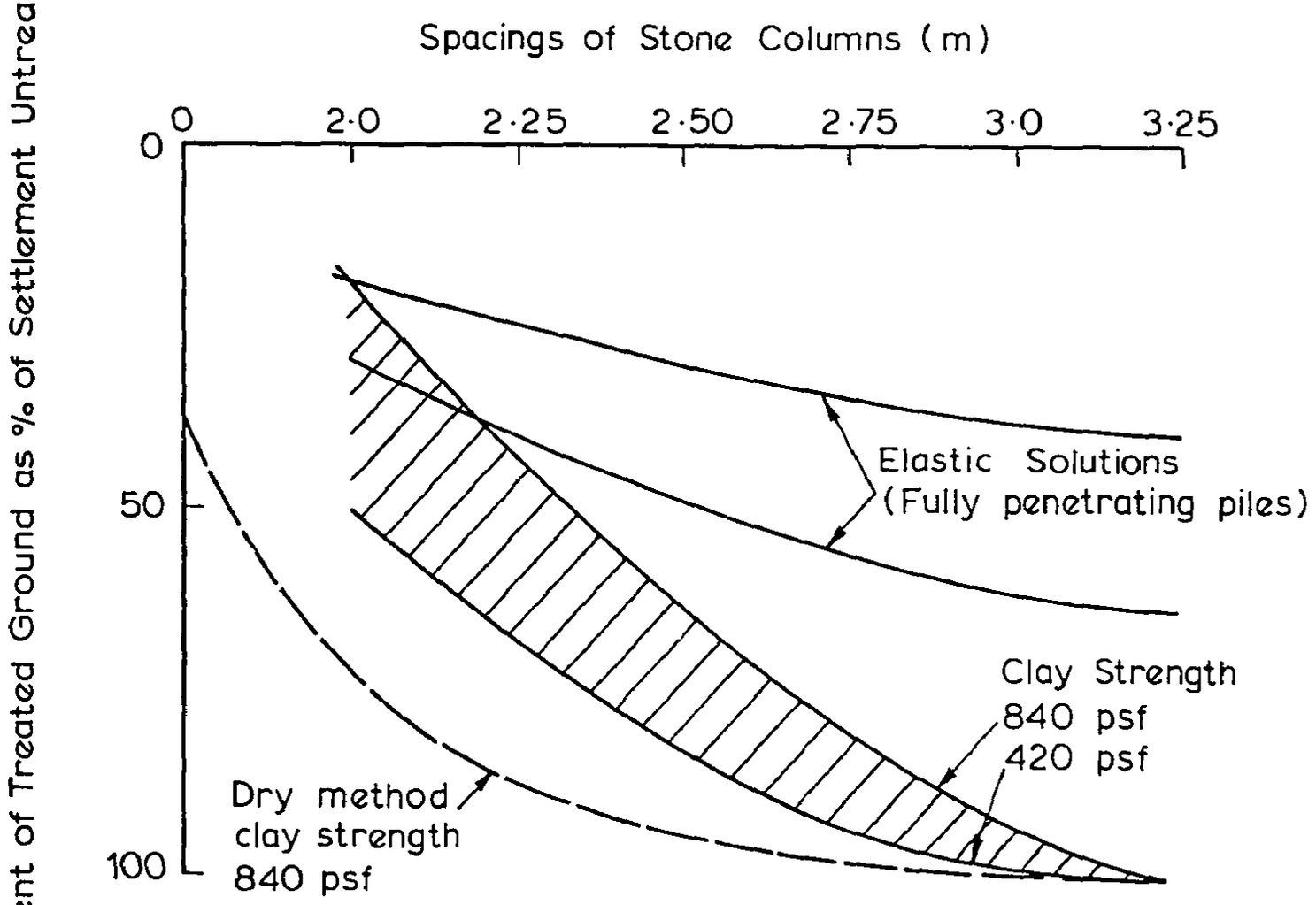

FIG. 5.13 COMPARISON OF ELASTIC SOLUTIONS WITH GREENWOOD'S SETTLEMENT DIAGRAM (after Greenwood, 1970)

the results presented in the previous section for fully penetrating piles.

Although the agreement between the two methods of prediction is good when the spacing of the piles is small, there is considerable discrepancy as the spacing increases, with the elastic solutions predicting larger settlement reductions. However, closer agreement would be obtained if the effect of local yield is taken into account. In addition, the elastic solutions are for a rigid base whereas Greenwood's reductions are for a firm base of clay, sand or harder ground which in practice will not be completely rigid resulting in smaller reductions in settlement.

Few settlement records for structures founded on soft cohesive soils reinforced with granular piles installed over a large area have been published. The result of an analysis of the available data is shown in Fig. 5.14 and discussed below.

Watt et al., (1967) have reported the results of loading tests on structures constructed on three different sites; Teesport, Hedon and Newport. Teesport is situated in Yorkshire in England and is the site of a large oil refinery. The six oil tanks for which data is presented, with the exception of tank 104 (T104), were constructed on cohesive soils reinforced with granular piles installed in a triangular grid at 1.90m spacing. For tank 104 a spacing of 2.13m was initially adopted although additional columns were installed in particularly soft areas. The authors have presented a table showing the maximum settlement measured along the perimeter of the tanks, differential settlement and for two tanks only, the settlement at the centre. The estimated settlements

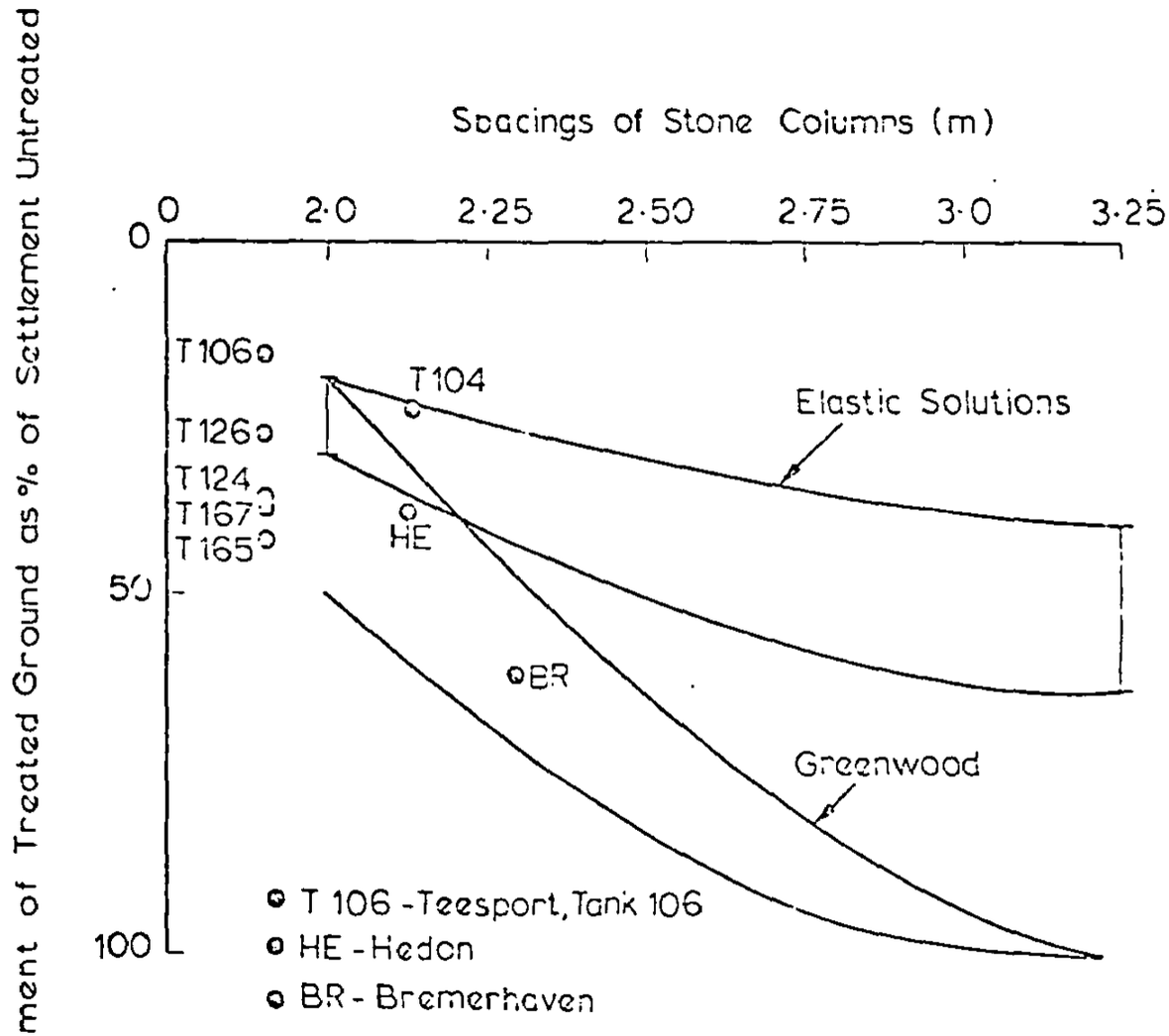

FIG. 5.14 COMPARISON BETWEEN OBSERVED SETTLEMENTS AND PREDICTIONS

for the centre and perimeter are also reported. For uniformity, a ratio of observed to estimated settlements has been calculated at the perimeter of each tank. These ratios are plotted in Fig. 5.14.

Hedon is situated on the Humber River in England. Granular piles were installed in a triangular grid at a spacing of 2.13m to an average depth of 6.71m before the construction of a 43.89m diameter tank. Consumption of the granular material indicated an average diameter of the piles of 1.03m. The elastic solutions presented can be applied directly to predict the ratio in settlement at this site because of the uniformity in the compressibility of the clay. The data corresponds to $d_e/d = 2.17$ and $h/d = 6.5$. Assuming the boulder clay on which the piles were founded is sufficiently stiff for the fully penetrating pile analyses to be applicable, interpolation of the results (Figs. 5.8 and 5.9) suggests a Settlement Ratio of .3-.35. The measured reduction in settlement at the perimeter of the tank of .38 is in good agreement with the prediction. Finally, the form of loading used at Newport was not widespread and thus the results are not applicable to the present investigation.

Greenwood (1970) has reported the results of a large scale field test at Bremerhaven (England) for a motorway embankment. Granular piles were installed through a shallow layer of peat and clay into fine uniform sand on a triangular grid at 2.3m spacing. Columns were either formed with sand of grain size 0-3mm or with gravel of size30-70mm. The test indicated the necessity of using gravel sizes to reduce the settlements. After 15 months the average settlements for the gravel piles, sand piles and untreated areas were 468 $\pm$ 31mm, 645 $\pm$ 75mm and 765 $\pm$ 13mm respectively. The reduction in settlement

for the piles formed with gravel is plotted in Fig. 5.14. At this site the elastic settlement results significantly overestimate the effectiveness of the stone columns in reducing the settlement. However, the range in values of $q/\gamma h$ is approximately .7-.9 indicating that a full elasto-plastic analysis is required for predicting the settlement.

5.3 STABILITY OF EMBANKMENTS SUPPORTED BY STONE COLUMNS

A mechanism for a general shear failure of an embankment supported by a large group of granular piles only exists at the edges of the reinforced area. In this section a method of evaluating a factor of safety against this type of failure from a slip circle analysis is briefly described. For the purposes of this analysis the factor of safety is defined as the resisting moments divided by the overturning moments.

In order that a conventional slip circle analysis can be utilised a row of piles is represented by a plane strain 'trench' of pile material with a volume equal to that of the row of piles. This assumption is considered to be acceptable because of the relative stiffness of the pile and soil materials, ie. when failure occurs the soil and piles would act as a combined mass rather than the soil moving between the piles as would be the case if conventional steel and concrete piles were being analysed.

The results of an analysis of a typical geometry is shown in Fig. 5.15. The analyses were performed using a standard computer program (Pells and Poulos, 1976) which allowed for the inclusion of

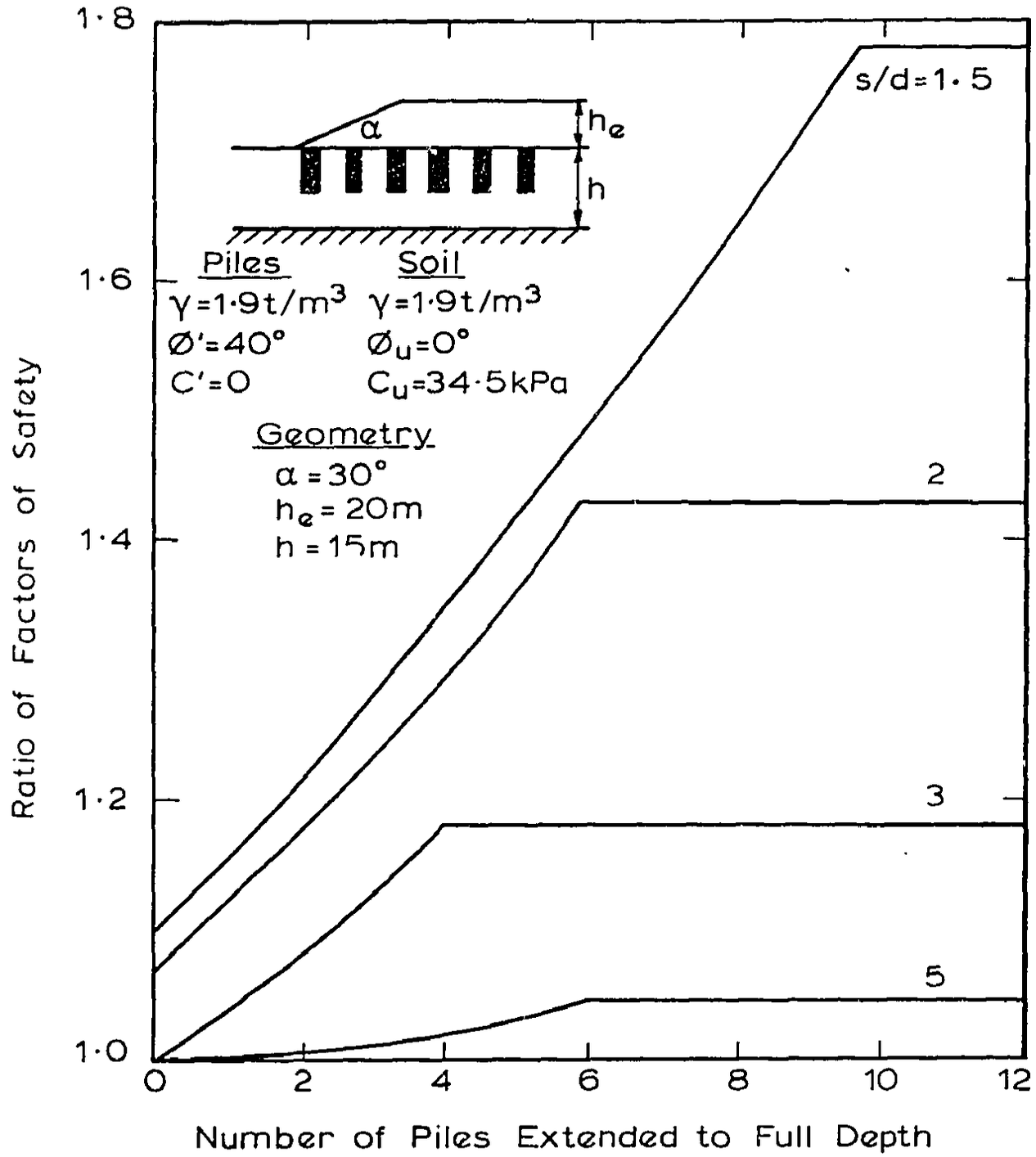

FIG. 5.15 RESULTS OF SLIP CIRCLE ANALYSES

soils with differing strength properties. The ratio of the factors of safety with piles to the factor of safety if no piles are installed is plotted against the number of piles extended to full depth. The elastic solutions for settlement indicated that no appreciable reduction in settlement was achieved by installing piles to less than half depth. Thus a convenient point to commence the analysis is to consider piles with differing spacings installed to half depth. For this case then, spacings of $s/d = 3$ and 5 resulted in no increase in the shearing capacity when all the piles were to half depth ie. the critical circle was deep seated and passed between the piles. The analysis was then repeated for a given spacing with increasing numbers of piles extended to full depth. A point is reached where if further piles are extended to full depth no further benefit is obtained. This then corresponds to the factor of safety if all piles are to full depth.

The results can be used as a basis for estimating the required layout of piles for a given factor of safety. In addition, the effect on stability of installation of piles beyond the toe of the embankment and varying the height of the embankment may be investigated by this method of analysis. The results verify that if the piles are closely spaced and installed to full depth the factor of safety of the embankment is increased markedly although for a particular geometry this improvement will depend on the material properties of the pile and soil.

5.4 SUMMARY AND CONCLUSIONS

In this chapter the behaviour of foundations resting on clays reinforced with granular piles installed in a regular pattern over a large area has been investigated. Elastic finite element results have

been presented showing the reduction in settlement due to the presence of the stiffer pile. These indicate that significant reductions in settlement occur only if the piles are closely spaced and installed to at least half depth of the clay layer. Although the results are limited in terms of the number of parameters they should provide a sound basis for estimating the reduction in settlement for a given layout of piles.

Comparisons between field data and the elastic solutions have been presented. Agreement is generally good although data is unavailable for piles whose spacing is greater than 2.3m.

Finally, the results of conventional slip circle analyses of an embankment resting on a soft clay stratum reinforced with granular piles demonstrate the applicability of this approach in determining a factor of safety. In addition, the usefulness of granular piles in acting as 'shear pins' resisting failure of the embankment has been demonstrated.

CHAPTER SIX

ANALYSIS OF 'SAND DRAIN' ACTION OF GRANULAR PILES

6.1 INTRODUCTION

The load-settlement behaviour of soft clays reinforced with granular piles is improved by the presence of the stiffer pile material and also because of the 'sand drain' action of the piles which promotes more rapid consolidation of the clay. This is an important advantage of stone columns in comparison with conventional piling systems. In this chapter the rate of settlement of flexible foun· 'o ~, supported by a clay stratum reinforced with a regular ttern ' anular piles, is examined. Comparisons are made between ' l~ment solutions to Biot's theory of consolidation and finite di ..uctions to diffusion theory for the rate of settlement of th Agreement is found to be generally good and because the diffusion theory solutions are more easily obtainable, a series of these solutions are presented in the form of a parametric study. These results, if used in conjunction with the elastic settlement reduction factors presented in Chapter 5, form the basis of a rational method of predicting the settlement-time behaviour of soft clays reinforced with granular piles.

In practice the rate of application of the load to the reinforced clay is such that dissipation of the excess pore pressures results in improvement in the strength and deformation properties of the clay before the load reaches its maximum value. However, water and oil storage structures are usually important exceptions to this. If the clay is suitable for the SHANSEP (an acronym for Stress History and Normalized Soil Engineering Properties) method of design to be employed (Ladd and Foott, 1974), then design based on the initial in-situ values of strength and deformation properties may be over-conservative. The SHANSEP method assumes that the soil's engineering pro-

perties can be normalised as a function of the stress system and over-consolidation ratio (OCR). Therefore, as consolidation takes place and the effective stresses increase, the strength and deformation properties of the clay improve.

Installation of granular piles increase the rate of consolidation of the clay layer to such an extent that only a comparatively short period of preloading is necessary. Excess pore pressures from diffusion theory solutions could then be used to estimate the stress system throughout the reinforced clay and thus establish new strength profiles for stability analyses similar to those described in Chapter 5. In addition, new deformation moduli could be established for prediction of settlements due to subsequent load applications.

6.2 CONSOLIDATION THEORY

In order to predict the rate of settlement of the reinforced soil a solution is required for the consolidation of the clay due to the expulsion of pore water by vertical flow and radial flow towards the granular piles.

6.2.1 Biot Consolidation Theory

The most rigorous theory of three dimensional consolidation is that due to Biot (1941) which combines the effects of diffusion and the elastic deformations resulting from the decrease in pore pressure. For a fully saturated isotropic soil skeleton the equation governing water flow in terms of cartesian co-ordinates x, y and z is given by

$$\frac{\partial u}{\partial t} = c_{v3} \nabla^2 u + \frac{1}{3} \frac{\partial \theta}{\partial t} \qquad (6.1)$$

where u = excess pore pressure

t = time

$\nabla^2 = \frac{\partial^2}{\partial x^2} + \frac{\partial^2}{\partial y^2} + \frac{\partial^2}{\partial z^2}$

θ = bulk total stress

$= \sigma_x + \sigma_y + \sigma_z$

c_{v3} = coefficient of consolidation in the vertical direction for three dimensional strain conditions.

In addition, consideration of equilibrium, compatibility and stress-strain relationships leads to a further three equations of the form

$$G\nabla^2 \rho_x + \frac{G}{1-2\nu_s'} \frac{\partial \varepsilon_v}{\partial x} - \frac{\partial u}{\partial x} = 0 \qquad (6.2)$$

where G = Shear modulus

ρ_x = displacement in the x-direction

ν_s' = Poisson's ratio of the soil skeleton

ε_v = Volume strain

and similarly for the y and z directions.

Equations 6.1 and 6.2 provide four equations which can be solved (together with the appropriate compatibility and stress-strain relationships) for the unknown pore pressure u and displacements ρ_x, ρ_y, ρ_z. Few analytic solutions to Biot's equations of consolidation have been produced and numerical methods of solution are usually adopted (Sandhu and Wilson, 1969; Christian and Boehmer, 1970; Booker, 1973). The finite element method is a convenient numerical technique for the solution of these equations. The finite element equations can

be derived in a number of ways. Sandhu and Wilson have used a Gurtin variational principle. However, solutions to Biot's theory presented in this chapter were obtained using a program written by Booker and Small (1975) in which a variational theorem involving the Laplace transform of the field quantities is used to derive the finite element equations.

Using this technique, a set of finite element equations are assembled using the elastic properties of the soil skeleton which can be expressed as

$$\begin{bmatrix} [K_E] & -[L]^T \\ -[L] & -(1-\alpha)\Delta t[\Phi] \end{bmatrix} \begin{bmatrix} \{\delta_{t+\Delta t}\} \\ \{q_{t+\Delta t}\} \end{bmatrix} = \begin{bmatrix} \{R_{t+\Delta t}\} \\ \{b_t\} \end{bmatrix} \qquad (6.3)$$

where the value of a variable at time t is denoted by a subscript and

$[K_E]$ = elastic stiffness matrix

$[\Phi]$ = a matrix governing flow through a rigid skeleton

$[L]$ = a coupling matrix linking deformation and flow

$\{\delta\}$ = vector of nodal deflections

$\{q\}$ = vector of nodal excess pore pressures

α = integration parameter (forward marching solutions are stable if $0 \leq \alpha \leq 0.5$)

Δt = increment in time

A forward marching technique is used to obtain values of nodal deflections and excess pore pressures at discrete times. With these solutions it is possible to calculate the degree of settlement for any point on the surface whereas diffusion theory solutions yield only an average degree of settlement. Furthermore, different material properties can be assigned to the sand and clay. However, the numerical solutions to

Biot's equations of consolidation do not differ significantly from the diffusion theory solutions. In this chapter a series of diffusion theory solutions are presented in the form of a parametric study of the factors affecting the rate of consolidation.

6.2.2 Diffusion Theory

The process of consolidation under two and three dimensional strain conditions involves a redistribution of bulk stress throughout the soil mass and thus the term $\partial\theta/\partial t$ (Equation 6.1) is generally non-zero. If however, this term is assumed to be zero the equations governing consolidation are identical to those of heat diffusion. An equation for consolidation involving two dimensional flow with one-dimensional strain conditions can be written with respect to cylindrical co-ordinates as

$$\frac{\partial u}{\partial t} = c_{vl} \frac{\partial^2 u}{\partial z^2} + c_{rl} \left[\frac{\partial^2 u}{\partial r^2} + \frac{1}{r} \frac{\partial u}{\partial r}\right] \qquad (6.4)$$

where c_{vl} = coefficient of consolidation in the vertical direction for one dimensional strain conditions

c_{rl} = coefficient of consolidation in the radial direction for one dimensional strain conditions

r = radial co-ordinate

z = vertical co-ordinate.

This equation is an extension of Terzaghi's (1925) theory of one dimensional consolidation. Its development and analytical solution has been reviewed by Barron (1948). The analytical solution is applicable for a pile which penetrates through the full depth of the consolidating layer.

Richart (1959) investigated the use of the finite difference method for solutions to problems which depart from the ideal case (ie. fully penetrating pile in a layered soil system). Hart et al., (1958) used this approach to analyse an illustrative problem in which the pile penetration varied although a simplifying assumption was made that the cylinder of clay directly beneath the pile did not drain. This was done to avoid the necessity of considering the special form of equation 6.4 when r = 0. It can however be readily shown that

$$\lim_{r \to 0} \frac{\partial u}{\partial r} = \frac{\partial^2 u}{\partial r^2} \qquad (6.5)$$

Therefore on the axis (r=0) equation 6.4 is replaced by

$$\frac{\partial u}{\partial t} = c_{v1} \frac{\partial^2 u}{\partial z^2} + 2c_{r1} \frac{\partial^2 u}{\partial r^2} \qquad (6.6)$$

Equations 6.4 and 6.6 are rewritten in an implicit finite difference form. A set of simultaneous equations for the unknown nodal values of u at time t + Δt are obtained by expressing the partial derivatives as an average value over the time interval t to t + Δt. The finite difference equivalents to these equations are given in Appendix 6A.

The implicit form of the equations is utilised because solution of the alternative set of equations (explicit form) can be prohibitively long and laborious as the maximum allowable time increment is dictated by a stability criterion. Solution of the implicit form of the equations is stable and no restriction is placed on the size of space or time increments. However, the finite differences must be reasonable approximations to the corresponding differentials and thus

the time interval chosen will depend on the rate of change of the pore pressures.

Solution of the equations leads to a set of excess pore pressures which are then used to calculate the average degree of pore pressure dissipation U_p, where

$$U_p = 1 - \frac{2\pi}{2\pi} \frac{\iint u_t \cdot r \cdot dr\, dz}{\iint u_0 \cdot r \cdot dr\, dz} \qquad (6.7)$$

where u_t = excess pore pressure at time t

u_0 = initial excess pore pressure, which is assumed here to be uniform throughout the mass.

6.2.3 Comparison Between Diffusion and Biot Theory Solutions

An important difference between diffusion theory solutions and solutions to Biot's theory of consolidation is that from the diffusion theory, only an average degree of pore pressure dissipation can be calculated whereas from the solutions to Biot's theory, both the degree of consolidation settlement and the average degree of pore pressure dissipation can be calculated. The degree of consolidation settlement is the quantity of engineering interest. Davis and Poulos (1972) have compared analytical solutions to Biot's consolidation theory with solutions from diffusion theory for a uniformly loaded strip footing and circle on a semi-infinite mass and for a uniformly loaded circle on finite layers. From these comparisons it was found that the average degree of pore pressure dissipation U_p approximates the degree of consolidation settlement U_s by defining the time factor T_v in terms of the one-dimensional coefficient of consolidation c_{vl}

for all cases, one-two or three dimensional.

The results discussed in this chapter are applicable to vertical granular piles installed in a regular pattern over a large area. In this case, except near the edges of the loaded area, the behaviour of all pile-soil units is virtually the same and thus the rate of settlement of the large group of piles may be analysed by considering a typical pile-soil unit as was the case for the settlement analyses discussed in the previous chapter. For a triangular arrangement, each pile may be considered as having a hexagonal domain of influence [Fig. 6.1(a)] and an equal area of influence is given by a circular domain of diameter $d_e = 1.05s$, where s is the pile spacing. For a square arrangement of piles, $d_e = 1.13s$. The pile-soil units analysed are cylindrical with diameter d_e and are divided into finite elements as shown in Fig. 6.1(b) for Biot theory solutions, and a finite difference grid as shown in Fig. 6.1(c) for the diffusion theory solutions.

In Fig. 6.2 the results of a comparison between finite element solutions to Biot's theory and finite difference solutions to diffusion theory are shown for a granular pile with varying degrees of penetration through the soil layer. The average degree of pore pressure dissipation U_p (diffusion theory) and degree of consolidation settlement U_s (Biot's theory) are plotted against the one-dimensional time factor T_{vl}. Although the discrepancy is significant for the fully penetrating pile, for values of L/h less than 0.8 the agreement between the solutions to the two theories is generally good.

The finite element solutions are for the pile and soil being

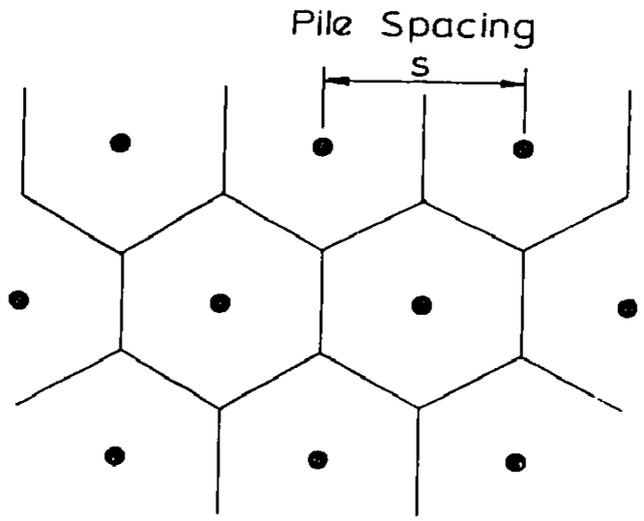

(a) Plan of regular triangular pattern of granular piles

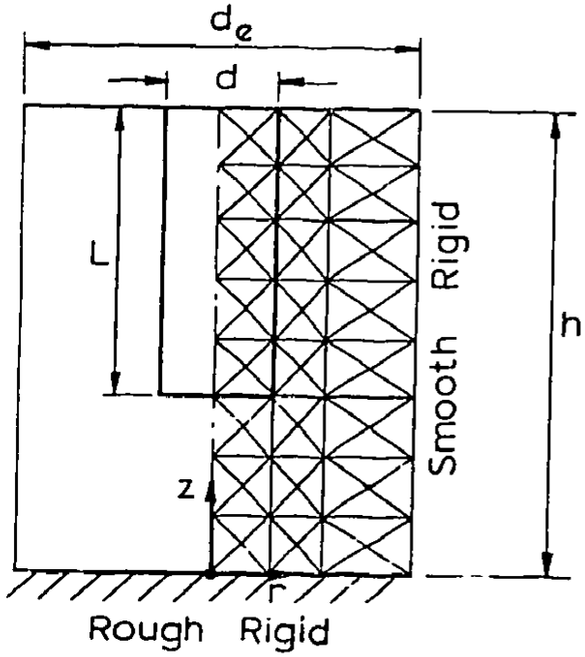

(b) Finite element model of a pile-soil unit

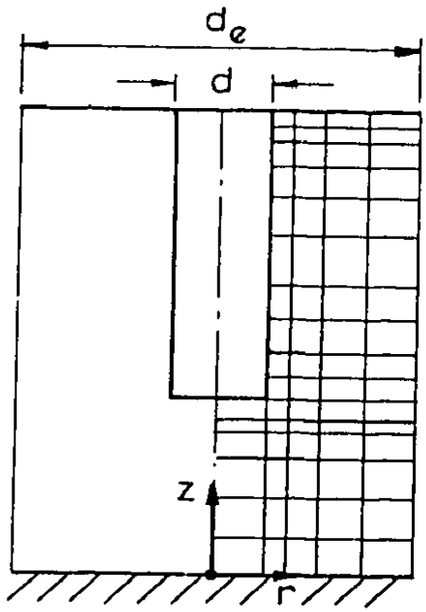

(c) Finite difference grid with variable spacing

FIG. 6.1 PILE-SOIL UNITS IN A REGULAR EXTENSIVE PATTERN OF GRANULAR PILES

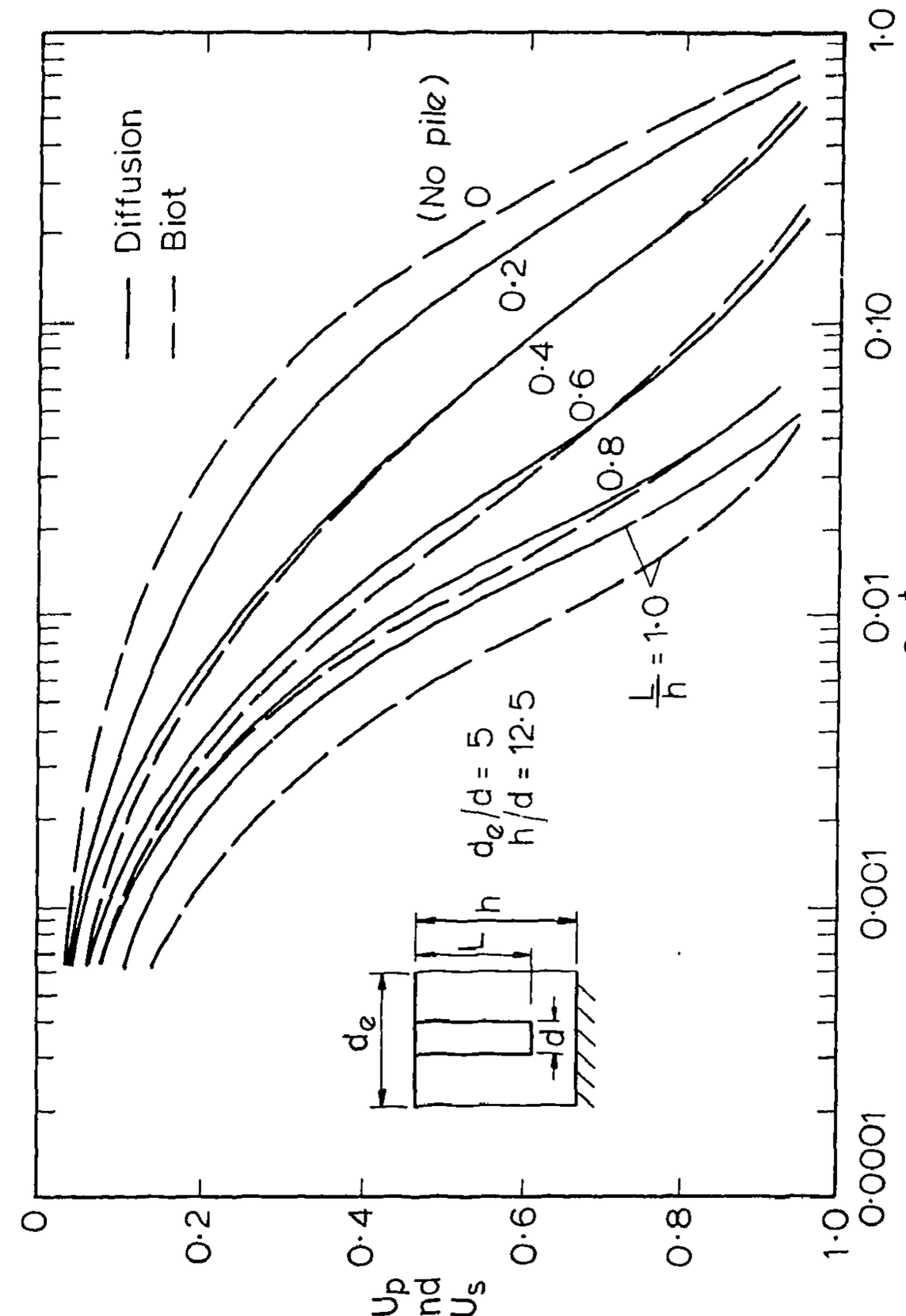

FIG. 6.2 RATE OF PORE PRESSURE DISSIPATION FOR d_e/d = 5 AND COMPARISON WITH BIOT RESULTS

ideal elastic materials. The soil and pile are homogeneous, E_p'/E_s = 20 where E_p' is the drained Young's modulus of the pile and E_s the undrained value for the soil. The drained Poisson's ratio of the pile material and soil (ν_p', ν_s') are 0.3. The undrained and drained Young's moduli of the soil (E_s, E_s') are related by the equation

$$\frac{E_s}{1.5} = \frac{E_s'}{(1+\nu_s')} \qquad (6.8)$$

The finite element mesh used for this comparison is shown in Fig. 6.3. The outer boundary is taken to be smooth, rigid and impermeable while the base is rough, rigid and impermeable (1-way drainage). The high permeability ratio of the pile and soil can be taken into account in one of two ways. The elements within the pile can be assigned a permeability much larger than the soil or the excess pore pressures within the pile can be specified as zero which corresponds to infinite permeability. For these analyses the excess pore pressures were specified as zero.

Settlement versus time plots for the nodes at the centre of the pile and at the outer edge of the cylindrical pile-soil unit are shown in Fig. 6.4 for the fully penetrating pile. The magnitudes of the settlements of these nodes are significantly different. However, the degree or rate of settlement (Fig. 6.5) is nearly identical. It is important to note that this also applies to partially penetrating piles. In Fig. 6.6 the final surface settlement profiles are shown for the various penetration lengths. The settlements at the outer edge (r/r_w = 5) correspond to those presented in Chapter 5 calculated using elastic finite element results.

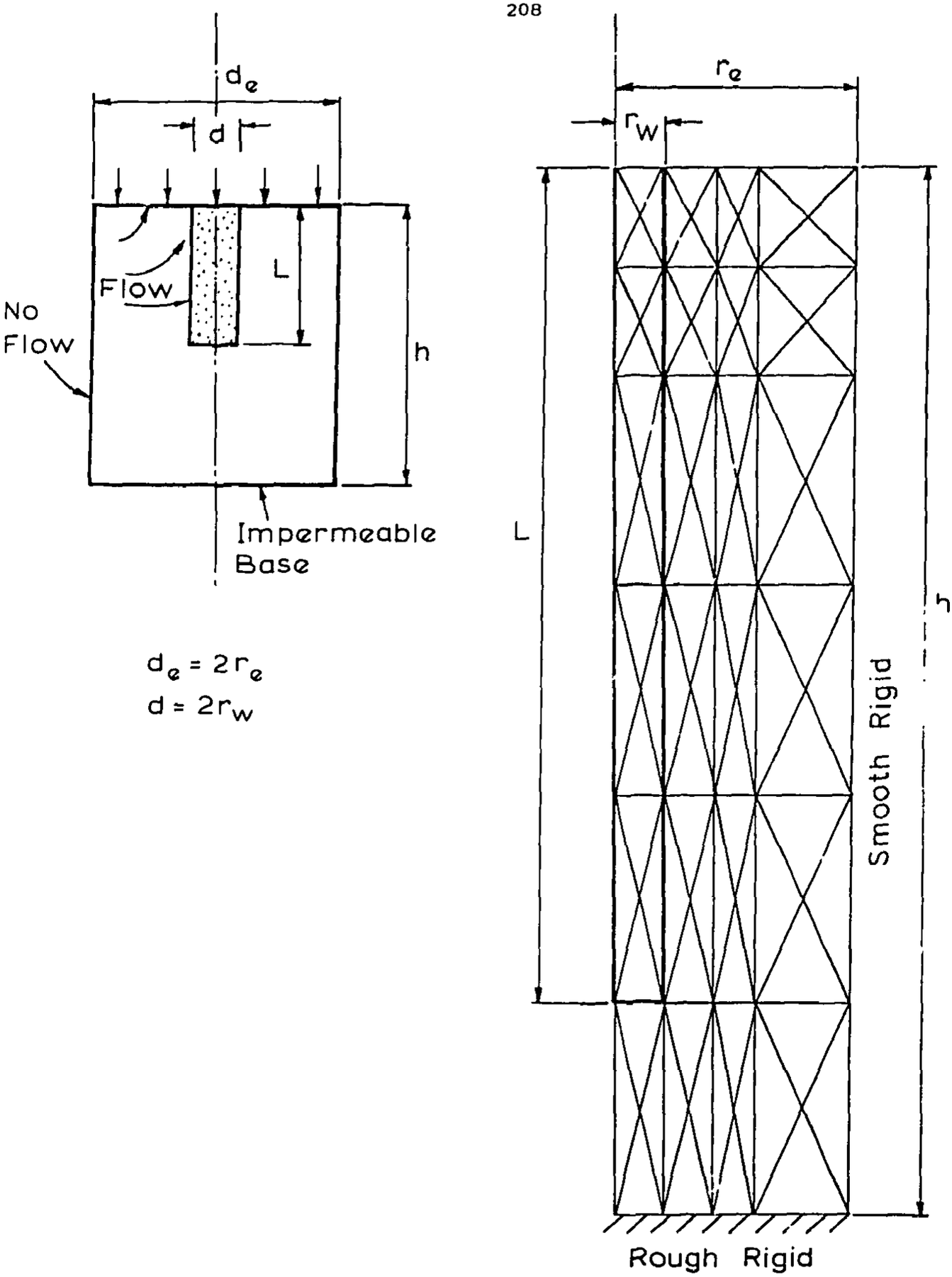

FIG. 6.3 MESH USED FOR COMPARISON OF BIOT AND DIFFUSION THEORY SOLUTIONS

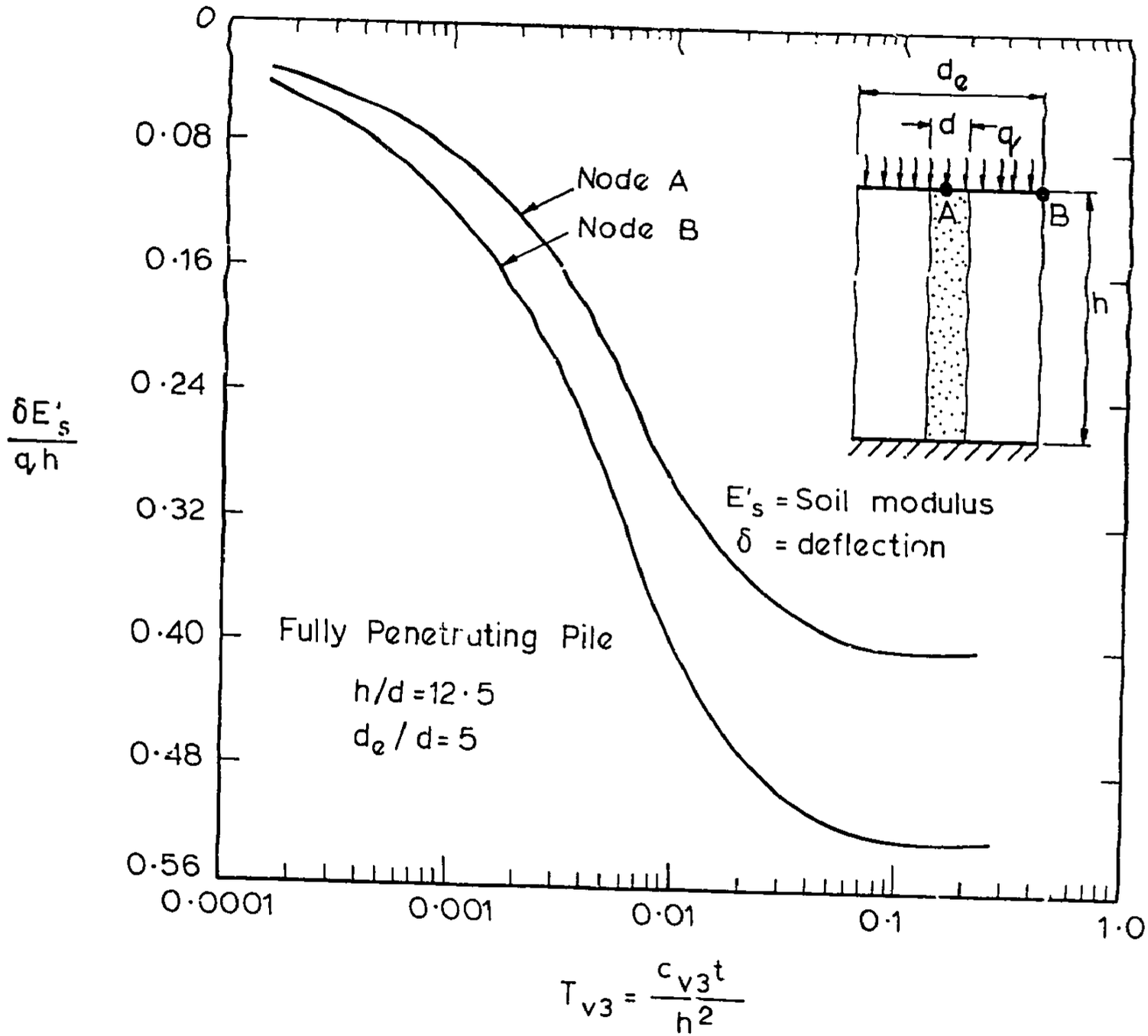

FIG. 6.4 SETTLEMENT VS TIME FOR FULLY PENETRATING PILE

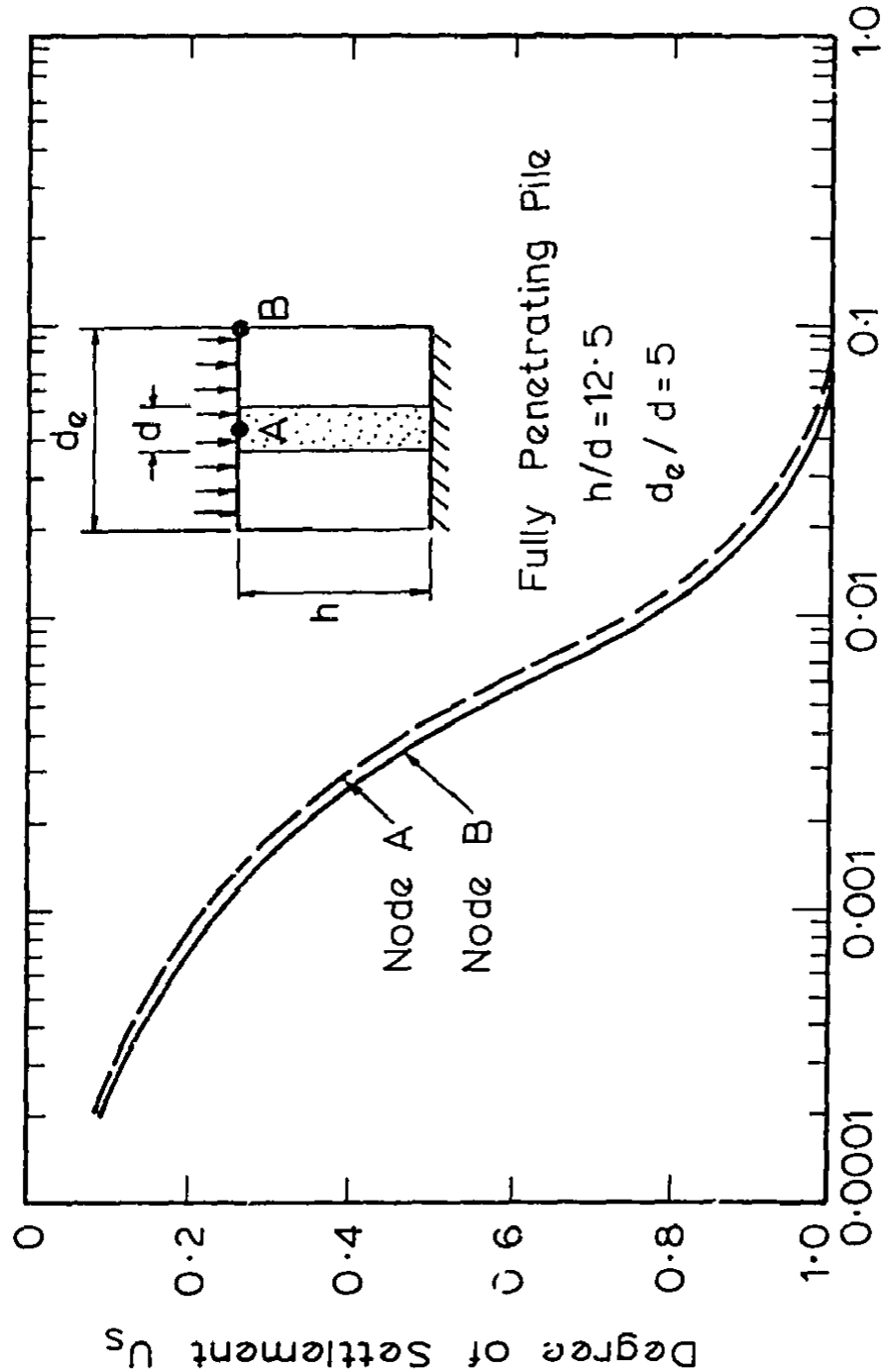

FIG. 6.5 DEGREE OF SETTLEMENT VS TIME

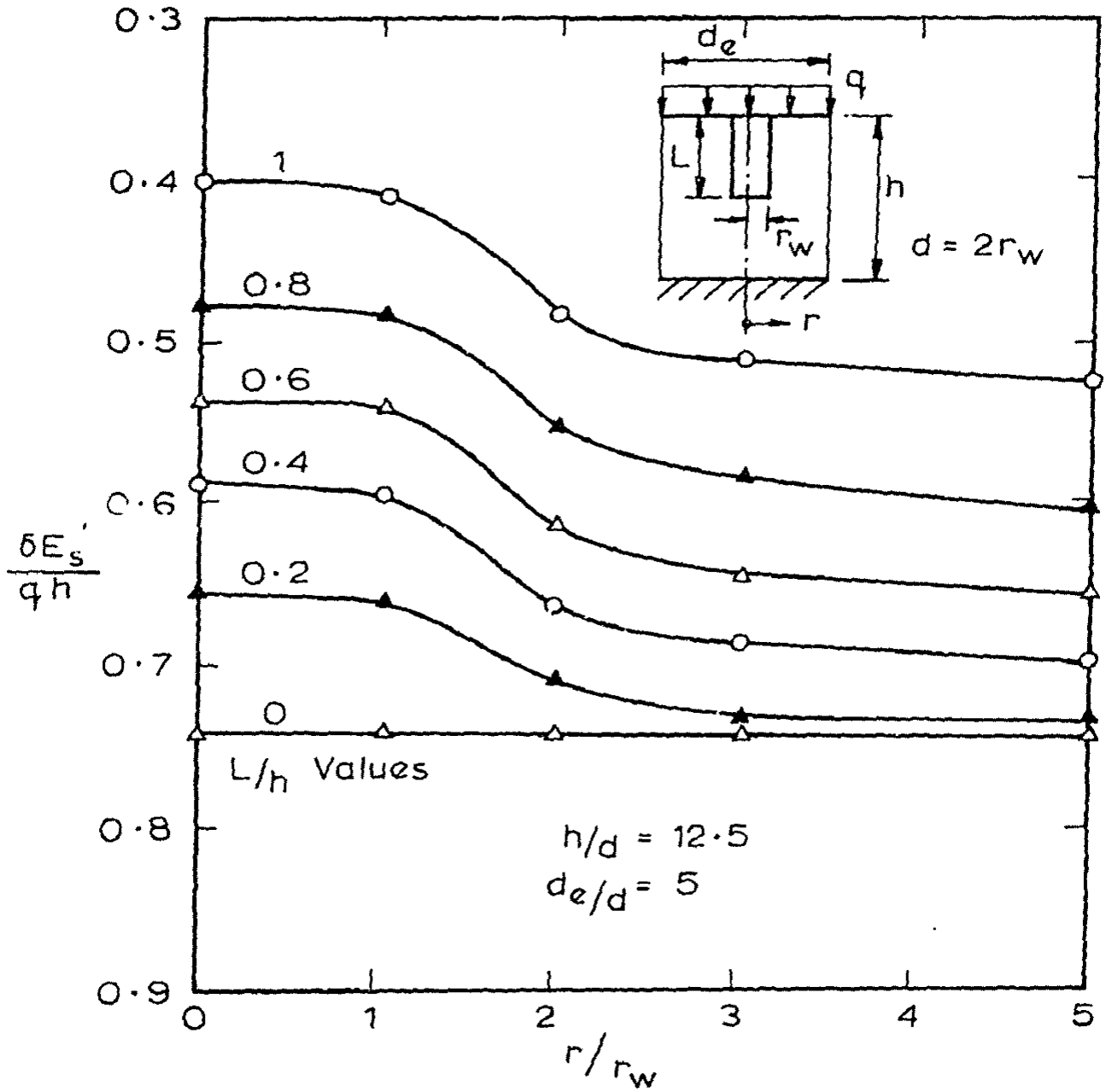

FIG. 6.6 FINAL VERTICAL SETTLEMENT PROFILES

Thus, from the Biot theory, solutions for both the magnitude and rate of settlement can be calculated from the one analysis. However, the results of the comparisons show that diffusion theory solutions provide close approximations to the degree of consolidation settlement. A series of diffusion theory solutions in the form of a parametric study of the increased rate of consolidation of the clay, due to the installation of the piles, is presented in the following section.

6.3 EFFECT OF PILE DIAMETER, SPACING AND DEGREE OF PENETRATION ON RATE OF PORE PRESSURE DISSIPATION

A series of diffusion theory solutions have been computed to quantify the increased rate of consolidation of the clay as the degree of penetration of the pile increases from L/h = 0 (no pile) to L/h = 1 (fully penetrating pile). In order to establish the fineness of the finite difference grids required for accurate solutions comparisons with the analytic solution for the fully penetrating piles were made for each geometry considered. Typical results of these comparisons are shown in Fig. 6.7 for $d_e/d = 5$ (h/d = 12.5, 25) and $d_e/d = 10$, h/d = 12.5. This close agreement is obtained using grids which consist of approximately 200 nodal points. Therefore, approximately this number of nodes were used for the analyses of the partially penetrating piles. In Fig. 6.8 a representative grid is reproduced to illustrate the fineness of the grids used for these analyses.

The results of the analyses for $d_e/d = 2, 5, 10$ for both h/d = 12.5 and 25 are shown in Figs. 6.9 to 6.14 for isotropic conditions. This range in values is considered representative of those found in

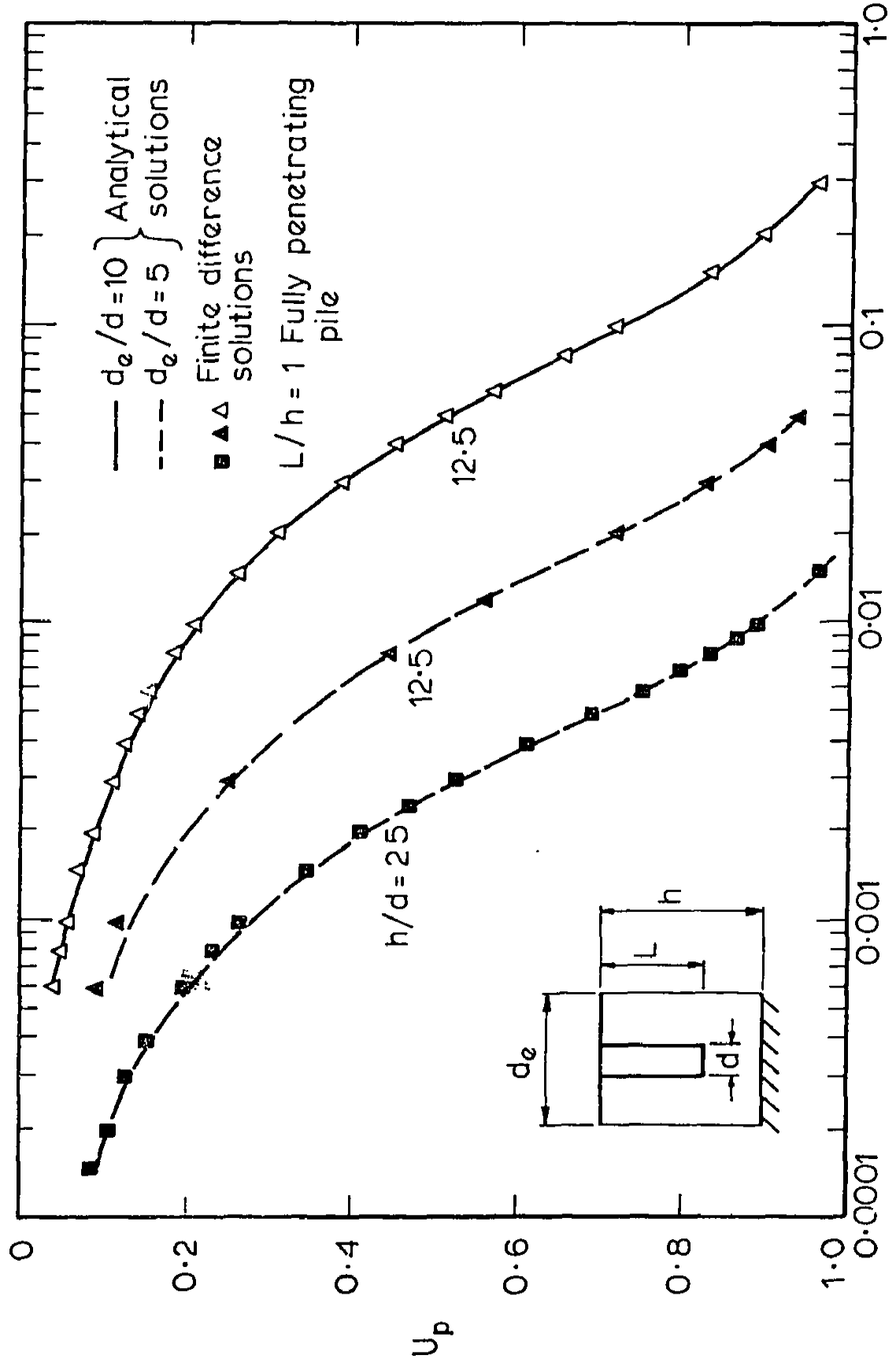

FIG. 6.7 COMPARISON BETWEEN ANALYTICAL SOLUTIONS AND FINITE DIFFERENCE SOLUTIONS

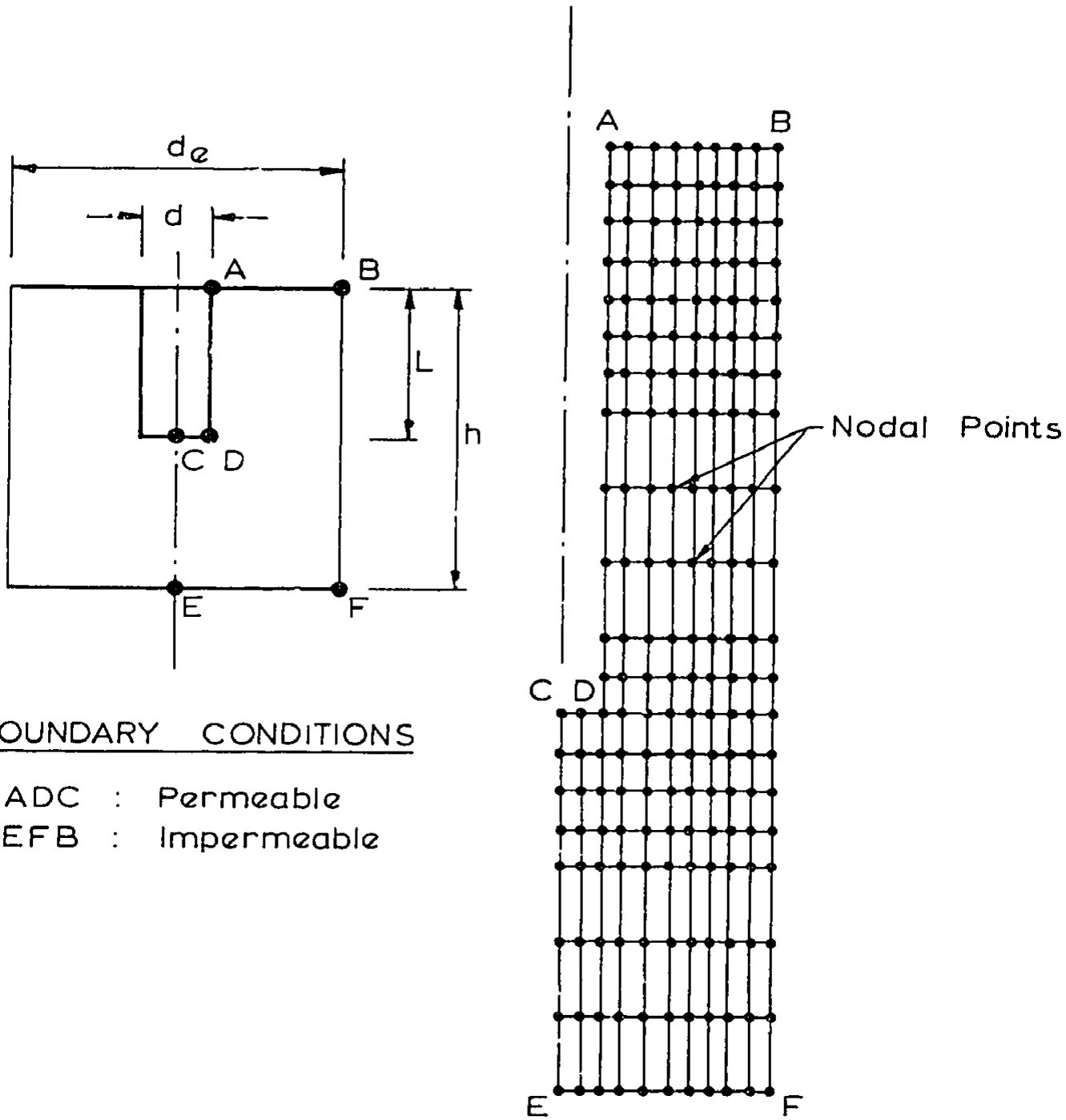

BOUNDARY CONDITIONS

BADC : Permeable
CEFB : Impermeable

FIG. 6.8 FINITE DIFFERENCE GRID USED FOR ANALYSIS OF $h/d = 12{\cdot}5$, $d_e/d = 5$, $L/h = 0{\cdot}6$ GEOMETRY

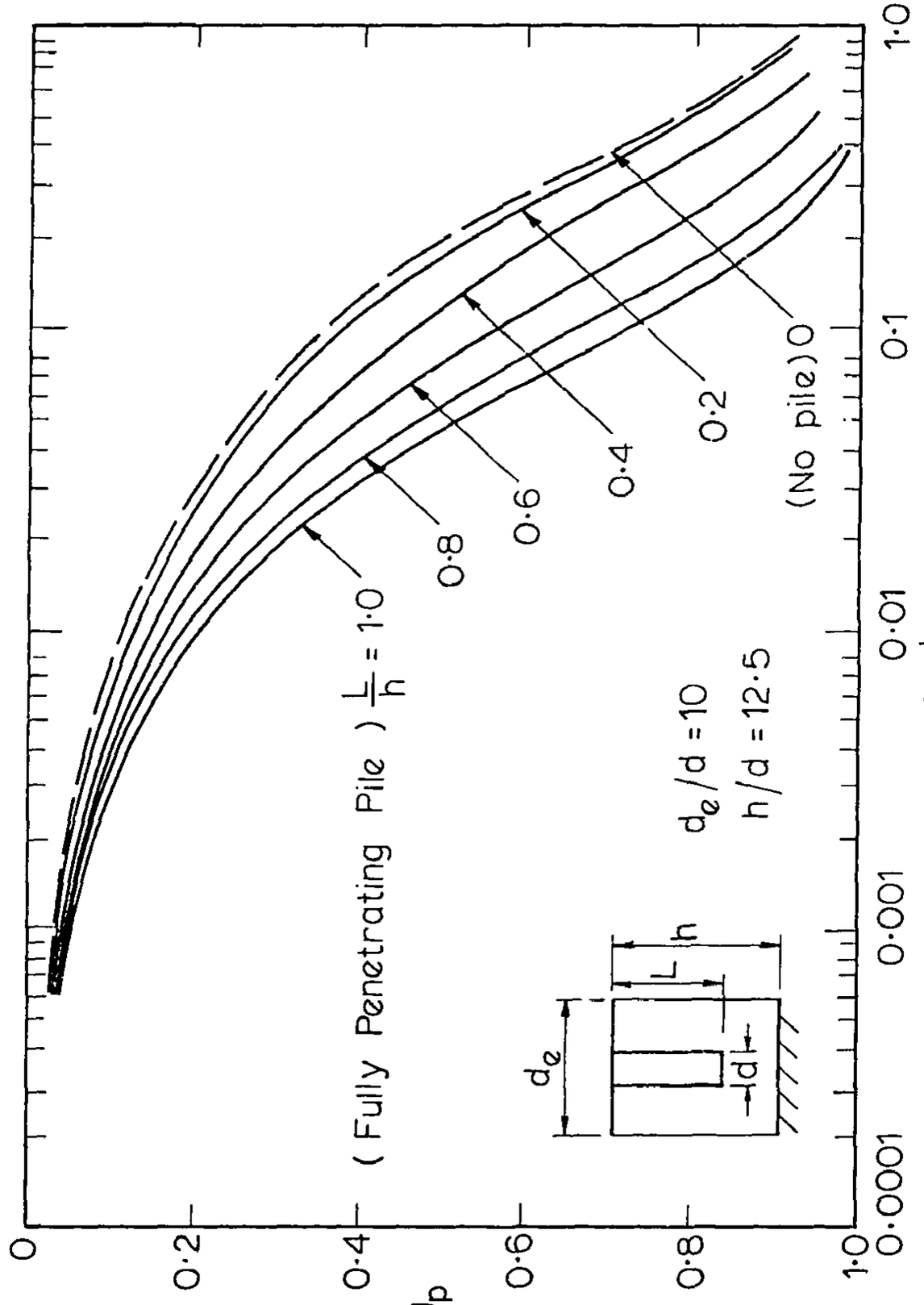

FIG. 6.9 RATE OF PORE PRESSURE DISSIPATION FOR d_e/d = 10

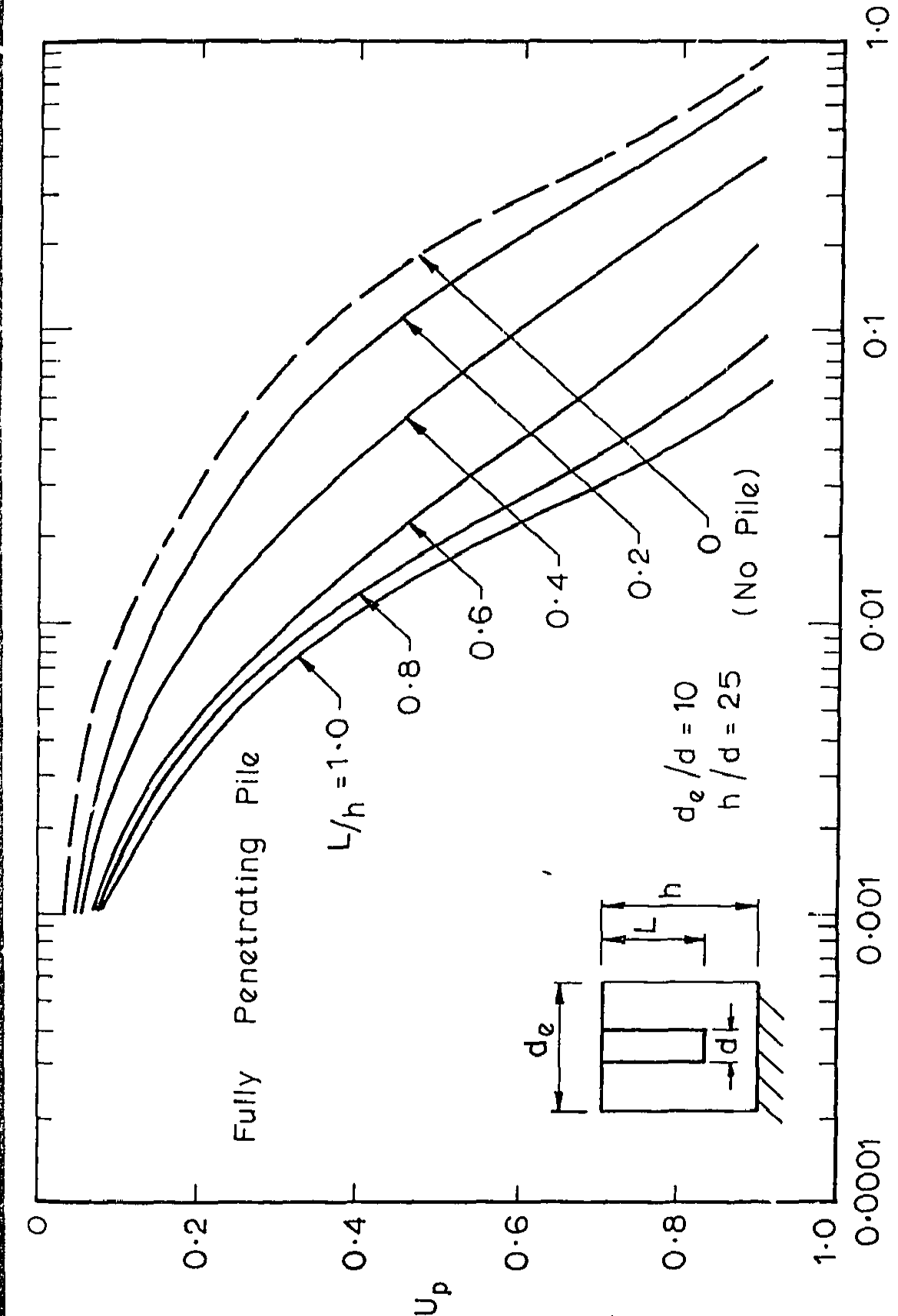

FIG. 6.10 RATE OF PORE PRESSURE DISSIPATION

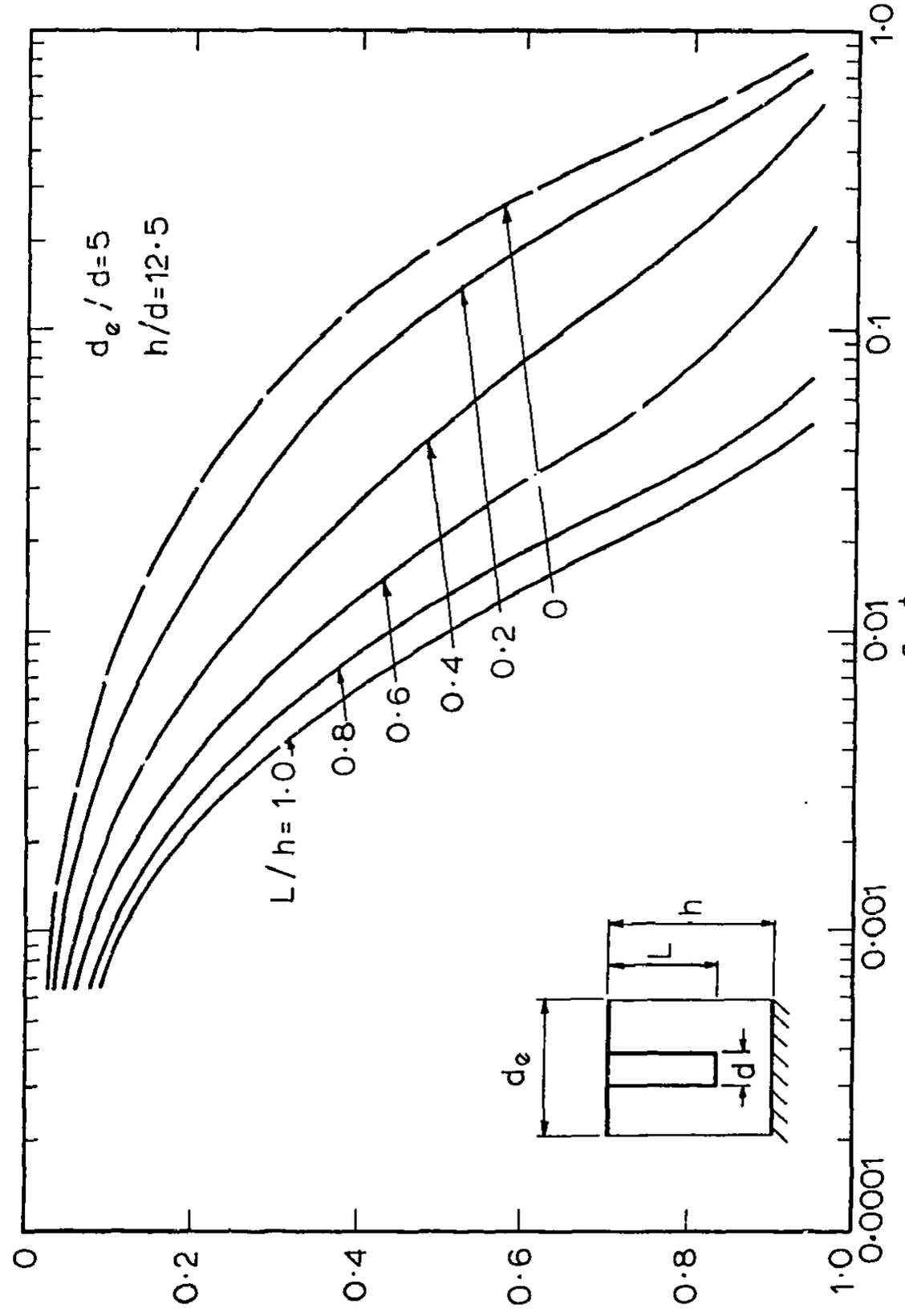

FIG. 6.11 RATE OF PORE PRESSURE DISSIPATION

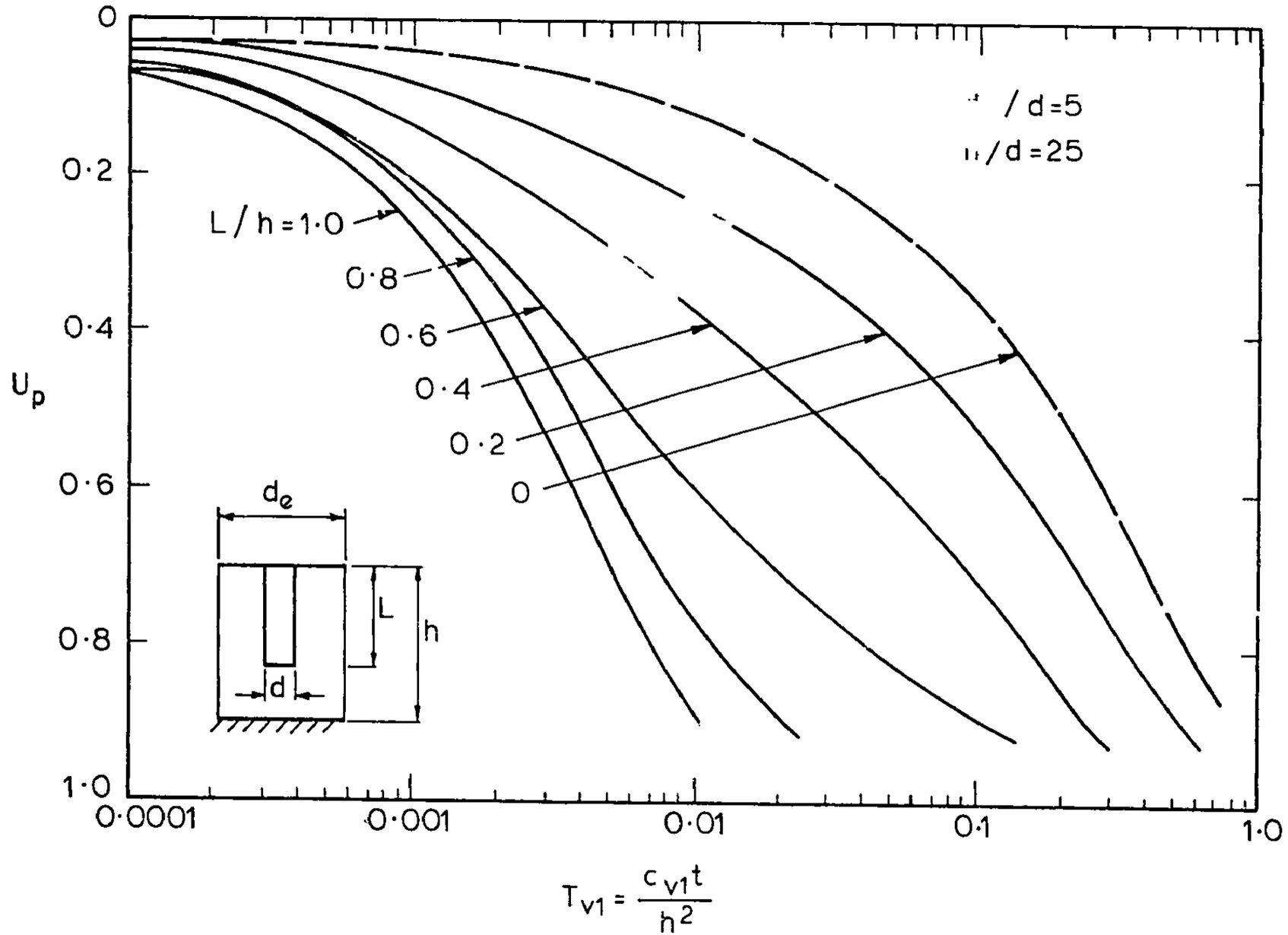

FIG. 6.12 RATE OF PORE PRESSURE DISSIPATION

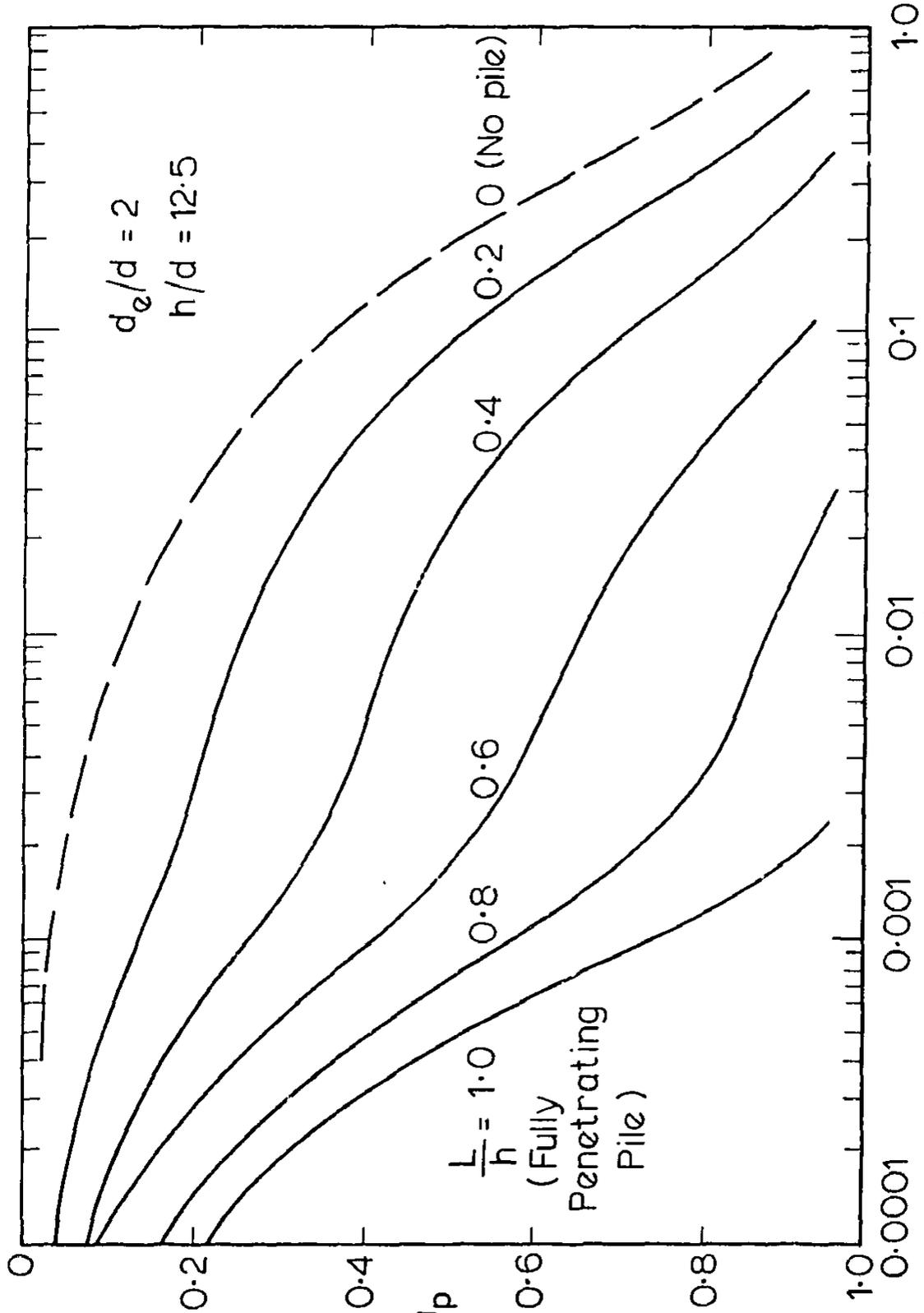

FIG. 6.13 RATE OF PORE PRESSURE DISSIPATION FOR $d_e/d = 2$

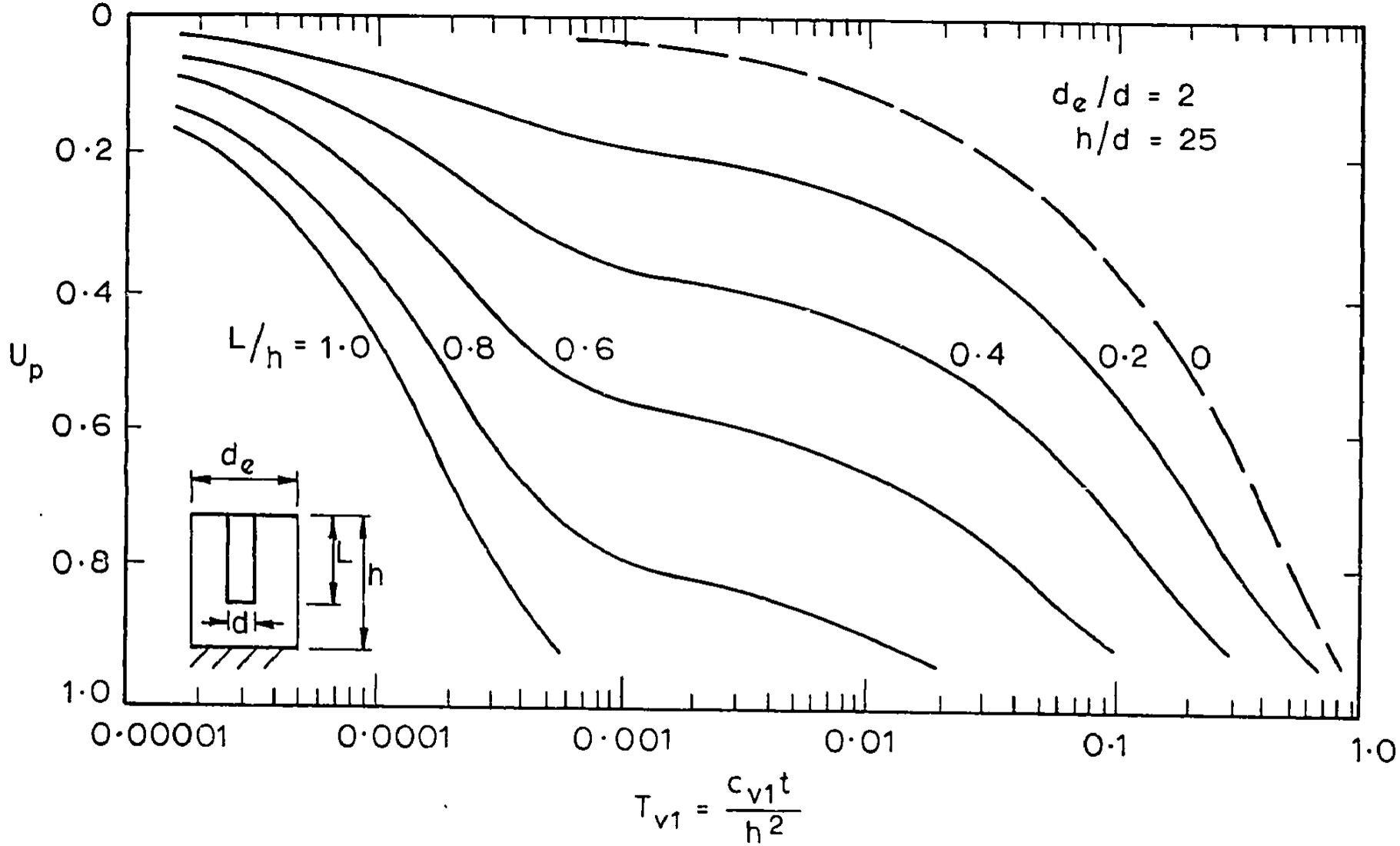

FIG. 6.14 RATE OF PORE PRESSURE DISSIPATION

practice. The results are for a permeable top and an impermeable base beneath the clay layer.

It is interesting to note in Figs. 6.13 and 6.14 the shape of the consolidation curves for $d_e/d = 2$. The change in shape with changing L/h is due to the rapid radial dissipation alongside the pile followed by the predominantly vertical flow from the clay beneath the pile. Because of the change in shape of the curves an investigation into the numerical accuracy of the solutions was undertaken. This was done in two ways.

Firstly, the number of nodal points in the finite difference grid were increased dramatically and the time intervals reduced. The effect on the solutions was found to be negligible. For example, solutions using 198 and 1131 nodal points were virtually identical . the case $d_e/d = 2$, $h/d = 25$ and $L/h = 0.6$, except for slight discrepan at early times. This slight discrepancy is to be expected as the excess pore pressures are set to zero at the first time step at the nodal points along the face of the pile and along the top surface. This has a comparatively larger effect for the grid with fewer nodal points, resulting in a slightly larger degree of pore pressure dissipation.

Secondly, for this geometry a degree of pore pressure dissipation U_R was calculated for the annulus of soil which embodies the pile. This was done to verify the assertion that the piles are so closely spaced that initially the dissipation of the excess pore pressures occur rapidly in this annulus of soil. In Fig [illegible] ted along with [illegible] which [illegible] of soil. The [illegible]

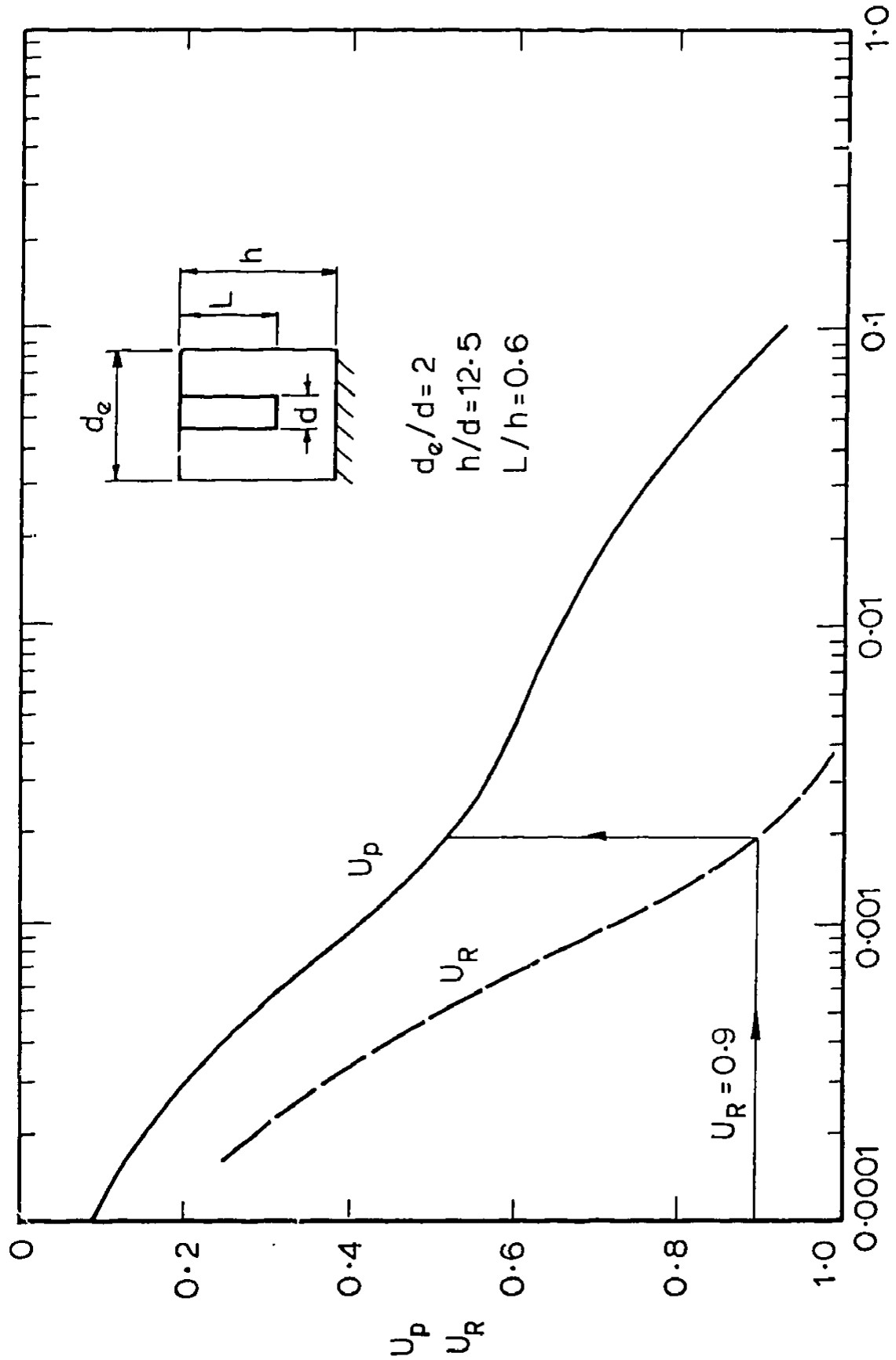

FIG. 6.15 INVESTIGATION OF NUMERICAL ACCURACY OF SOLUTIONS

point of inflection in the solution for U_p. This suggests that the initial portion of the solutions for these close spacings is due to the rapid radial dissipation and the point of inflection occurs when the flow is changing from predominantly radial alongside the pile to vertical from the cylinder of clay beneath the pile. Thus, the results of this investigation show that the solutions are numerically accurate.

The solutions presented in Figures 6.9 to 6.14 illustrate the increased rate of consolidation of the clay due to the installation of the piles. A convenient method of quantifying this increased rate is by comparing the rate with piles to the rate without piles ie. the one dimensional consolidation conditions. This comparison has been made by evaluating the ratio of time factors, T_{vl} for the 'with piles' solution to the 'without piles' solution when $U_l = 0.5$. The results of these comparisons are shown in Fig. 6.16. These results illustrate the importance of the degree of penetration of the piles on the rate of consolidation. For example, when $h/d = 25$ and $d_e/d = 5$, if the degree of penetration is increased from 0.4 to 0.8 (ie. the volume of pile material doubled), the rate of consolidation is increased by a factor of seven. Thus, if a given rate of consolidation is required, these results could be used to optimise the spacing, degree of penetration and diameter of the piles. If, for example, the rate required is ten times that for one dimensional consolidation conditions and the diameter of the piles chosen represent a value of $h/d = 25$, then if the piles are spaced such that $d_e/d = 5$, the degree of penetration required is .43, whereas if the piles are spaced such that $d_e/d = 10$, then a degree of penetration of 0.8 is necessary. The first alternative requires twice the volume of pile

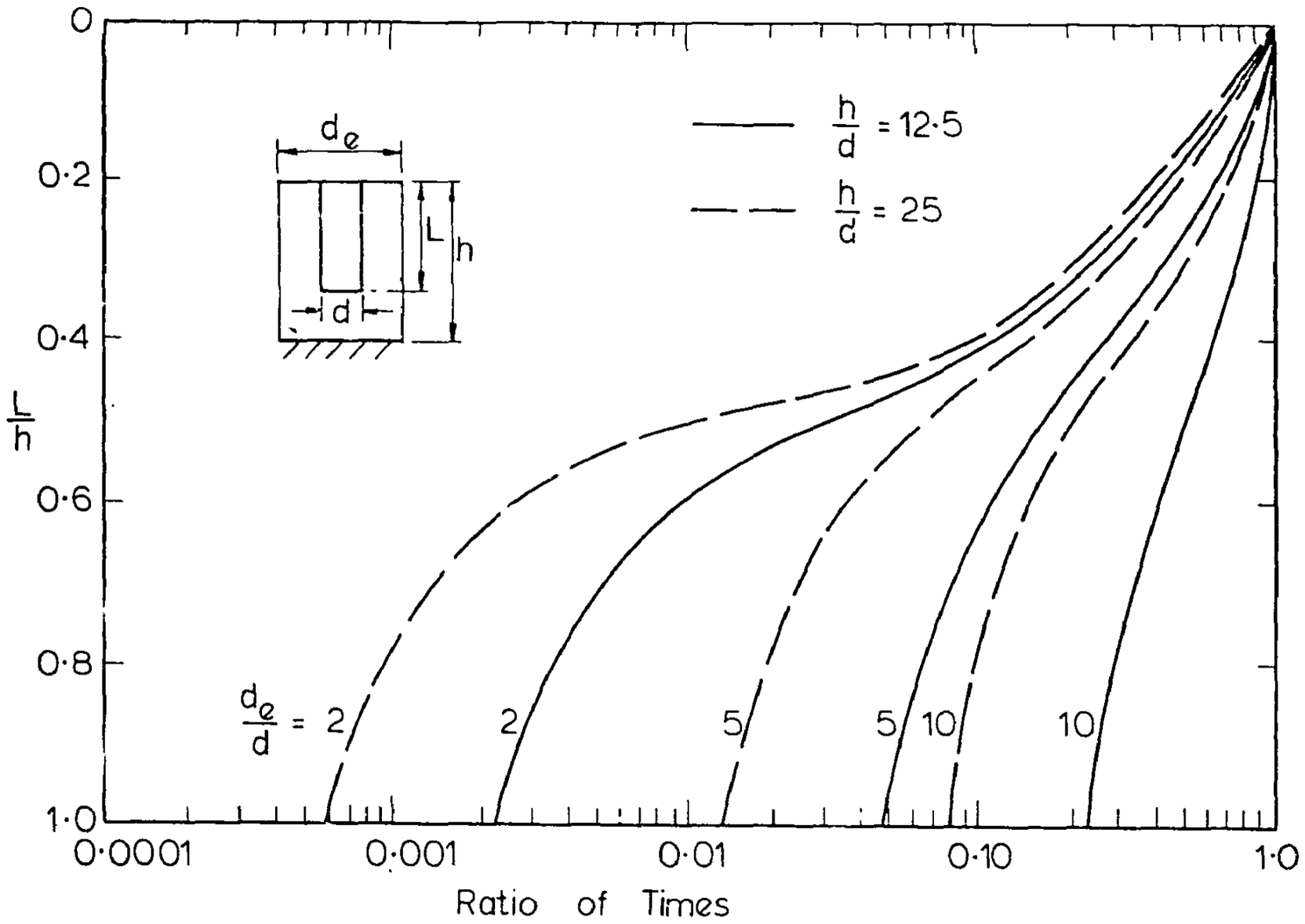

FIG. 6.16 EFFECT OF DEGREE OF PENETRATION ON RATE OF PORE PRESSURE DISSIPATION

mater.

6.4 EFFECT OF ANISOTROPY AND DRAINAGE CONDITIONS ON RATE OF PORE PRESSURE DISSIPATION

In Figs. 6.17 to 6.22 the increased rate of consolidation of the clay as the degree of penetration of the pile increases is shown when the coefficient of consolidation in the radial direction is twice the vertical. The rate of pore pressure dissipation is faster than for isotropic conditions which results in a displacement to the left of the curves shown in Figs. 6.9 to 6.14. This displacement illustrates the relative importance of radial drainage for the geometry being considered. The results of the comparison of time factors T_{vl} for the 'with piles' solution to the 'without piles' solution when $U_{l'} = 0.5$, is shown in Fig. 6.23.

In many anisotropic clays the ratio of horizontal to vertical permeability is much larger than two to one. To illustrate the effect of increasing the anisotropy on the rate of consolidation, solutions are presented in Figs. 6.24 to 6.27 for ratios of $c_{rl}:c_{vl}$ of 3, 4, 6 and 10 for the geometry $d_e/d = 5$, $h/d = 12.5$ and L/h varying from 1.0 to 0. If the ratios of the times for 50% consolidation under isotropic and anisotropic conditions are plotted against the degree of anisotropy (Fig. 6.28), the increased importance of the degree of penetration as the anisotropy increases is clearly demonstrated. The solutions for $L/h = 1.0$, 0.8 and 0.6 are nearly linear for this geometry because the rate of dissipation of the excess pore pressures is controlled predominantly by radial drainage. Thus, if the permeability in the radial direction is doubled, then the rate of consolidation is approximately

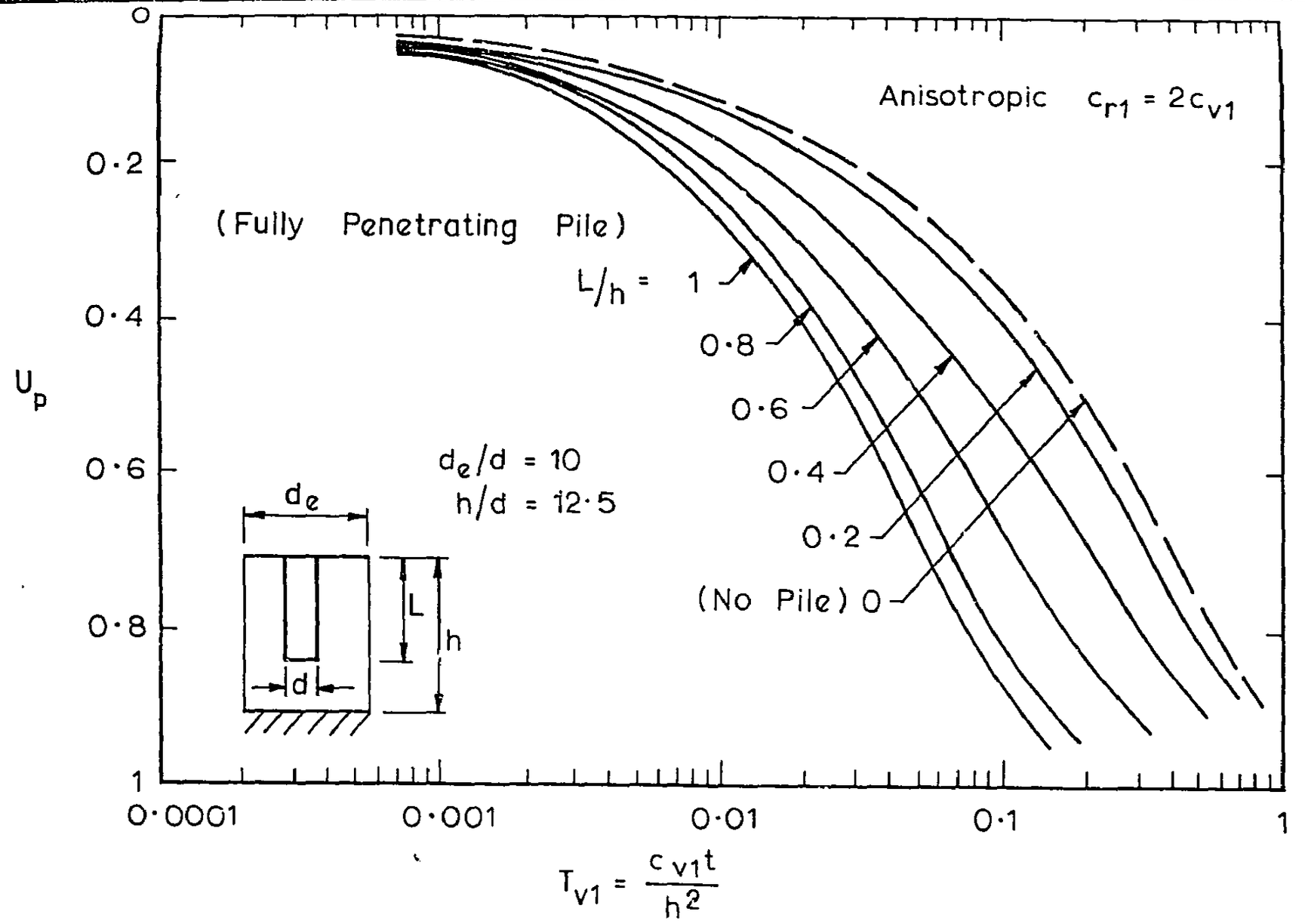

FIG. 6.17 RATE OF PORE PRESSURE DISSIPATION

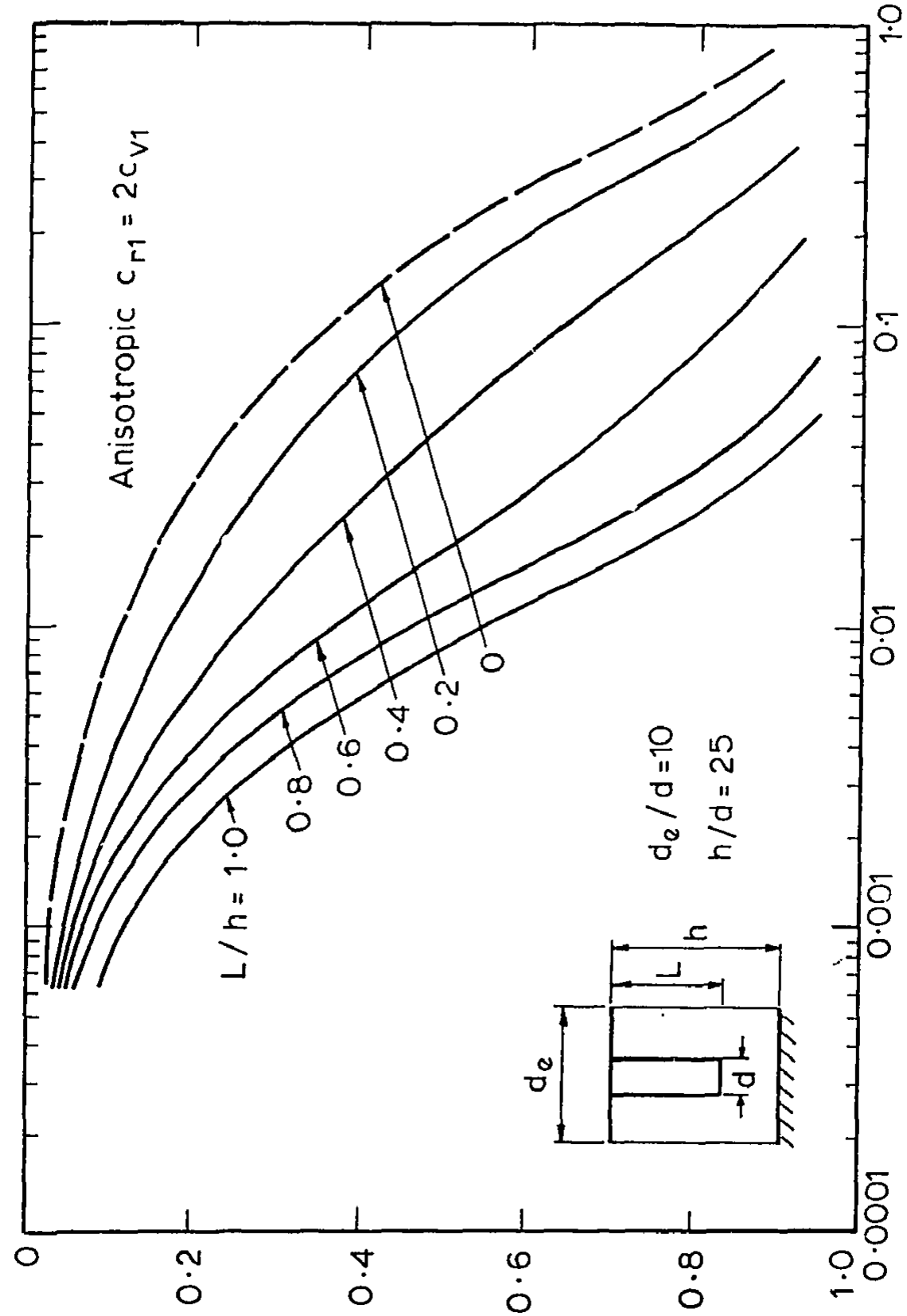

FIG. 6.18 RATE OF PORE PRESSURE DISSIPATION

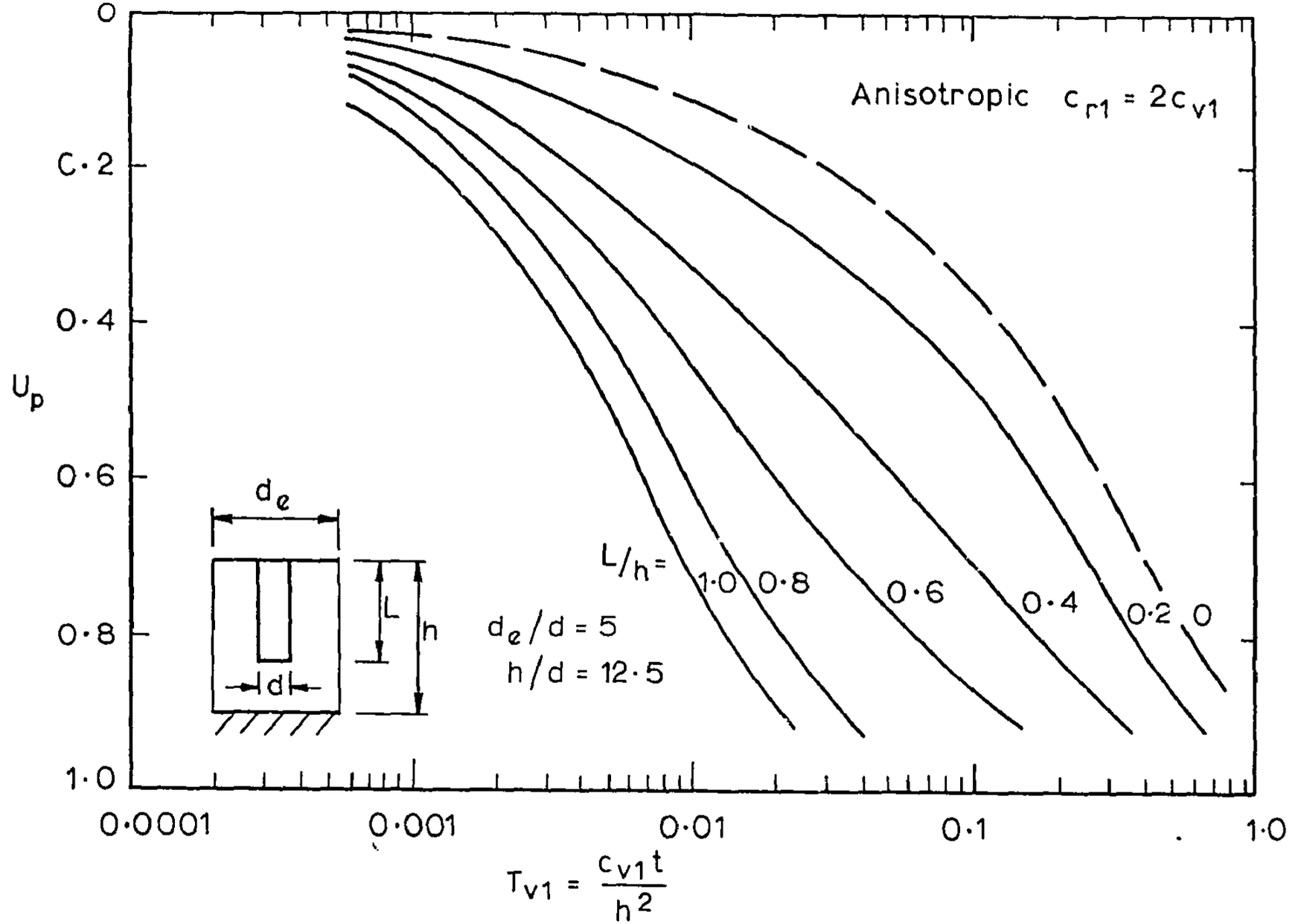

FIG. 6.19 RATE OF PORE PRESSURE DISSIPATION

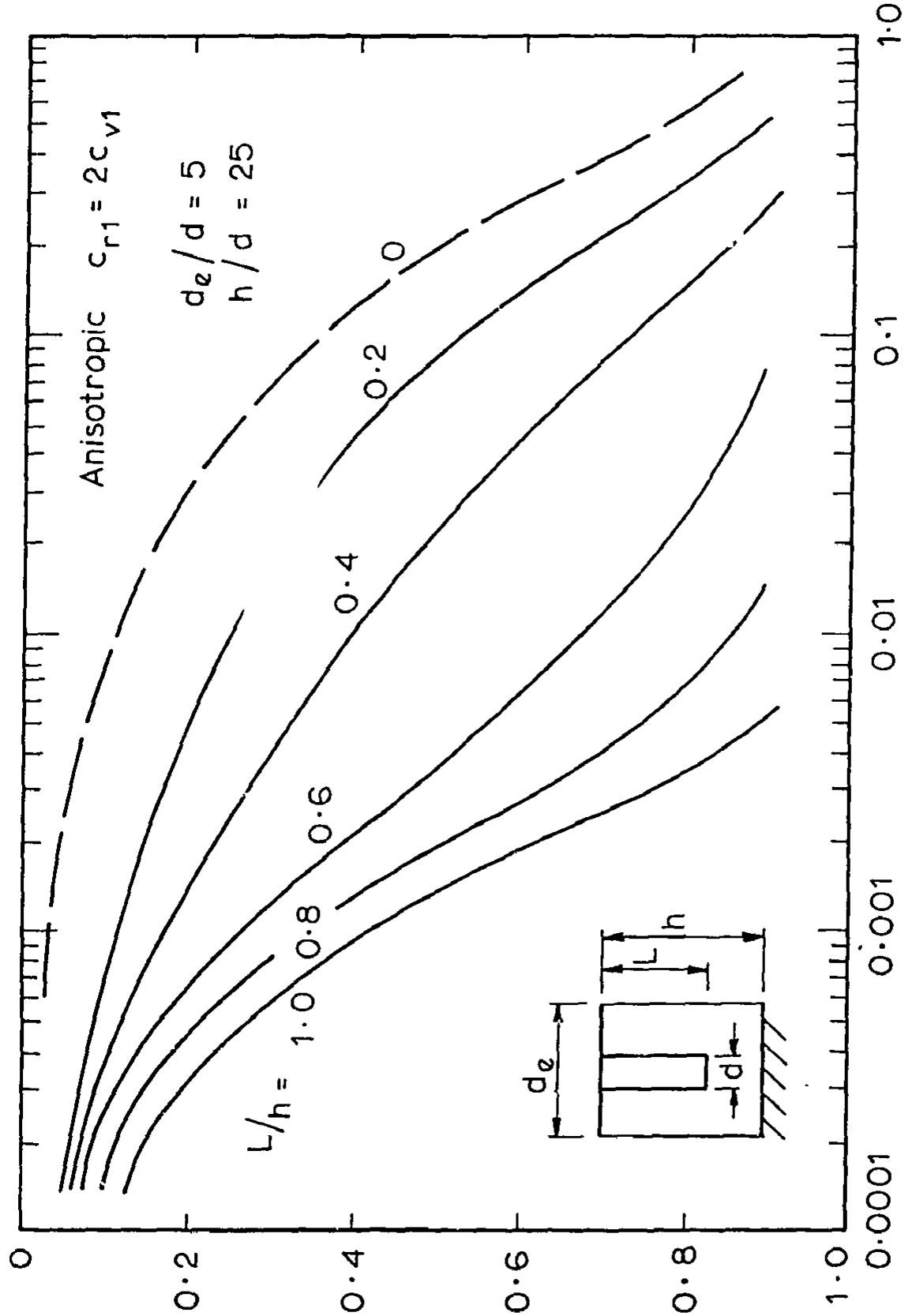

FIG. 6.20 RATE OF PORE PRESSURE DISSIPATION

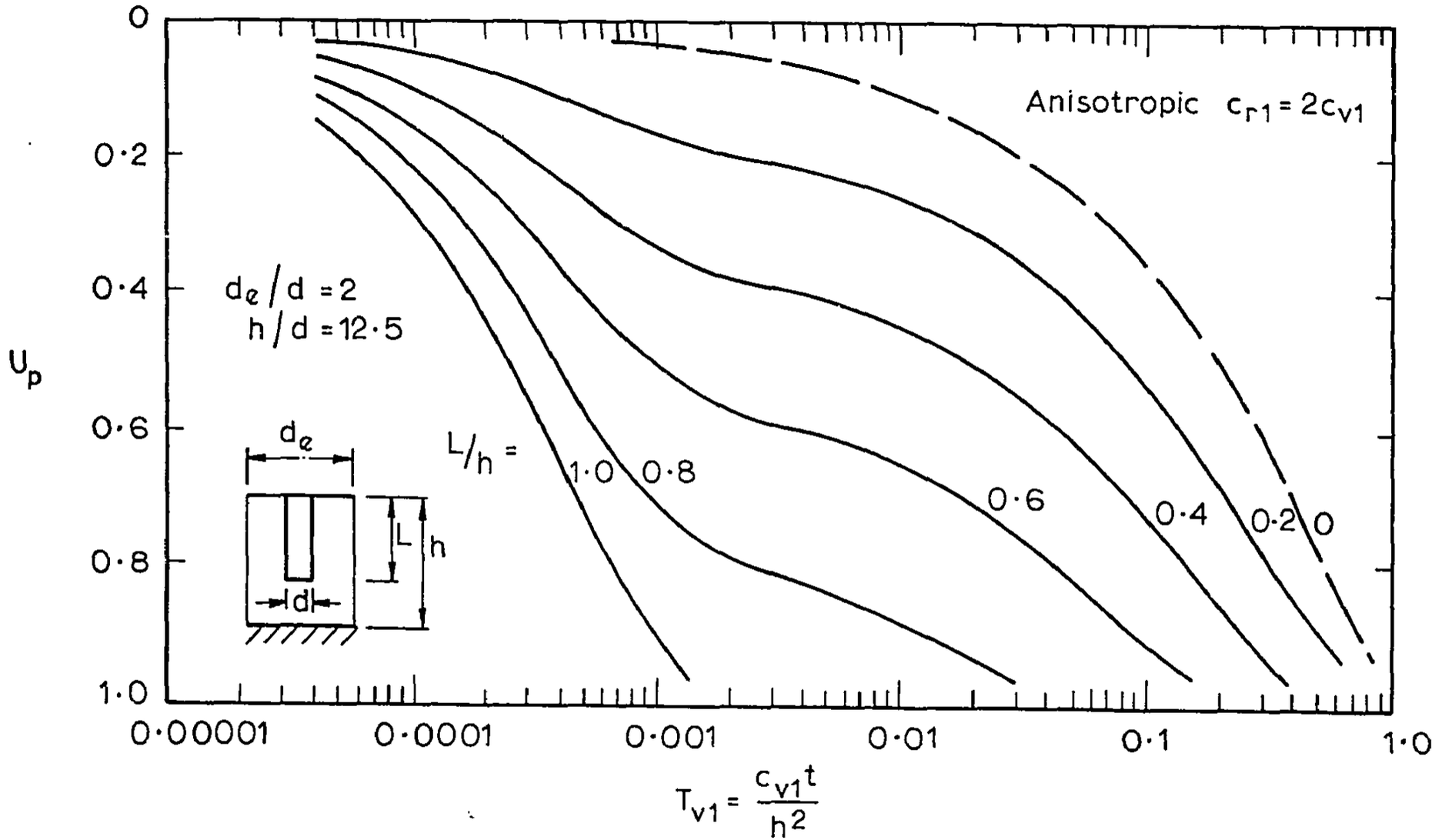

FIG.6.21 RATE OF PORE PRESSURE DISSIPATION

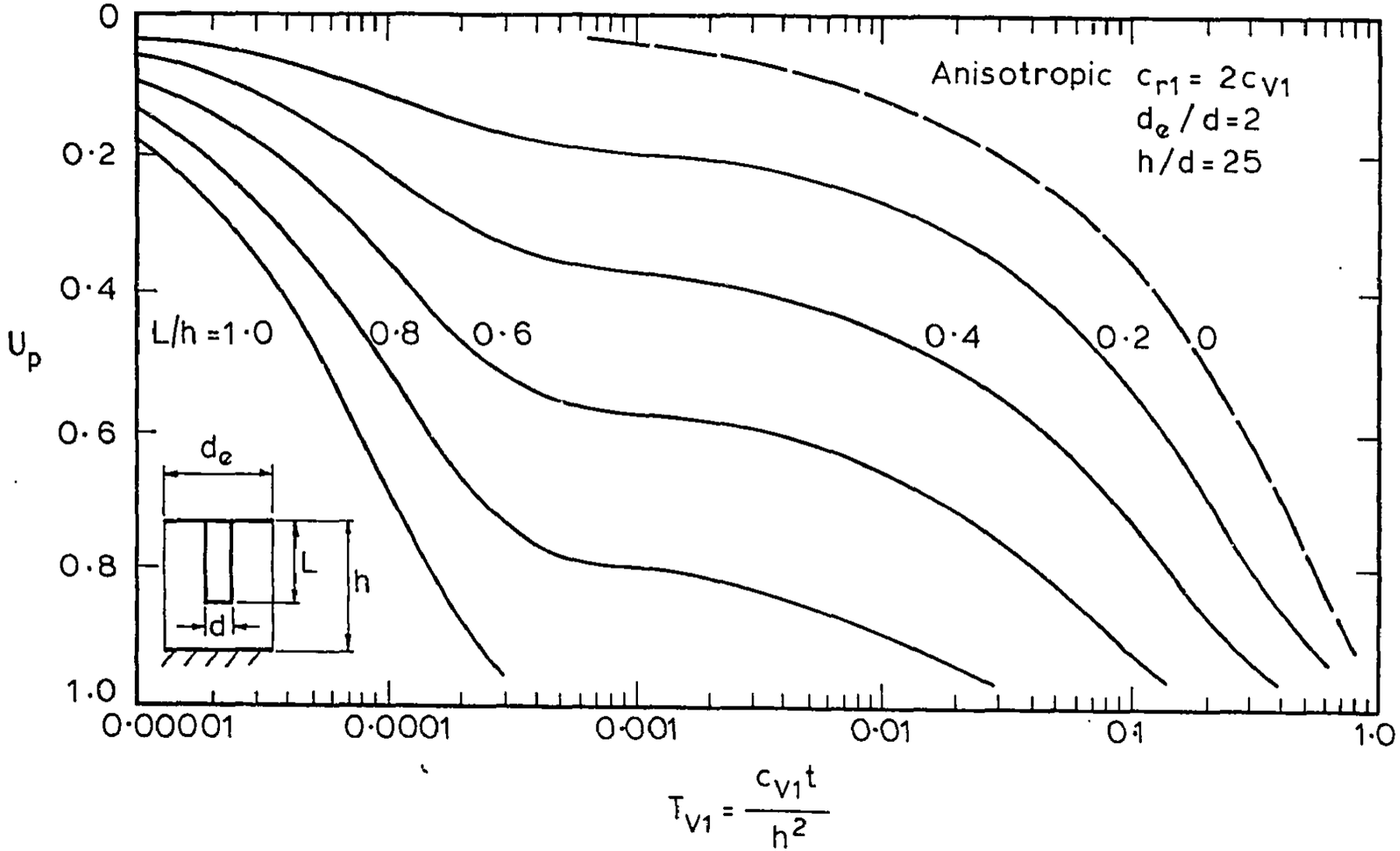

FIG. 6.22 RATE OF PORE PRESSURE DISSIPATION

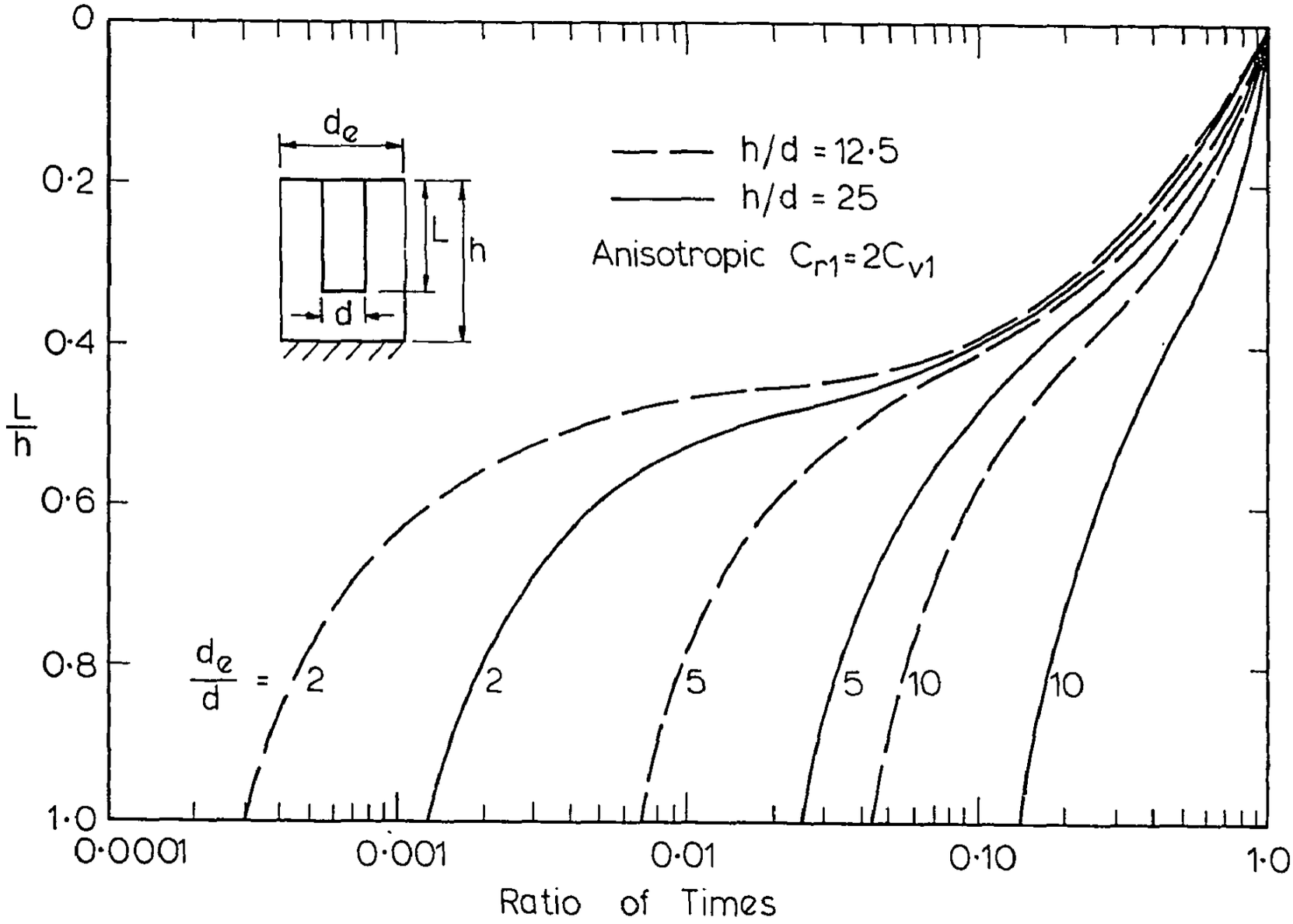

FIG. 6.23 EFFECT OF DEGREE OF PENETRATION ON RATE OF PORE PRESSURE DISSIPATION FOR ANISOTROPIC CONDITIONS

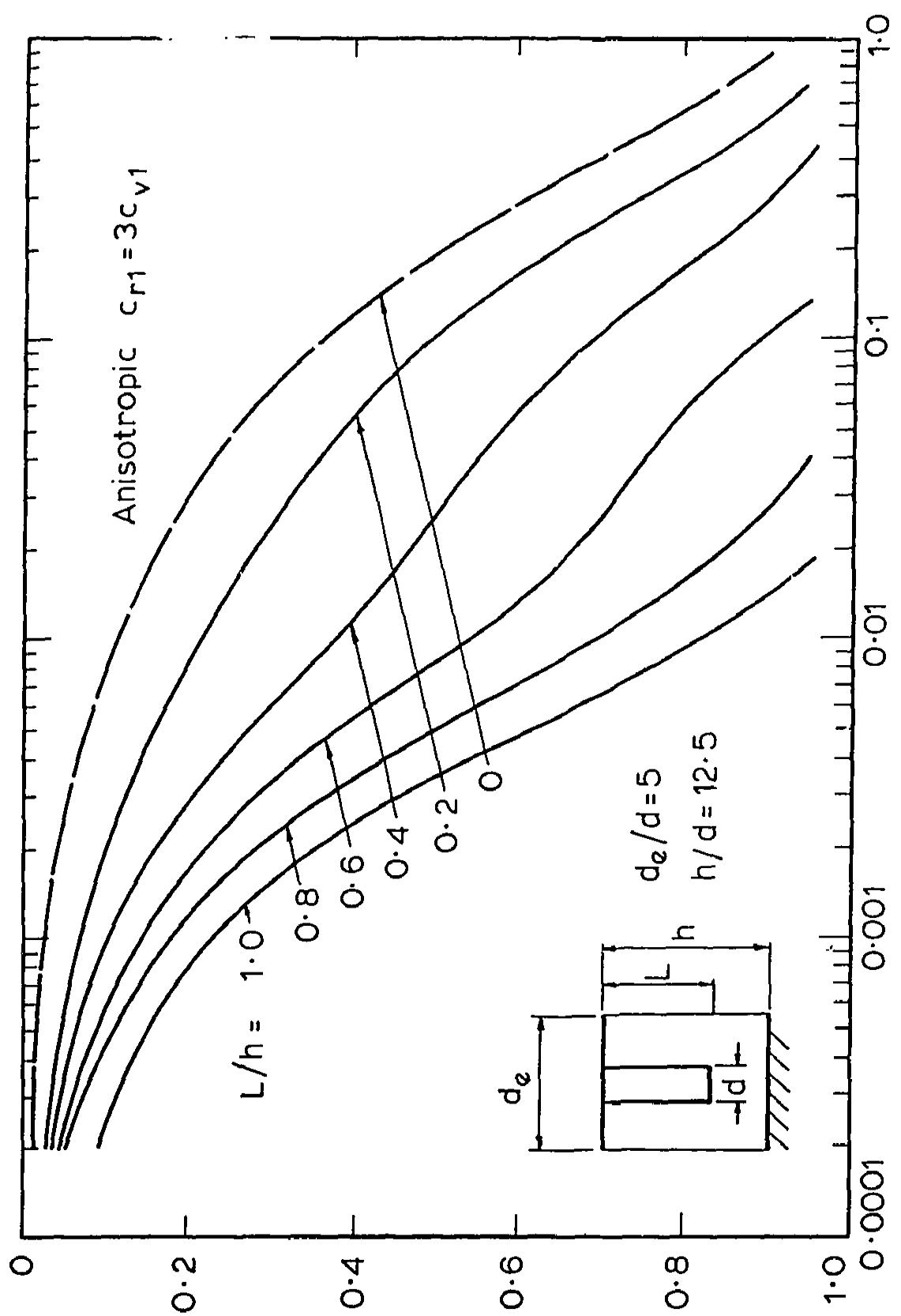

FIG. 6.24 RATE OF PORE PRESSURE DISSIPATION FOR $c_{r1} = 3c_{v1}$

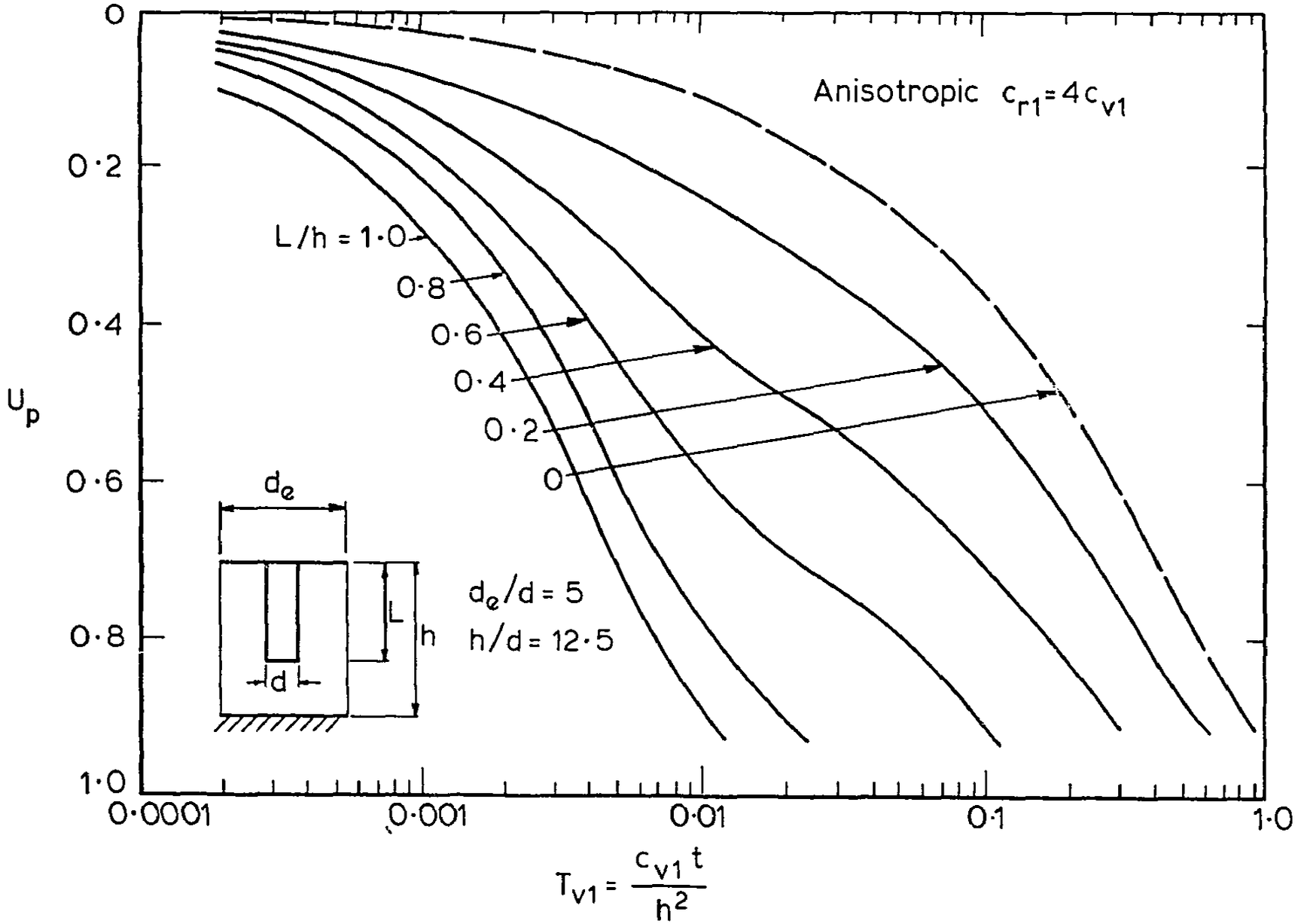

FIG. 6.25 RATE OF PORE PRESSURE DISSIPITATION FOR $c_{r1}=4c_{v1}$

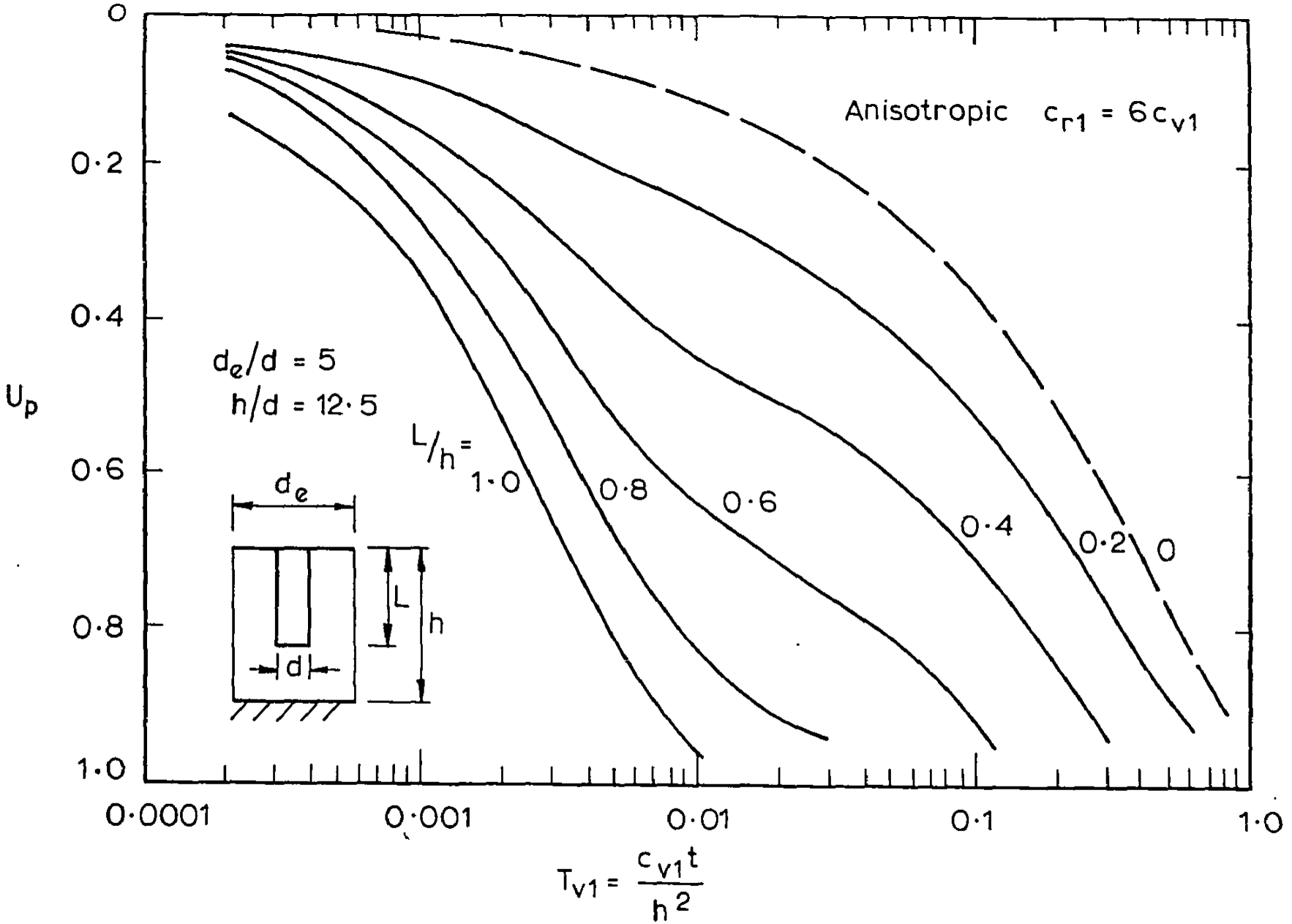

FIG. 6.26 RATE OF PORE PRESSURE DISSIPATION FOR $c_{r1} = 6c_{v1}$

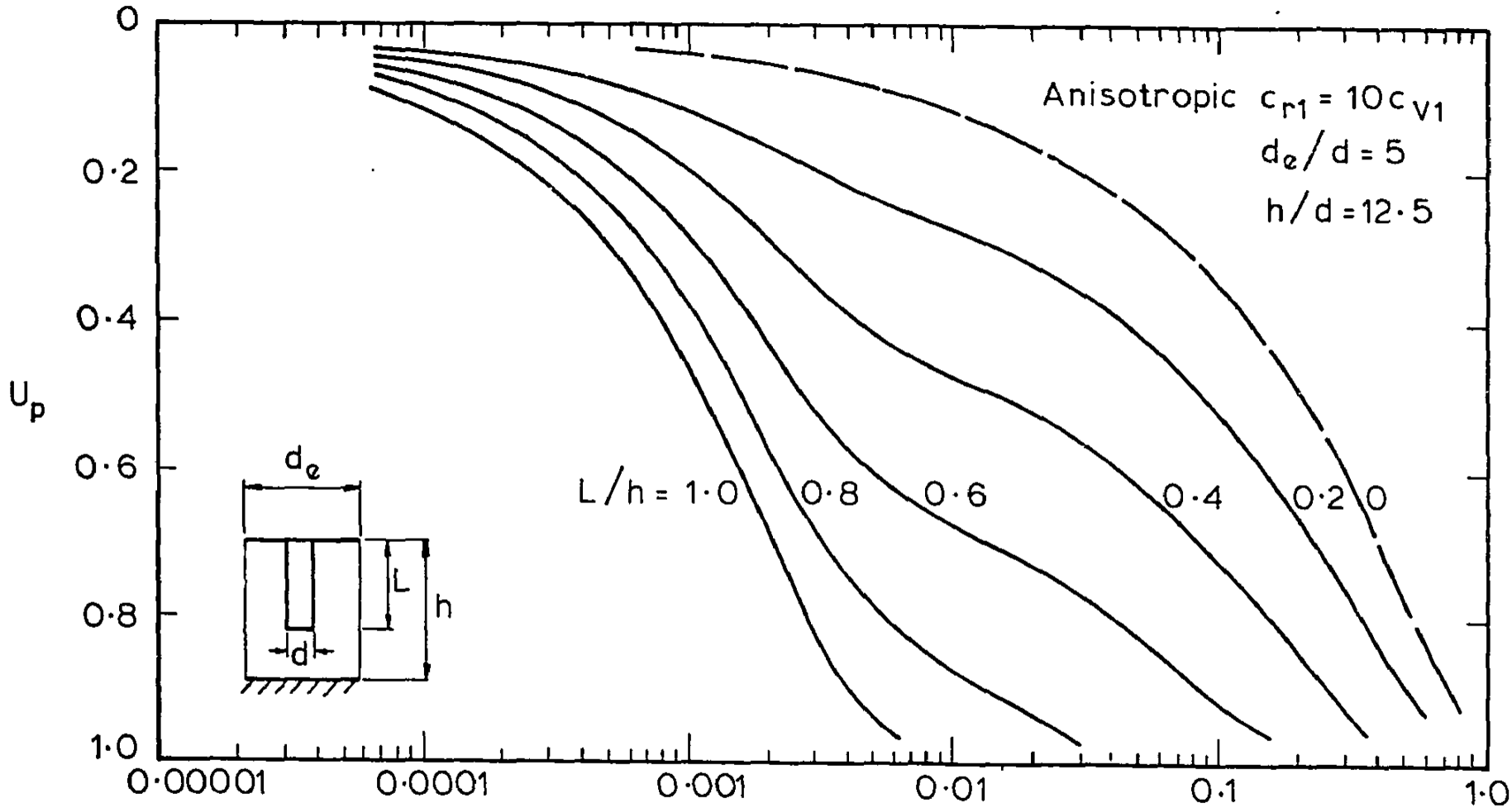

FIG. 6.27 RATE OF PORE PRESSURE DISSIPATION FOR $c_{r1} = 10 c_{v1}$

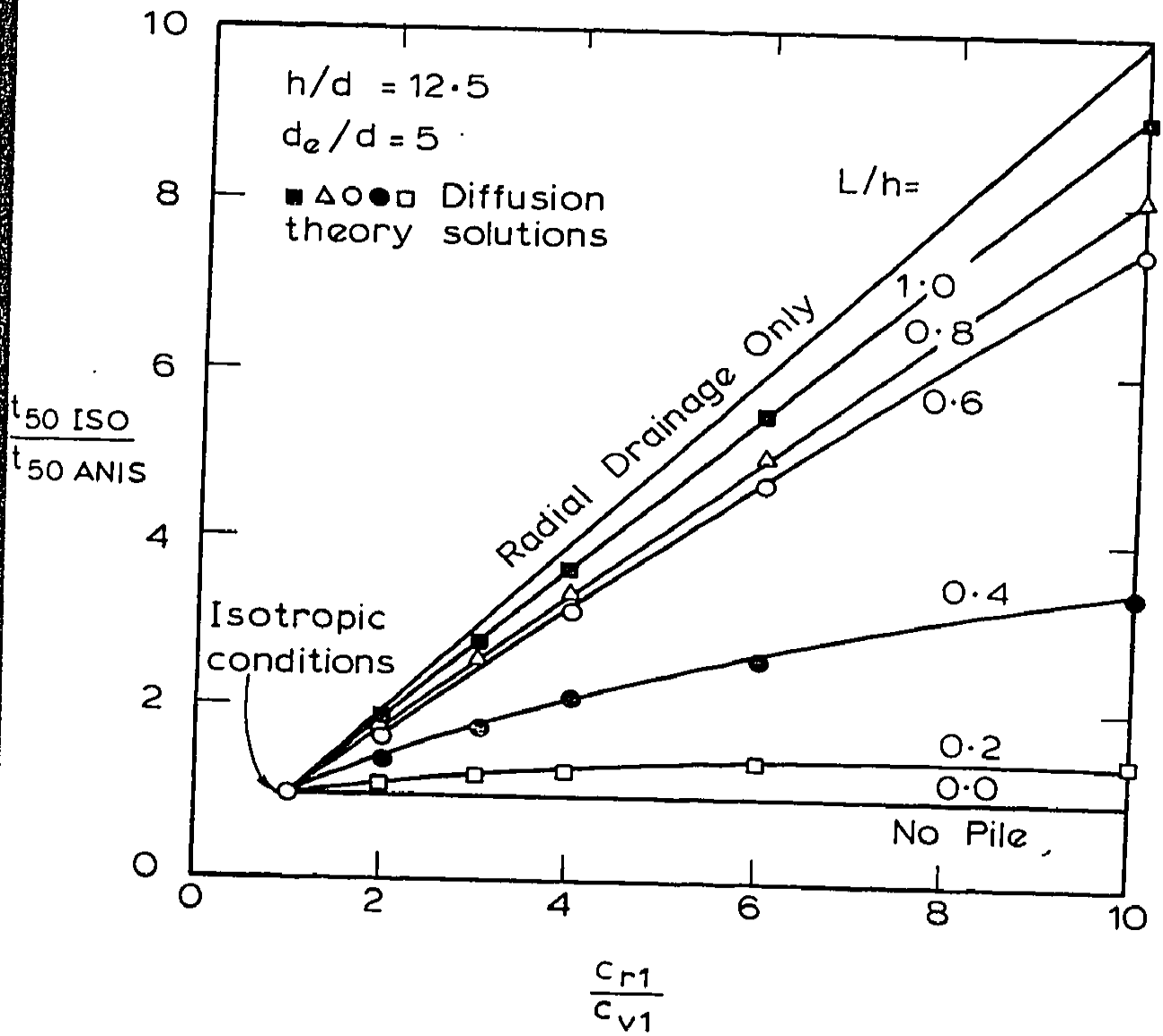

FIG. 6.28 THE EFFECT OF ANISOTROPY ON THE RATE OF CONSOLIDATION

doubled. However, for smaller values of L/h (0.4, 0.2) vertical drainage becomes relatively more important and thus increasing the radial permeability by a factor of two does not cause a corresponding increase in the rate of consolidation. Finally these results show that for clays with larger radial permeabilities than vertical, increasing the degree of penetration of the piles leads to more efficient use of the pile material.

As expected, when the top and bottom of the consolidating layer are permeable, the piles are not as effective in increasing the rate of consolidation compared to when the base of the layer is impermeable. The curves of Figs. 6.9 to 6.14 are thus displaced to the right. This displacement is illustrated in Fig. 6.29 for the isotropic case when $d_e/d = 5$, $h/d = 5$.

6.5 EXAMPLE ILLUSTRATING THE USE OF SOLUTIONS PRESENTED IN CHAPTERS 5 AND 6

To illustrate the use of the solutions presented in Chapters 5 and 6, the following example is considered.

A large flexible raft which exerts a pressure of 70 kN/m^2 is to be constructed on a soft homogeneous normally consolidated clay of depth 10m which overlies dense sands. Oedometer tests on samples taken from mid depth of the layer give the following results:

Initial void ratio	(e_o)	= 0.7
Compression index	(C_c)	= 0.45
Recompression index	(C_r)	= .05

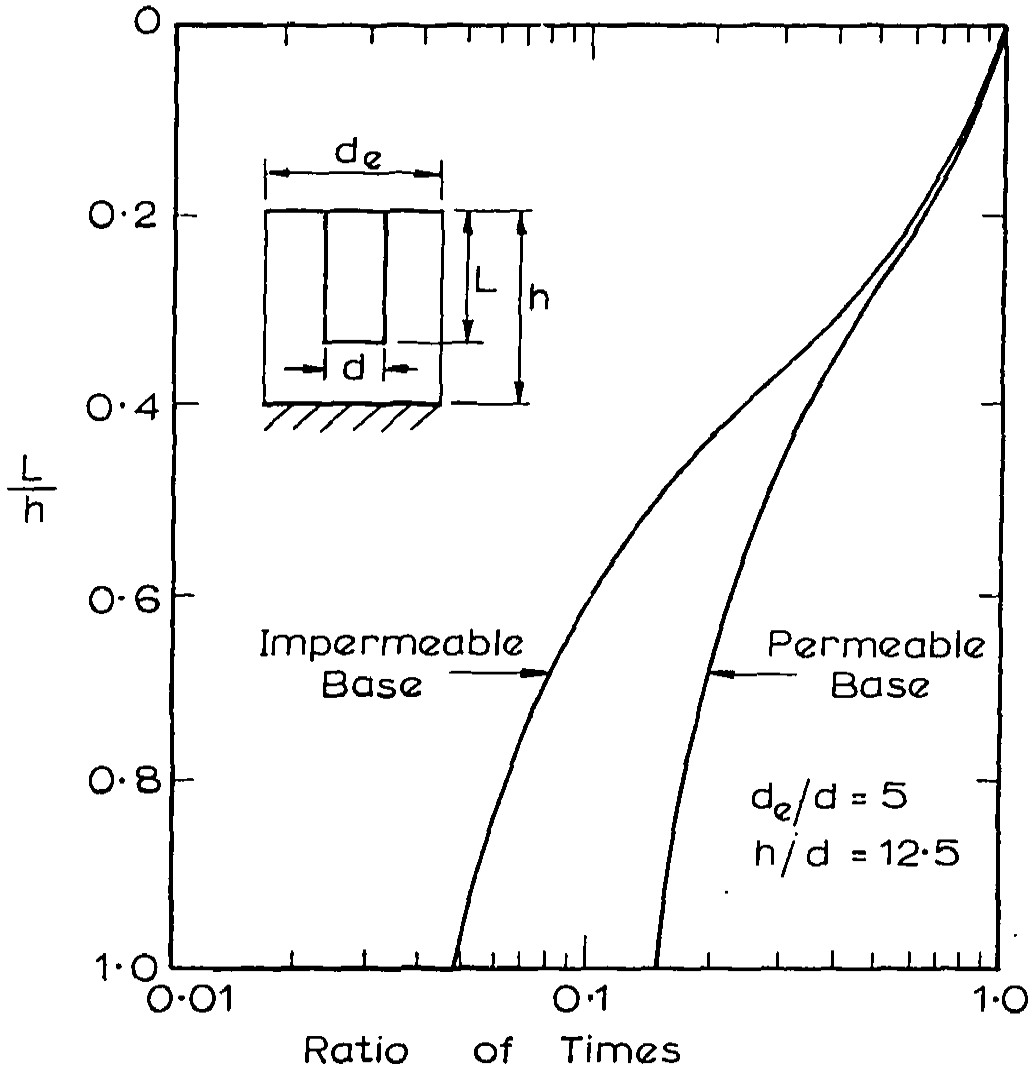

FIG. 6.29 EFFECT OF PERMEABILITY OF BASE ON RATE OF PORE PRESSURE DISSIPATION

One-dimensional coefficient of consolidation (c_{vl}) = 2.5 m^2/year

Bulk density of clay (γ_t) = 18 kN/m^3

The maximum allowable settlement of the raft is 250mm. The water table is taken to be at the surface.

One-dimensional settlement theory predicts a settlement of 1145mm which exceeds the allowable value of 250mm. Stabilisation by granular piles is considered an economical alternative. The vibro-flotation rig installs piles using the wet process of construction with an average diameter of 1m. The following example calculations are presented for three possible alternatives.

(A) Installation of the Piles Followed by Construction of the Raft

If the piles are installed to full depth of the soft clay (10m) in a triangular grid at a spacing of 1.90m; then from Figs. 5.6 and 5.7: For h/d = 10 and d_e/d = 2 the Settlement Ratio is .20 to .30, depending on the distribution of modulus with depth.

Settlement range = (.20)(1145) to (.30)(1145)

= 229 ~ 344mm

Therefore, even if the piles are installed at this close spacing the reduction in settlement is not sufficient to satisfy the maximum allowable settlement criterion.

(B) Installation of the Piles Followed by a Short Period of Preloading and the Commencement of Construction (assuming Preload not Removed)

If the piles are installed and the site preloaded by 3m of fill with density 19 kN/m^3 then from the diffusion theory results (Fig. 6.13) consolidation is taken to be complete when $T_{v1} = .002$ which corresponds to a time t where

$$t = \frac{T_{v1} h^2}{c_{v1}}$$

$$\therefore \quad t = \frac{(.002)(10)^2}{2.5} \text{ years}$$

$$\therefore \quad t = .08 \text{ years}$$

The preloading need only be left for a month before construction commences.

Calculation of Settlement of Raft

After 1 month the effective stress in the clay at mid depth σ_f' is approximated by

$$\sigma_f' = (3)(19) + (5)(18-9.8) \ kN/m^2$$
$$= 98 \ kN/m^2$$

The void ratio corresponding to this effective stress is given by

$$e_1 = e_o - C_c \log_{10} \frac{\sigma_f'}{\sigma_o'}$$

where σ_o' = initial effective stress at mid depth

= 41.0 kN/m^2

$\therefore$ $e_1 = 0.7 - 0.45 \log_{10} (\frac{98.0}{41.0})$

$e_1 = .53$

The final effective stress in the clay σ_{ff}' is approximated by

$\sigma_{ff}' = 70 + (3)(19) + (5)(18-9.8)$

= 168 kN/m^2

(i) Settlement without piles

$$\text{Settlement} = \left[\frac{C_c \log_{10} \frac{\sigma_{ff}'}{\sigma_f'}}{1 + e_1}\right] H$$

where H = thickness of the clay layer (assumed still to be 10m)

$$= \left[\frac{0.45 \log_{10} (\frac{168.0}{98.0})}{1.53}\right] 10$$

= 688mm

(ii) Settlement of raft (with piles)

From Figs. 5.6 and 5.7 for h/d = 10 and d_e/d = 2 the Settlement Ratio is .2 to .3

Settlement range = (.2)(688) ~ (.3)(688)

= 138 - 207mm

The range in predicted settlements is now acceptable.

(C) Installation of the Piles Followed by One Month of Preloading, Removal of Preload and then Commencement of Construction

At many sites the removal of the preload, before commencement of construction, is essential. This sequence of stabilisation is now considered.

If the piles were not installed but the ground preloaded, then the preload removed, one-dimensional settlement theory predicts a raft settlement of 280mm. Applying the Settlement Ratio of .2 - .3 results in a predicted range in settlement (with piles) of:

Settlement range = 56 - 84mm

This range of predicted settlement is also acceptable. An important assumption in the above examples is that the differential settlements due to the presence of the piles has been accounted for in the design of the raft.

6.6 SUMMARY AND CONCLUSIONS

Installation of granular piles in a regular pattern over a large area leads to an increased rate of consolidation due to the 'sand drain' action of the piles.

In this chapter comparisons have been made between finite element solutions to Biot's theory of consolidation and finite difference

solutions to simple diffusion theory for piles with varying degrees of penetration. It has been shown that by a suitable adjustment of the time scale, the discrepancy between the solutions is small except for piles which are nearly fully penetrating. A series of diffusion theory solutions are presented to show the effect of geometric factors, (such as pile penetration, spacing and soil layer depth), on the rate of consolidation of the clay.

The study indicates that the effectiveness of granular piles in increasing the rate of consolidation is increased dramatically by simultaneous reduction of pile spacing and increased pile penetration. The relative importance of the degree of pile penetration is increased with increasing anisotropy of the clay. In addition, because granular piles can increase the rate of consolidation of a clay layer to such an extent, an efficient mode of usage would be to install the piles and then subject the reinforced layer to a comparatively short period of preloading, which would result in significant reduction in settlement due to subsequent loading, and an increased load carrying capacity.

The solutions enable predictions of the rate of consolidation of the reinforced clay and can be used for optimising the spacing, diameter and degree of penetration of the piles for a required rate of consolidation.

Finally, an example to illustrate the use of the solutions presented in Chapters 5 and 6 is considered. The calculations emphasise the effectiveness of granular piles in increasing the rate of consolidation and reducing settlements.

APPENDIX 6A

FINITE DIFFERENCE EXPRESSIONS FOR DIFFUSION THEORY EQUATION

The diffusion theory equation can be written as

$$\frac{\partial u}{\partial t} = c_{vl} \frac{\partial^2 u}{\partial z^2} + c_{rl} \left[\frac{\partial^2 u}{\partial r^2} + \frac{1}{r} \frac{\partial u}{\partial r}\right] \tag{6A.1}$$

Referring to Fig. 6A.1 and letting

$$w_1 = \frac{\Delta z_1}{\Delta z_1 \, \Delta z_2 (\Delta z_1 + \Delta z_2)} \tag{6A.2}$$

$$w_2 = \frac{\Delta z_2}{\Delta z_1 \, \Delta z_2 (\Delta z_1 + \Delta z_2)} \tag{6A.3}$$

$$p_1 = \frac{\Delta r_1}{\Delta r_1 \, \Delta r_2 (\Delta r_1 + \Delta r_2)} \tag{6A.4}$$

$$p_2 = \frac{\Delta r_2}{\Delta r_1 \, (\Delta r_1 + \Delta r_2)} \tag{6A.5}$$

$$q_1 = \frac{1}{2r \, (\Delta r_1 + \Delta r_2)} \tag{6A.6}$$

$$\alpha_1 = c_{vl} \, \Delta t \tag{6A.7}$$

$$\alpha_2 = c_{rl} \, \Delta t \tag{6A.8}$$

then at time t the finite difference equivalents to the differentials can be written as

$$\frac{\partial u}{\partial t} = \frac{u_{o,t+\Delta t} - u_{o,t}}{\Delta t} \tag{6A.9}$$

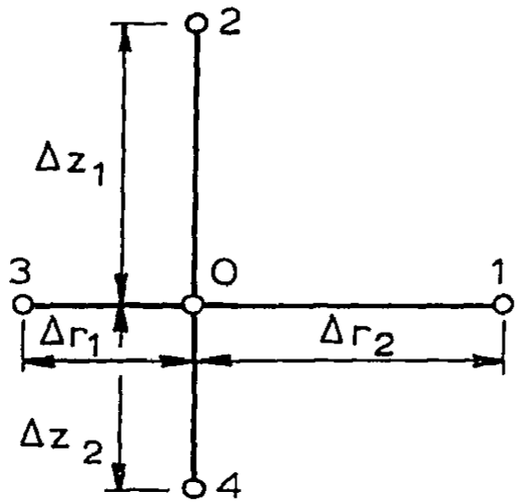

(a) Definition of spacing and numbering scheme for nodal points

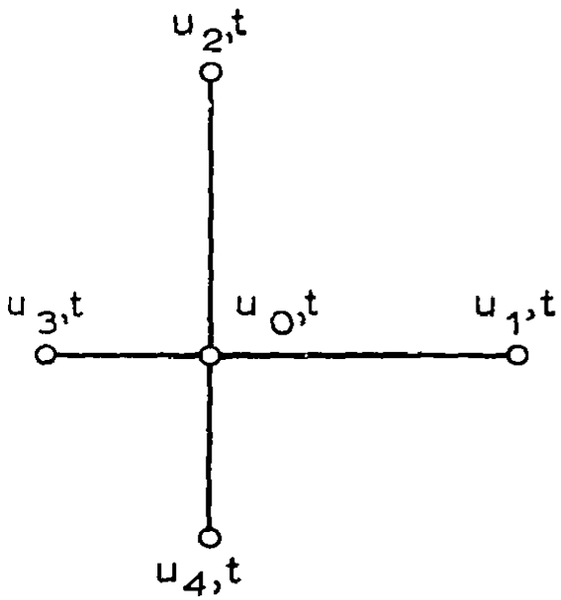

(b) Excess pore pressures at time t

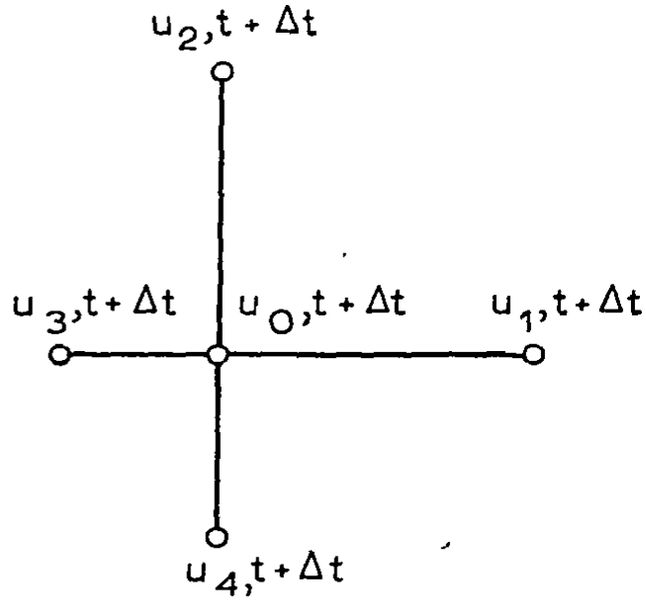

(c) Excess pore pressures at time $t + \Delta t$

FIG. 6A.1 DEFINITION OF TERMS USED IN APPENDIX 6A

$$\frac{\partial^2 u}{\partial z^2} = 2\{(u_{4,t} - u_{o,t})\, w_1 - (u_{o,t} - u_{2,t})\, w_2\} \qquad (6A.10)$$

$$\frac{\partial^2 u}{\partial r^2} = 2\{(u_{1,t} - u_{o,t})\, p_1 - (u_{o,t} - u_{3,t})\, p_2\} \qquad (6A.11)$$

$$\frac{1}{r}\frac{\partial u}{\partial r} = \frac{1}{r}\left(\frac{u_{1,t} - u_{o,t}}{\Delta r_1 + \Delta r_2}\right) \qquad (6A.12)$$

For the implicit form of the equations, average values for the differentials are used over the time interval Δt. An equation for the unknown nodal value of excess pore pressure at time $t + \Delta t$ ($u_{o,t+\Delta t}$) in terms of the known values at time t is assembled for each grid point, ie.

$$\{a\}^T\{u\}_{t+\Delta t} = \{b\}^T\{u\}_t \qquad (6A.13)$$

where $\{u\}$ = vector of excess pore pressures at the node being considered and the adjacent nodes

= $\{u_o, u_1, u_2, u_3, u_4\}$

and the subscripts t, $t+\Delta t$ refer to the time. The vectors $\{a\}^T$ and $\{b\}^T$ contain the following terms:

$$\{a\}^T = \{a_o, a_1, a_2, a_3, a_4\} \qquad (6A.14)$$

where $$a_o = 1 + \alpha_1(w_1 + w_2) + \alpha_2(p_1 + p_2) \qquad (6A.15)$$

$$a_1 = -\alpha_2(p_1 + q_1) \qquad (6A.16)$$

$$a_2 = -\alpha_1 w_2 \qquad (6A.17)$$

$$a_3 = \alpha_2(q_1 - p_2) \qquad (6A.18)$$

$$a_4 = -\alpha_1 w_1 \quad (6A.19)$$

$$\{b\}^T = \{b_o, b_1, b_2, b_3, b_4\} \quad (6A.20)$$

where $$b_o = 1 - \alpha_1 (w_1 + w_2) - \alpha_2 (p_1 + p_2) \quad (6A.21)$$

$$b_1 = -a_1 \quad (6A.22)$$

$$b_2 = -a_2 \quad (6A.23)$$

$$b_3 = -a_3 \quad (6A.24)$$

$$b_4 = -a_4 \quad (6A.25)$$

The boundary condition r = 0

For nodal points on the axis r = 0, a special form of equation 6A.1 is used as

$$\lim_{r \to 0} \frac{1}{r} \frac{\partial u}{\partial r} = \frac{\partial^2 u}{\partial r^2} \quad (6A.26)$$

Thus, equation 6A.1 is replaced by

$$\frac{\partial u}{\partial t} = c_{vl} \frac{\partial^2 u}{\partial z^2} + 2c_{rl} \frac{\partial^2 u}{\partial r^2} \quad (6A.27)$$

For these nodal points the vectors $\{a\}^T$ and $\{b\}^T$ contain the following terms:

$$a_o = 1 + \alpha_1 (w_1 + w_2) + 2\alpha_2 (p_1 + p_2) \quad (6A.28)$$